Analysis of telomere length dynamics and telomerase activity in neurosenescence and neurodegenerative diseases of the central nervous system

Dissertation

To fulfil the requirements for the degree of

"Doctor of Philosophy" (Ph.D.)

Submitted to the Faculty Council of the School of Medicine

Friedrich Schiller University, Jena

by

Quratul Ain, M.Phil

Born on 10.06.1985 in Okara, Pakistan

Dissertation, Friedrich Schiller University Jena, 2018

Reviewers:

1. Prof. Dr. O.W. Witte

Hans-Burger Department of Neurology, University Hospital, Jena

2. Prof. Dr. Regine Heller

Institut for Molecular Cell Biology, University Hospital, Jena

Universitätsklinikum Jena

3. Prof. Dr. Thomas Arendt

Paul-Flechsig Institut for Brain Research. University Hospital, Leipzig

Date of public disputation: 03.07.2018

In the name of God, most Gracious, most Compassionate

O mankind, if you should be in doubt about the Resurrection, then [consider that] indeed, We created you from dust, then from a sperm-drop, then from a clinging clot, and then from a lump of flesh, formed and unformed – that We may show you. And We settle in the wombs whom We will for a specified term, then We bring you out as a child, and then [We develop you] that you may reach your [time of] maturity. And among you is he who is taken in [early] death, and among you is he who is returned to the most decrepit [old] age so that he knows, after [once having] knowledge, nothing. And you see the earth barren, but when We send down upon it rain, it quivers and swells and grows [something] of every beautiful kind.

(AlQuran; 22:5)

To my family and late Dr. Hadi Hasan Shaheed

TABLE OF CONTENTS

LIST OF ABBREVIATIONS

A	Area
AD	Alzheimer's disease
AF 488	Alexa fluor 488
ALS	Amyotrophic lateral sclerosis
ALT	Alternative lengthening of telomeres
ANOVA	Analysis of variance
AS	Asymptomatic
ß-III tub	Beta III tubulin
Bp	Base pair
BSA	Bovine serum albumin
CA-II	Carbonic anhydrase II
CHAPS	3- ((3-cholamidopropyl)dimethylammonio)-1-propanesulfonic acid
CNS	Central nervous system
c-Rel	Canonical NF-κB subunit
Ct	Threshold cycle
DABSYL	4-(dimethylamine)azo benzene sulfonic acid
DAPI	4',6-diamidino-2-phenylindole
DMSO	Dimethyl sulfoxide
ET	Energy transfer
EU	European union
FACS	Fluorescence-activated cell sorting (FACS)
FITC	Fluorescein isothiocyanate
FISH	Fluorescent *in situ* hybridization
FSC	Forward side scatter
GAPDH	Glyceraldehyde-3-phosphate dehydrogenase
H	Height
HR	Homologous recombination
HT-QFISH	High throughput quantitative fluorescent *in situ* hybridization
Iba-1	Ionized calcium binding adapter molecule 1
IQ-FISH	Interphase quantitative fluorescent *in situ* hybridization
Kb	Kilo base
MDD	Major depressive disorders
MFI	Mean fluorescence intensity
NeuN	Neuronal nuclei
NF-κB	Nuclear factor kappa-light-chain-enhancer of activated B cells
PBS	Phosphate buffered saline
PCNA	Proliferating cell nuclear antigen
PCR	Polymerase chain reaction
PFA	Paraformaldehyde
PI	Propidium iodide
PNA	Peptide nucleic acid
POT1	Protein protection of telomeres 1
PS	Presymptomatic
qPCR	Quantitative reverse transcriptase polymerase chain reaction
Q-FISH	Quantitative fluorescent *in situ* hybridization
Rap1	Repressor activator protein 1
RelA	V-Rel avian reticuloendotheliosis viral oncogene homolog A
ROS	Reactive oxygen species
RP	Reverse primer

RT	Room temperature
RTL	Relative telomere length
TAE	Tris-acetate ethylene diamine tetra acetic acid buffer
TBS	Tris buffer saline
TERC	Telomerase RNA component
TERT	Telomerase reverse transcriptase
TIN2	TRF1-interacting nuclear factor 2
TPP1	Tripeptidyl peptidase
TRAP	Telomeric repeat amplification protocol
TRF	Terminal restriction fragment length analysis
TRF1,2	Telomeric repeat binding factor 1, 2
TS	Telomere substrate
S	Symptomatic
SEM	Standard error of the mean
SOD1	Superoxide dismutase 1
SPF	Specific pathogen-free
SSC	Side scatter
S100-ß	S100 calcium binding protein B
UV	Ultra violet

Units

Sec	Second
Min	Minute
AU	Arbitrary unit
IU	International unit
U	Unit
µl	Microlitre
ml	Millilitre
L	Litre
amoles	Attomoles
µM	Micromol
mM	Millimol
M	Molar (mol/litre)
µg	Microgram
ng	Nanogram
mg	Milligram
g	Gram
µm	Micrometer or Micron
mm	Millimeter
%	Percent
°C	Degree celsius
Rpm	Rotation per minute
Vol	Volume

SUMMARY

Telomeres are specialized nucleoprotein structures that protect chromosomal ends, and their lengths are species-specific. Telomeres serve as a mitotic clock as they get shortened with each round of replicative cycle until the cell reaches a state of replicative senescence. Thus, telomeres are crucial for genome integrity and cell viability and are thought to influence organismal lifespan. However, a direct correlation between telomere length and life expectancy across several species is not established. Telomere length and respective chromosomal integrity can be preserved by the activity of the enzyme telomerase, which is also involved in many other cellular functions related to tissue homeostasis and ageing. Different biochemical and genetic factors have been proven to impact telomere lengths and integrity. Likewise, it has been shown that ultra-long telomeres in inbred mouse strains arise as a result of consanguineous breeding strategies and lack of genetic refreshment. Most of the knowledge about the structural and functional biology of telomeres was obtained from observations made in somatic cell types. However, the role of telomeres in the brain is still not well understood because of the low replicative capacity of this organ, which is further restricted to certain cell populations excluding neurons. However, recent observations also suggest atypical cell cycle activity in nominally postmitotic neurons under certain stress conditions. Therefore, in this study we assessed the telomere length dynamics and telomerase activity in the ageing and diseased murine brain.

In the first part of the study, we determined the impact of ageing and different breeding strategies on the relative telomere length (RTL) in the brain of two C57BL/6 strains as a function of cell cycle activity. We show that telomere shortening eventuates in the ageing murine brain in both, a replication-dependent and also -independent manner. This observation was restricted to conditions of hermetic inbreeding and found to be more pronounced in the dividing cell moiety of the brain. Moreover, the C57BL/6 mouse colony, which was held in the absence of genetic refreshment, exhibited a substantially faster rate of age-associated telomere erosion in neural cell populations of the brain. Additionally, in contrast to the conventionally inbred strain, telomerase reverse transcriptase (TERT) activity remained unchanged with ageing in the genetically non-refreshed strain. Sustained levels of TERT activity in the hermetically inbred mice with ageing coincided with upregulated levels of RelA, a central nervous system (CNS)-prevailing subunit of the classical NF-κB cascade for which a feed-forward interaction with TERT has recently been demonstrated in a malignant environment. In contrast, reduced TERT activity level in the refreshed murine strain was

associated with a significant age-associated reduction in the expression of c-Rel, another subunit of the classical NF-κB cascade.

In the second part of the study, we analyzed the telomere length and telomerase activity in a murine model mimicking amyotrophic lateral sclerosis (ALS) pathology. ALS is a relentless neurodegenerative disorder, which is currently understood to originate from a complex, multi-facetted pathobiology implicating a precocious ageing process. Using the hSOD1^{G93A} transgenic mouse model, our data revealed unexpected telomere lengthening in the cortex and spinal cord, which paralleled disease progression and the development of severe neurological deficits. Furthermore, the different pattern of telomerase activity observed for several brain regions and the spinal cord with disease progression points to region-specific regulation of telomerase activity in the mature and diseased CNS.

In conclusion, our study provides evidence for a differential regulation of telomere length and telomerase activity in the ageing and diseased CNS. Further studies are needed to investigate the role of specific neural cell types in the telomere erosion process, in particular of post-mitotic neurons and specifically of motor neurons in an ALS-like environment, and to define a putative mechanistic link between TERT and NF-κB in the senescent brain. Likewise, it will be interesting to reveal the mechanisms responsible for the observed telomere lengthening alongside with the progression of ALS-related neurodegeneration.

ZUSAMMENFASSUNG

Telomere sind spezialisierte Nukleoprotein-Komplexe, die chromosomale Endstrukturen schützen und deren Längen Spezies-spezifisch sind. Telomere dienen als ‚mitotische Uhr', da sie sich mit jedem Zellzyklus verkürzen, bis die Zelle einen Zustand der replikativen Seneszenz erreicht. Telomere sind daher entscheidend für die Genomintegrität und die Lebensfähigkeit der Zelle. Außerdem wird angenommen, dass sie die Lebenszeit von Organismen beeinflussen, obwohl eine direkte Korrelation zwischen Telomerlänge und Lebenserwartung, über mehrere Spezies hinweg, nicht etabliert ist. Die Telomerlänge und assoziierte chromosomale Integrität können durch die Aktivität des Enzyms Telomerase erhalten werden. Die Aktivität der Telomerase ist auch an vielen anderen zellulären Funktionen beteiligt, die mit Gewebehomöostase und Alterung zusammenhängen. Verschiedene genetische und biochemische Faktoren beeinflussen die Telomerlänge und -integrität. In ähnlicher Weise wurde gezeigt, dass ultralange Telomere in Inzucht-Mausstämmen ein Resultat konsanguiner Zuchtstrategien und fehlender genetischer Auffrischung darstellen. Wichtige Erkenntnisse über die strukturelle und funktionelle Biologie der Telomere wurden über Beobachtungen an verschiedenen somatischen Zelltypen gewonnen. Die Rolle der Telomere im Gehirn ist jedoch aufgrund der geringen Replikationskapazität dieses Organs, die außerdem auf bestimmte Zellpopulationen beschränkt ist und Neurone ausschließt, noch nicht gut verstanden. Jedoch gibt es neuerdings Hinweise, dass unter bestimmten zellulären Stresskonditionen eine unkonventionelle Zellzyklusaktivierung auch in nominell postmitotischen Neuronen stattfinden kann. Daher untersuchten wir in dieser Studie die Telomerlängendynamik und die Telomeraseaktivität im alternden und erkrankten murinen Gehirn.

Im ersten Teil der Studie untersuchten wir den Einfluss von zellulärer Alterung auf die relative Telomerlängendynamik im Gehirn in Abhängigkeit von Zellzyklusaktivität, u.z. vergleichend in zwei C57BL/6-Stämmen mit unterschiedlicher Zuchtstrategie. Wir konnten zeigen, dass eine Telomerverkürzung unter hermetischen Inzuchtbedingungen im alternden murinen Gehirn sowohl in replikationsabhängiger als auch -unabhängiger Weise stattfindet. Dieser Effekt war beschränkt auf Tiere mit hermetischer Inzuchtgenetik und stärker in replikativen als in non-replikativen Zellpopulationen ausgeprägt. Darüber hinaus zeigte die C57BL/6-Kolonie, die ohne genetische Auffrischung gehalten wurde, eine Akzelleration an Alters-assoziierter Telomer-Erosion in neuralen Zellpopulationen des Gehirns. Außerdem blieb das relative TERT-Aktivitätsniveau im genetisch nicht-aufgefrischten Stamm, im

Gegensatz zum konventionellen Inzuchtstamm, im Alter unverändert. Das stabilisierte TERT-Aktivitätsniveau, das für den gealterten hermetischen Inzucht-Stamm detektiert wurde, ging mit einer hochregulierten Expression von RelA einher. RelA ist eine im zentralen Nervensystem (ZNS) vorherrschende Untereinheit der klassischen NF-κB-Kaskade, für die kürzlich in einem Tumormodell eine positive Interaktion mit TERT nachgewiesen wurde. Im Gegensatz hierzu war das reduzierte TERT-Aktivitätsniveau im genetisch aufgefrischten Stamm mit einer signifikanten Alters-assoziierten Reduktion der Expression von c-Rel, einer anderen Untereinheit der klassischen NF-κB-Kaskade, assoziiert.

Im zweiten Teil der Studie wurde die Telomerlänge und Telomeraseaktivität in einem murinen Modell, welches der Amyotrophen Lateralsklerose (ALS) ähnliche Krankheitskonditionen nachbildet, analysiert. Bei der ALS handelt es sich um eine infauste neurodegenerative Erkrankung, der eine komplexe multifaktorielle Pathobiologie zugrunde liegt, die wiederum einen vorzeitigen Alterungsprozess impliziert. Unter Nutzung des hSOD1G93A transgenen Mausmodells zeigen unsere Daten eine unerwartete Telomerverlängerung sowohl im Cortex als auch im Rückenmark, die mit dem Krankheitsverlauf und der Entwicklung schwerer neurologischer Defizite korreliert. Darüber hinaus weist das unterschiedliche Muster der Telomeraseaktivität in den verschiedenen Hirnregionen und im Rückenmark, welches im Laufe der Krankheitsprogression beobachtet wurde, auf eine regionsspezifische Regulierung der Enzymaktivität im adulten und erkrankten ZNS hin.

Zusammenfassend liefert die Studie Hinweise für eine differentielle Regulation der Telomerlänge und Telomeraseaktivität im alternden und erkrankten ZNS. Weitere Studien sind erforderlich, um die Rolle spezifischer neuraler Zelltypen im Telomer-Erosionsprozess, insbesondere von postmitotischen Neuronen und speziell von Motorneuronen, unter ALS-ähnlichen Bedingungen zu untersuchen und eine mutmaßliche mechanistische Verbindung zwischen TERT und NF-κB im seneszenten Gehirn zu konsolidieren. Ebenso wird es interessant sein, jene Mechanismen zu identifizieren, die in Assoziation mit dem Fortschreiten der ALS-ähnlichen Neurodegeneration für die beobachtete Telomerverlängerung verantwortlich sind.

1 INTRODUCTION

1.1 Telomeres

Telomeres are highly conserved, non-coding DNA elements at the terminal ends of eukaryotic chromosomes (Moyzis et al., 1988). Mammalian telomeres are basically nucleoprotein structures comprising hexameric 5'-TTAGGG-3' repeats, which are shielded by a hexa-protein complex, the Shelterin complex (Fig. 1). The extension of telomere motif repetitions ends in a long G-rich single strand overhang (Wright et al., 1997). Telomeric repeat binding factor 2 (TRF2) is crucial for binding to the duplex DNA and promotes the invasion of the 3' overhang into the duplex telomere repeat motif, which folds back to form a bigger loop structure, the T-loop. TRF1 can also interact with the duplex DNA but it is not crucial for the interaction with telomeric substrate (Griffith et al., 1999). Other proteins of the Shelterin complex are the protein protection of telomeres 1 (POT1), repressor activator protein 1 (Rap1), tripeptidyl peptidase 1 (TPP1), and TRF1-interacting nuclear factor 2 (TIN2). POT1 is important for the formation of a smaller loop structure at the 3' overhang, which is named as the D-loop, whereas Rap1, TPP1 and TIN2 interact with TRF1, TRF2 and POT1. In the absence of the Shelterin complex, the chromosomal ends are recognized as broken ends, thus leading to the activation of the DNA repair machinery (reviewed by De Lange, 2005). This suggests that presence of telomere repeat sequence at the end of each chromosome *per se* is not enough and requires interaction with Shelterin complex to protect the chromosomal ends.

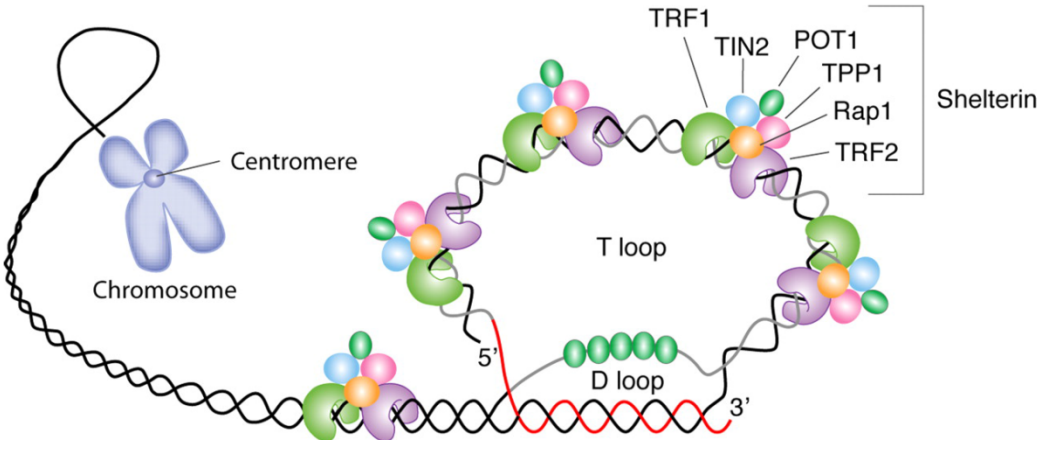

Fig. 1: Structure of telomeres. Schematic diagram representing the arrangement of proteins in the Shelterin complex at the telomere sequence, involving two loop structures, the T-loop and D-loop (Calado and Young, 2008).

The biological function of these repetitive telomere motifs was initially described by H. J. Muller in 1938 who proposed that chromosomal ends are capped by certain terminal genes and that these genes are indispensable for chromosomal stability. He termed these terminal genes "telomeres" (Muller, 1938). Muller's idea was further supported by Barbara McClintock who provided evidence that the broken chromosomal ends can fuse together, while the intact chromosomal termini are protected against such fusions (McClintock, 1941, 1942). Therefore, telomeres perform a critical function to preserve the integrity of the genomic DNA by protecting the chromosomes from end-to-end fusions (reviewed by O'sullivan and Karlseder, 2010). However, whenever a eukaryotic cell divides, these protective chromosomal ends get truncated and are not completely replicated due to the so-called 'end replication problem' of DNA polymerase enzyme. Since the DNA polymerase enzyme is a unidirectional enzyme, it cannot replicate few bases at the 3' template with each replicative cycle, which results in a loss of nucleotides at the terminal telomere repeats (Levy et al., 1992) (Fig. 2).

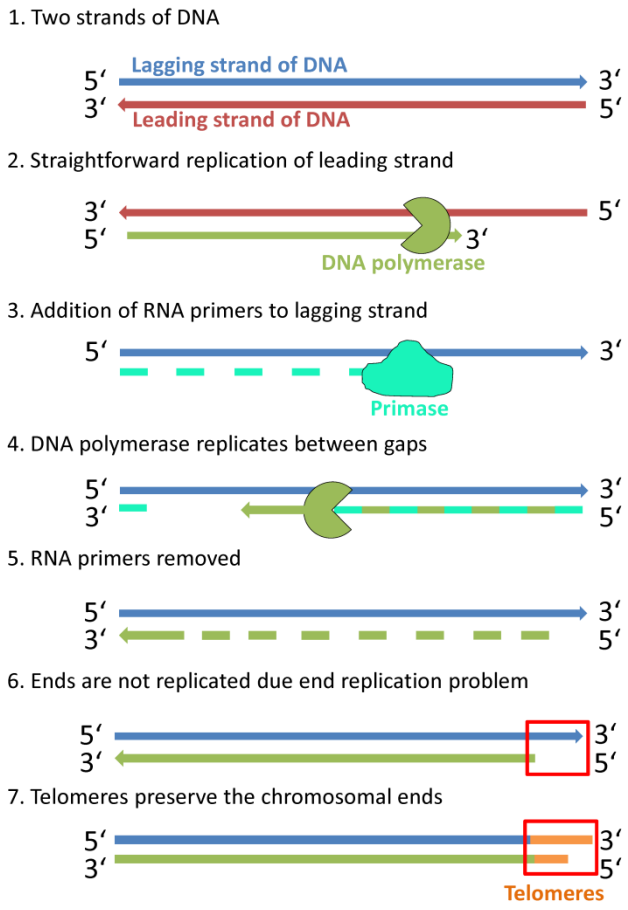

Fig. 2: End replication problem. Scheme explaining telomere shortening by the end replication problem of DNA polymerase enzyme (image idea adopted from the blog (https://blogs.scientificamerican.com/guest-blog/the-hallmarks-of-cancer-4-limitless-replicative-potential/)

Though telomeres get mainly shortened as a result of numerous rounds of cell division during lifetime, other genetic and environmental factors also contribute to the chromosomal attrition. Regular loss of telomere sequences has striking consequences with respect to species preservation and evolution since it limits cellular and organismal lifespan by inducing a state of permanent growth arrest in eukaryotic cells, called senescence (Shay and Wright, 2000). In this respect, the presence of critically short telomeres, rather than a reduction of the average telomere length, appears to be crucial for the initiation of replicative senescence and therefore, is considered as a biomarker of ageing (Hemann and Greider, 2000).

1.1.1 Replenishment of telomeres

The end replication problem of DNA polymerase is solved by a ribonucleoprotein complex, the telomerase enzyme, which is capable of *de novo* addition of $TTAGGG_{(n)}$ repeats to the chromosomal ends (Greider and Blackburn, 1987). Telomerase is a reverse transcriptase enzyme, consisting of two basic subunits in mice and humans: 1) the RNA component (TERC: telomerase RNA component), which serves as a template for the addition of telomeric repeats to the 3´ end of the chromosome; 2) a catalytic subunit (TERT: telomerase reverse transcriptase) which catalyzes the synthesis of the TTAGGG sequence (Fig. 3) (Garforth et al., 2006). Dyskerin is another protein, which interacts with TERT and is responsible for maintaining the stability and proper functioning of the enzyme (Cohen et al., 2007). In most somatic cells, telomerase is expressed at very low levels, whereas it is highly expressed in embryonic tissue (Wright et al., 1996) and reactivated in immortal tumor cells (Kim et al., 1994). Telomerase is a multitasking enzyme and performs many cellular functions other than addition of telomere repeats (reviewed by Chiodi and Mondello, 2012). Likewise, it is involved in cellular survival, proliferation, gene regulation and cellular signaling. Thereby, the catalytic subunit TERT maintains cell survival in cancer cells and also improves neural cell survival by inhibiting apoptotic pathways (Kang et al., 2004). Inhibition of TERT activity in neurons increases their vulnerability to amyloid ß-peptide-induced oxidative stress and mitochondrial damage (Zhu et al., 2000). Recently, TERT has been shown to tightly regulate NF-κB-related gene expression by forming a feed-forward loop with the RelA subunit of canonical NF-κB (Ghosh et al., 2012).

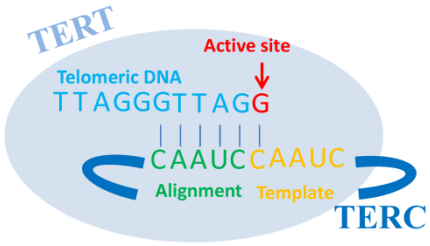

Fig. 3: Structure and function of telomerase complex. The two basic subunits TERT and TERC of the active telomerase enzyme. Image idea adopted from web link http://www.public.asu.edu/~jchen61/ChenLab/Research.html

1.1.2 Methods to determine telomere length

Several methods have been developed to measure relative or absolute telomere length within different cell types and tissues, individual chromosomes or even individual arms of chromosomes and isolated genomic DNA. Such methods vary in their sensitivity to identify the shortest telomeres, and each technique currently available has its own advantages and limitations. The very first tool established to measure telomere length is the terminal restriction fragment length analysis (TRF), which is based on classical Southern blot technique and allows determine the mean telomere length in a given genomic DNA sample from cells or tissue. TRF analysis is quite laborious and although it has certain limitations it is still considered as a gold standard and used to validate other methods for quantification of telomere lengths. Moreover, TRF requires a large amount of sample DNA and has a limited accuracy for telomere length measurement as it detects both telomeric and sub-telomeric regions. TRF analysis is also totally insensitive to detect shorter telomeres because of the low hybridization signal associated with them (Baird, 2005; Vera et al., 2012; Montpetit et al., 2014).

Other methods based on real time quantification of telomeric repeats in genomic DNA, e.g. by polymerase chain reaction (PCR) are also widely used, especially for population studies. PCR-based telomere length determination was originally developed by Cawthon in 2002, which again like TRF analysis provides the relative quantification of the mean $TTAGGG_{(n)}$ tract length in a given sample by assessing the ratio of telomere repeats copy number to the reference gene copy number (T/S ratio) (Cawthon, 2002). Unlike to the TRF analysis, this method is more rapid and robust, requires less amount of DNA and does not amplify sub-telomeric regions, which makes it more accurate and reliable (Vera et al., 2012). Later on, different adaptations were elaborated to improve this assay. Cawthon in 2009 developed a multiplex assay, in which both the telomere and single copy gene were amplified in the same

well to make the measurements more precise (Cawthon, 2009). The multiplex assay again only permitted a relative quantification of the telomere repeats and thus did not provide absolute telomere length measures. This issue was resolved by introducing a standard curve created from serial dilutions of telomere constituting oligomers and the reference gene sequence, both displaying known transcript length in terms of kilobases (O'Callaghan and Fenech, 2011). With all these adaptations, it is possible to get relative or absolute estimates of telomere lengths at the single cell level. Still, the main limitation of this method is associated with the incompetency to measure telomeres on single arms of the chromosomes and therefore the incapability to estimate the percentage of very short telomeres (Vera et al., 2012). Other methods like Flow-FISH and quantitative (Q)-FISH which rely on fluorescent *in situ* hybridization (FISH) either coupled to flow cytometry or digital imaging microscopy respectively, are highly sensitive and serve as specific tools for telomere length quantification at the level of single cells or even single chromosomes (Vera et al., 2012; Montpetit et al., 2014). FISH methods are basically carried out using a synthetic peptide nucleic acid (PNA) probe , which is highly specific to the TTAGGG repeat sequence (Vera et al., 2012). Q-FISH can be performed on metaphase spreads of cells, interphase cells as an Interphase (I) Q-FISH or high throughput (HT) Q-FISH, as well as on tissue slices to achieve an absolute quantification of telomeres of individual chromosomes, thereby allowing the detection of short telomeres (Vera et al., 2012; Aida et al., 2014). On the other hand, the Flow-FISH method provides the average measurement of telomere length and thus again compromises the analysis of individual short telomeres (Vera et al., 2012; Montpetit et al., 2014). Q-FISH methods are not very suitable for population-based studies since it is technically demanding, time consuming and laborious.

1.1.3 Factors affecting telomeres and their integrity

Telomeres are highly conserved among all the vertebrate species (reviewed by Calado and Dumitriu, 2013). However, telomere length greatly varies across different species and is genetically determined for each species (Manning et al., 2002). In humans, the telomeric repeats are 10-15 kb long (Allshire et al., 1989), while in inbred laboratory mouse strains telomeres are 5 to 10 times longer, reaching 150 kb (Kipling and Cooke, 1990) although they have much shorter lifespan than humans. This observation led to the speculation that telomere length has no correlation with organismal lifespan (Hemann and Greider, 2000). Moreover, these ultra-long telomeres in inbred mouse strains are assumed to arise from the lack of genetic exchange and excessive cross-mating within small, inbred mouse colonies (Hemann

and Greider, 2000; Manning et al., 2002). In humans, telomere length exhibits great intra- and inter-individual variations and is affected by various factors including genetic and environmental variables (Vasa-Nicotera et al., 2005; Dlouha et al., 2014). In a recent study, Dlouha and colleagues analyzed the relative telomere length in several tissues including brain and peripheral blood leukocytes from human subjects with ages ranging from 29 weeks postnatally to 88 years. They found a great degree of intra-individual variability in the relative telomere length (RTL) of different tissues (Dlouha et al., 2014). Likewise, in mice the telomere length of different tissues was also found to be highly variable within the same organism (Prowse and Greider, 1995; Coviello-McLaughlin and Prowse, 1997). The differences in telomere lengths of different tissues within the same individual argue for a tissue-specific regulation of telomere lengths (Coviello-McLaughlin and Prowse, 1997). Likewise, the reported heritability factor for the telomere length in leucocytes ranged between 36-82%, which shows that telomere lengths are moderately to strongly heritable (Vasa-Nicotera et al., 2005; Andrew et al., 2006). The genetic origin and the mode of telomere length inheritance is still a topic of debate. Some studies reported a maternal origin and X-linked inheritance, in terms of stronger mother-offspring correlation (Nawrot et al., 2004; Broer et al., 2013). On the contrary, some earlier studies showed a significant link with autosomal inheritance, thereby associating the telomere length with chromosome 12 and 14 (Vasa-Nicotera et al., 2005; Andrew et al., 2006). Other studies supported a paternal mode of inheritance and presented a strong correlation between father-offspring telomere length (Nordfjäll et al., 2005; Njajou et al., 2007; Nordfjäll et al., 2010). Paternal contribution to telomere length inheritance was also indicated by strong correlation between grandparents-grandchild pairs (Nordfjäll et al., 2010). Telomere lengths in human blood cells have also been demonstrated to be positively correlated with the paternal age at the time of the offspring's birth (Unryn et al., 2005; De Meyer et al., 2007; Broer et al., 2013).

Telomere lengths greatly vary between the two genders, with females displaying longer telomeres as compared with men (Nawrot et al., 2004; Mayer et al., 2006; Gardner et al., 2014; Dalgård et al., 2015). In addition, the age-associated telomere attrition rate is faster in males as compared with females, which ranged between 24-25 and 16-19 bp per year for men and women, respectively (Nawrot et al., 2004; Nordfjäll et al., 2005; Möller et al., 2009). The longer telomeres in females may be at least partly attributed to the estrogen-mediated transcriptional regulation and activation of TERT (Misiti et al., 2000). A recent study in a rat model for menopause has also shown anti-ageing effects of exogenous estrogen via TERT activation (Cen et al., 2015). Moreover, females may also be protected against reactive

oxygen species (ROS)-induced telomere damage due to the scavenging effects of estrogen (reviewed by Aviv, 2002).

In addition to the above-mentioned hereditary and gender-related effects, telomere length dynamics in humans are also shaped by an individual's life style and many environmental factors. Smoking causes oxidative damage to DNA and hence increases the rate of telomere shortening (Song et al., 2010). Thereby, the rate of telomere shortening seems directly proportional to the amount of cigarettes consumed per day (Valdes et al., 2005; Song et al., 2010). Likewise, obesity also leads to an elevated level of ROS (reviewed by Marseglia et al., 2014) and thus might negatively influence telomere stability. Similarly, Valdes and colleagues showed that white blood cells from obese women displayed shorter telomeres as compared to non-obese ones (Valdes et al., 2005). In contrast, dietary intake of antioxidants like omega-3 fatty acids (Farzaneh-Far et al., 2010), vitamin C and E (Xu et al., 2009) and moderate levels of physical exercise (Ludlow et al., 2008) preserve the chromosomal ends.

1.1.4 Replicative senescence and telomere integrity

Cultured diploid cells have a finite replicative capacity and after multiple rounds of mitotic cell divisions, the cells reach a limit where they cannot divide anymore. This limit, where the mitotic activity of cells ceases and senescence is induced, is called "Hayflick limit" (Hayflick, 1965). The underlying mechanism for the proposed Hayflick limit can be explained by the telomere hypothesis (Harley et al., 1992). The recurrent replication cycles in cells with low or no telomerase activity inevitably leads to the development of critically short and dysfunctional telomeres. Moreover, the shortening of chromosomal extremities with each round of cell replication to a certain checkpoint results in replicative arrest induced by DNA damage responses (Fumagalli et al., 2012). Although telomere shortening leads to replicative arrest, these senescent cells remain alive and perform their metabolic functions (Harley et al., 1992). As aforementioned, telomere shortening is also promoted by oxidative stress. The Guanine-rich sequence of the telomere repeats increases their susceptibility and makes them vulnerable towards ROS, which results in a persistent damage and attrition of the telomere tracts (Kawanishi and Oikawa, 2004; Coluzzi et al., 2014). Moreover, short and dysfunctional telomeres also arise due to frailty in the telomere-associated proteins such as the Shelterin complex and the telomerase enzyme (O'sullivan and Karlseder, 2010).

In conclusion, the capping of the chromosomal ends by telomeres is crucial for chromosomal stability and genome integrity and once the telomeres are shortened and become

dysfunctional, it can lead to the development of ageing-associated degenerative diseases, cancer and rare inherited disorders (Wu et al., 2003; Vulliamy et al., 2006; Willeit et al., 2010).

1.2 The ageing and diseased brain

The brain is highly vulnerable to pathological ageing as indicated by the strong, age-related increase in the incidence of neurodegenerative disorders. In comparison to other organs, brain tissue shows a high susceptibility towards oxidative stress, caused by high levels of ROS production, which arise from the high metabolic rate and oxygen consumption of this organ. ROS along with the trace elements copper and iron modify biological molecules like lipids, proteins and nucleic acids including the mitochondrial and telomeric DNA, which can result in cellular damage (Floyd and Carney, 1992; Hollensworth et al., 2000; Jeng et al., 2013; Coluzzi et al., 2014). There is substantial evidence pointing to protein damage by ROS, including breakdown of important metabolic enzymes essential for physiological brain function (Smith et al., 1991). The prevalence of non-dividing neurons, which cannot compensate DNA damage, e.g. by replication-dependent homologous recombination, leads to further accumulation of cellular damage, entailing inflammation, enhanced astrocytic reactivity, calcium dysregulation and mitochondrial dysfunction, factors which ultimately will impair normal brain function with ageing (reviewed by Sibille, 2013).

Changes in the expression levels of specific sets of genes, related to certain cell types and biological processes in the ageing brain, have been reported in many studies. Gene expression in the brain is also modulated by age-associated DNA damage, mediated, e.g., by increased oxidative stress. Transcriptional profiling of human frontal cortical tissue from individual subjects with ages ranging from 26 to 106 years displayed reduction in the expression levels of genes involved in synaptic and mitochondrial functions, transport of proteins, cellular stress management, DNA repair and antioxidant mechanisms at ages beyond 40 years (Lu et al., 2004). Moreover, these genes down-regulated with ageing displayed striking DNA damage in their promotor regions, which was partially mediated by oxidative stress as assessed by *in vitro* studies using human cortical neurons (Lu et al., 2004). In contrast, glial genes involved in inflammatory pathways and cellular defense mechanisms often appear up-regulated (Erraji-Benchekroun et al., 2005). In conclusion, such studies suggest that lack of genome integrity, including telomeric DNA alterations, is one of the hallmarks of brain ageing.

1.2.1 Telomere length dynamics in the ageing and diseased brain

Telomere attrition has been strongly implicated in the senescent-related ageing process of somatic cells. Therefore, progressive telomere shortening up to a critical length is assumed to drive the cell into replicative senescence, and has been regarded as a biomarker for ageing. In spite of increasing evidence concerning the role of telomere integrity in genome stability in general and in the healthy ageing process of organs with high cell turnover rate, the importance of telomere length dynamics for the ageing process itself and development of age-related CNS pathologies remains largely unaddressed. Accordingly, there are only few reports available in this context (Takubo et al., 2002; Takubo et al., 2010).

The fact that the terminally differentiated brain predominantly consists of cell types that are thought to have only moderate (glial) or even no (neuronal) cell cycle activity could partially explain the lack of knowledge currently available on the contribution of telomeres to neurosenescence. According to the prevailing notion, glial cells are the only cell types in the brain retaining a lifelong moderate proliferative potential, whereas neurons are believed to be devoid of cell cycle activity as soon as they become terminally differentiated (Nakamura et al., 2007). However, the two groups of K. Herrup and T. Arendt have recently provided convincing evidence for a continuous and active suppression of the cell cycle machinery in quiescent neurons (Herrup and Yang, 2007; Arendt, 2012). Loss of control on cell cycle activity in neurons might end up in an aberrant cell cycle re-entry and related neuronal apoptosis-like death (Arendt and Brückner, 2007; Zhang and Herrup, 2011). Moreover, up to 10-20% of the quiescent cortical neurons in the healthy ageing brain and in brains from patients with Alzheimer's disease show an altered DNA content, which thus may serve as a potential marker for cell cycle re-entry (Mosch et al., 2007; Fischer et al., 2012). Furthermore, such an atypical cell cycle activity and concomitant increase in DNA content have also been linked to mediate development of Alzheimer dementia (Arendt and Brückner, 2007; McShea et al., 2007; Arendt, 2012) and other neurodegenerative disorders like Parkinson's disease (Höglinger et al., 2007) and amyotrophic lateral sclerosis (Ranganathan and Bowser, 2003). Aberrant, unscheduled cell cycle activity in neurons has been shown to remain abortive in most cases and thus is distinct from a true cell division cycle. The impact of such an abortive cell cycle activity on telomere length is still uninvestigated.

In spite of the common notion that brain neural cells are mostly postmitotic and therefore do not undergo any telomere attrition, there are few studies which report about telomere instability in the mammalian brain. In an early study, Coviello-McLaughlin and Prowse

(1995) described a remarkable telomere length reduction in the brain of mice. Similarly, Flanary and Streit also demonstrated telomere shortening in the cortex and cerebellum of the rat brain up to the age of 5 months, with cortex harboring the shortest telomeres (Flanary and Streit, 2003). Microglia, being capable of mitotic cell division, were thought to be the only putative causal agent responsible for the reduction in average telomere lengths (Flanary and Streit, 2003). However, their findings are contradictory to a contemporary report showing that telomere length in male and female rat brain tissue remains unchanged up to an age of 15 months, whereas telomere length in more replicative tissues such as pancreas, liver, lungs and kidneys was found to be reduced at this age as compared to the neonates (21 days) and young rats (3 months) (Cherif et al., 2003). Moreover, at 15 months of age, no increment was observed in the percentage of very short telomeres in brain tissue, though the moiety of short telomeres was augmented in other tissues (Cherif et al., 2003). Studies on brain samples from human subjects with ages ranging from 0-104 years also suggested that cerebral cortex, like non-replicative myocardium, preserves the telomeres during chronological ageing (Takubo et al., 2002; Takubo et al., 2010). Interestingly, telomeres from human cerebral white and gray matter showed marginal decline in lengths until the age of 70-79 years, whereas specimens from later age categories ranging from 80 to 100 years presented longer telomeres, with centenarians displaying the longest telomeres. Such observations suggested that individuals with longer life span may retain constitutively longer telomeres from their birth onwards (Nakamura et al., 2007). Additionally, under physiological conditions, gray matter comprising in particular neuronal nuclei devoid of cell cycle activity presented significantly longer telomeres than the white matter, which encompasses oligodendrocytes with preserved proliferative capability (Nakamura et al., 2007). Strikingly, centenarians with such prevailing longer telomeres presented lower rate of cancer incidence (Nakamura et al., 2007). The conclusion that individuals with longer life span might retain constitutively longer telomeres from their birth is noteworthy and requires further investigations, including tissues that retain telomere lengths independently of age.

Changes in both telomere length and telomerase expression and activity have been associated with many neurodegenerative and psychiatric disorders. For instance, reduced levels of telomerase activity and high oxidative stress accompanied by increased telomere attrition are significantly linked to acute and chronic psychological stress (Epel et al., 2004). Moreover, telomere lengths in blood samples of patients suffering from various neurodegenerative disorders like Alzheimer disease (AD) (Panossian et al., 2003; Thomas et al., 2008; Kota et al., 2014) and psychiatric disorders like schizophrenia were significantly shorter than those of

healthy controls (Kao et al., 2008). Lukens and colleagues found a direct correlation between the telomere lengths of blood leucocytes and cerebellar tissue in AD patients (Lukens et al., 2009). However, in the intra-tissue comparison, telomere length in cerebellum from AD patients remained unaltered as compared to respective controls and thus appeared not to be involved in the disease-associated telomere shortening process. Likewise, no telomere attrition as compared to healthy controls was observed, e.g., in cerebellar gray matter of patients with bipolar disorders and schizophrenia (Zhang et al., 2010) and in cortical and cerebellar gray matter of patients suffering from major depressive disorders (MDD) (Zhang et al., 2010; Verhoeven et al., 2014). Thus, telomere shortening in blood samples of patients with neurodegenerative and psychiatric disorders are likely to be unrelated to brain telomere length and might not serve as an indicator of telomere shortening in this organ (Lukens et al., 2009; Zhang et al., 2010). In another study using Q-FISH, a significant decrement in telomere length of hippocampal neurons from AD patients was observed as compared with the controls (Franco et al., 2006). In contrast, Thomas and colleagues found a significant AD-associated increment in telomere length of up to 49% using a polymerase chain reaction-based method (Thomas et al., 2008). The contradictory results described for telomere length quantification in AD patients might arise from the high technical variability found across the studies. This issue therefore requires further analysis.

1.2.2 Telomeres and Amyotrophic lateral sclerosis (ALS)

Amyotrophic lateral sclerosis (ALS) is the most frequent age-associated neurodegenerative disorders of the motor system, characterized by the irreversible and progressive loss of motor neurons located in the cerebral cortex, brain stem and along the ventral horns of the spinal cord (Kiernan et al., 2011; Brettschneider et al., 2013). The disease usually manifests with the development of paralyses, involving skeletal and respiratory muscles (reviewed by D'Amico et al., 2013) starting at an average age of 65 years (Turner et al., 2012), with peak incidences being found between 50 and 75 years of age (van Es et al., 2017). ALS is characterized by a rapid clinical progression, leading to the demise of the patients within 20-48 months after the onset of symptoms (Paulukonis et al., 2015). The underlying cellular, biochemical and molecular pathomechanisms are numerous and complex, and incompletely understood. However, many studies have shown the association between oxidative stress levels and malfunction of cellular processes leading to motor neuron degeneration in ALS (reviewed by D'Amico et al., 2013). Likewise, an increment in the protein nitration at tyrosine residues, which converts it to 3-nitrotyrosine and serves as a biomarker for protein translational

modification caused by oxidative stress, was found in both sporadic and familial ALS patients carrying SOD1 mutations (Beal et al., 1997). Moreover, a study carried out in hSOD1^{G93A} transgenic animals overexpressing the mutant human SOD1 gene showed an increased oxidative damage to proteins isolated from the spinal cord tissue (Poon et al., 2005). Therefore, ALS pathomechanisms might also involve ROS-mediated telomere attrition and thus add up to the neurodegenerative process, though this has not been elucidated yet. At present, there are few studies, which show a link between telomeres, telomerase enzyme and ALS disease entities. ALS patients displayed shorter telomere lengths in their blood leucocytes as compared with respective healthy controls, and showed reduced levels of TERT expression, as assessed in leucocytes and postmortem spinal cord tissue (De Felice et al., 2014). Recently, shorter telomere length arising from the absence of telomerase activity in double transgenic mTerc$^{-/-}$;SOD1^{G93A} mice, a mouse model for ALS-like pathology with short telomeres, was associated with earlier disease onset and reduced life expectancy (Linkus et al., 2016). Interestingly, the induction of telomerase enzyme in hSOD1^{G93A} mutant mice by the pharmacological compound AGS-499 was shown to delay ALS onset and progression by improving the survival of spinal motor neurons by up to 60% (Eitan et al., 2012). In spite of these findings, region-specific changes in telomere length and telomerase activity and the possible influence on ALS disease manifestation are not yet clear. In particular, a study specifically assessing telomere length at early and late disease stages does not yet exist.

2 AIMS OF THE STUDY

Several studies have shown that changes in telomere length contribute to DNA damage response, chromosomal instability, cellular senescence and apoptosis, and that they correlate with disease- and ageing-associated pathologies (Tümpel and Rudolph, 2012). One open question is whether telomeres in postmitotic cells of the CNS, in particular neurons, are also subjected to age-related telomere attrition. This issue is highly relevant in order to define factors involved in the increased prevalence of neurodegenerative disorders in the human ageing population (Rolyan et al., 2011).

Telomere length is tightly regulated by the enzyme telomerase, which consists of a reverse transcriptase (TERT) and a RNA component (TERC). The telomerase enzyme also performs many non-canonical functions and is involved in several regulatory pathways for cell survival, gene transcription, cell signaling and cellular restitution mechanisms (reviewed by Chiodi and Mondello, 2012). At the molecular level, telomerase regulates NF-κB-dependent transcription and, reciprocally, NF-κB interacts with TERT via a feed forward loop (Ghosh et al., 2012). In addition, the neuroprotective role of telomerase has been evidenced by the induction of telomerase enzyme in a murine model of ALS, showing improved neuronal survival and delayed disease onset and progression (Eitan et al., 2012). The importance of telomere-dependent and telomere-independent telomerase functions and TERT transcriptional regulation in the ageing CNS are still undefined. Moreover, though telomere integrity and telomerase activity have been linked to ALS-like pathology, region-specific telomere length dynamics and telomerase activity in brain and spinal cord, and their possible contribution to the disease pathogenesis and progression are not yet been fully explored. Therefore, our project aimed to elucidate:

i. Age-associated telomere length dynamics in cortical neural cells of the mouse brain
ii. Telomere length alterations in the CNS as a function of disease progression in the murine hSOD1^{G93A} strain, an experimental model of ALS pathology
iii. Changes in telomerase activity in different brain regions in association with CNS ageing and ALS-like pathology
iv. A possible role of NF-κB subunits in telomerase function in the aged and diseased brain

In particular, we wanted to determine:

- whether telomere length in the ageing brain is influenced in a cell cycle-dependent and -independent manner
- whether inbreeding, which is known to be a strong genetic factor that influences telomere length in mice, also has an impact on telomeres in the ageing brain. For this, studies were performed in a standard C57BL/6 strain and compared with a derivative sub-strain devoid of genetic refreshment for at least 90 generations
- whether telomere length in the CNS of the hSOD1^{G93A} strain is altered with disease progression
- whether TERT activity is influenced by CNS ageing and during the course of ALS-related disease progression, the latter being assumed to underlie a precocious ageing process
- whether the activity of NF-κB, as a master regulator of age-related genetic reprogramming, correlates with TERT activity and contributes to influence telomere length in the geriatric brain

3 MATERIALS AND METHODS

3.1 Animals

To study the impact of physiological ageing on brain telomere length dynamics and telomerase activity, male C57BL/6 mice at an age of 3 months and 24-28 months from two distinct colonies were used. One colony of the C57BL/6 mice, named here as B6Je, were kept under hermetic inbreeding conditions without any genetic refreshment for at least 90 generations; the second colony, denoted here as B6J, was cross-bred under regular genetic refreshment for at least 50 generations. Likewise, mutant hSOD1 mice (B6.Cg-Tg (SOD1*G93A)1GurJ, denoted as hSOD1^{G93A}) were chosen to evaluate the influence of ALS-like neurodegenerative pathology on relative telomere lengths and telomerase activity. Three different stages of disease progression were assessed i.e., asymptomatic (7 weeks), pre-symptomatic (16 -17 weeks) and symptomatic stages (19 -21 weeks, clinical score 1 or 2; Tab. 1). Clinical scoring of mutant mice was performed daily in the animal facility at the Jena University Hospital, where the animals were bred and housed. Additionally, clinical symptoms were finally analyzed immediately before sacrificing the mice. For both, aged and ALS mutant animals, subcategories according to the ages of the animals were further specified for each set of experiment. All animals were housed in specific pathogen-free (SPF) conditions at the Institute of Laboratory Animal Care and Welfare (IVuT) at the Jena University Hospital under controlled conditions for humidity (70-80%), temperature (22-24°C) and light/dark cycle (14 hour day / 10 hour night cycle) with food and water *ad libitum*. All animal procedures were performed in accordance with the ARRIVE guidelines and conformed to current EU regulations on the Protection of Animals Act with approval of the regional animal welfare authorities (TVA number: 02-046/14).

3.1.1 Clinical scoring of hSOD1^{G93A} mutant mice

Mutant hSOD1^{G93A} mice were scored for clinical manifestation of different stages of the ALS-like disease according to Tab. 1. Mice with clinical score 1 or 2 were assigned to the symptomatic group of hSOD1^{G93A} mutant mice.

3.2 Trans-cardial perfusion of mice

Animals were deeply anesthetized with volatile isofluran / isofluran CP and immediately transcardially perfused with 25 ml of ice-cold sterile PBS/TBS (5 ml/min) for 5 min prior to the tissue extraction in order to remove blood contaminations and avoid artifacts in the

downstream applications. Briefly, mice were put in a sealed glass jar containing tissue paper soaked in isofluran until the animal was deeply anesthetized and no longer reactive to painful stimuli, but with preserved residual cardiac circulation. Fore and hind limbs were fixed into a plastic tray with the help of tape. For continuous provision of anesthesia, a 15 ml falcon tube with a small isofluran-soaked pad was inverted on the nose of the pre-anesthetized animal. The animal was euthanized by diaphragm perforation. The abdomen was cut open with a sharp scissor (FST GmbH, Essen, Germany) and the heart was exposed. A small blade cut was made in the apex of the left ventricle and cannulated with a knob cannula. The cannula was arrested in the left ventricle using a fastener. Afterwards, a small cut was made into the right atrium to let venous blood pouring out. Then, the animal was perfused until the perfusion buffer was of clear aspect. The procedure was followed by decapitation and brain extraction for further downstream applications.

Tab. 1: Clinical scoring of hSOD1^{G93A} mutant mice.

Clinical Score	Clinical Manifestation
0	During tail suspension, mice extend the hind limbs completely away from the lateral midline and are able to hold this for 2 sec (repeated 2-3 times)
1	Signs of weakness during tail suspension like complete / incomplete failure to extend the hind limbs away from the lateral midline or tremor of legs
2	Unable to walk normally and drag part of their feet or curl the toes few times during locomotion
3	Signs of rigid paralysis as the mice are unable to do any forward motion or to move their joints
4	Mice fail completely to get into upright position

3.3 Development of neural cell isolation protocol

Though protocols for neural cell isolation from embryonic and early postnatal murine brain are well established, procedures available for cell purification from mature CNS are poorly elaborated, and require basic validation for reproducibility, efficiency and specificity. Therefore, in order to evaluate the telomere length dynamics from young (3 months) and aged (25-27 months) murine cortical tissue, a working protocol had to be established and validated, starting with trial and optimization of several steps already described in the literature.

3.3.1 Isolation protocol described by Guez-Barber et al. (2012)

As first practical guideline, we applied a protocol described by Guez-Barber and colleagues in 2012, developed for neural cell extraction from adult wild type rat brains using enzymatic digestion followed by a purification via a percoll gradient and subsequent FACS (Guez-Barber et al., 2012). Accordingly, whole cortical tissue was isolated from 3 months old male C57BL/6 mice, incubated with accutase enzyme (Millipore, Darmstadt, Germany) for 30 min and triturated during the incubation. All steps were carried out at 4°C as recommended by the author. However, the tissue was very difficult to triturate due to the incomplete digestion by the enzyme. After trituration, cells were purified with a percoll gradient according to the author's description, and purification rate and cellular yield were assessed by immuno-staining with the neuronal marker NeuN (mouse monoclonal antibody, clone A60; 1:250; Millipore, Darmstadt, Germany). Cell nuclei were counter-stained with DAPI solution and examined by fluorescence microscopy. The preparation showed a lot of debris and stained nuclei in big tissue clumps, which confirmed incomplete tissue digestion (Fig. 4A).

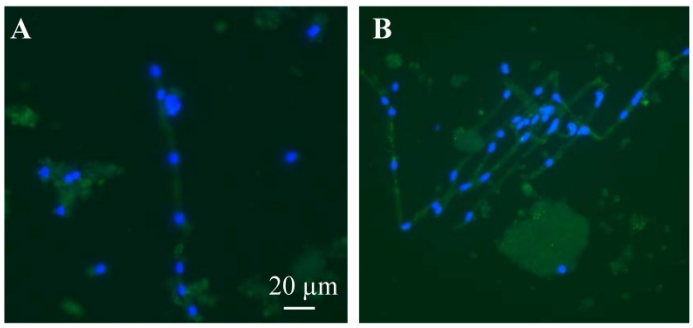

Fig. 4: Representative photomicrographs showing the development of cortical cell isolation protocol used on 3 months old C57BL/6 male mice. Isolated cells were immuno-stained with the neuronal marker NeuN (green) and counter-stained with the nuclear marker DAPI (blue). (A) Neural cell isolates following application of an accutase-based protocol described by Guez-Barber (2011). (B) Isolated cortical cells after application of several modifications to the same protocol as described in the text. N = 3, objective = 40 x magnification, scale bar = 20 µm.

Several approaches were evaluated to improve the accutase enzyme-based protocol. First, instead of using both hemispheres of a brain, only a small piece of cortical tissue (30 mg) was digested at different incubation times (20, 30 and 40 min at 4°C). Next, DNAse was used to avoid cellular clumping through nucleic acid elimination from the damaged cells. Furthermore, an OptiPrep instead of percoll gradient (Axis Shield Diagnostics, Dundee, Scotland) was implemented to improve cell isolation and purification, as described by Brewer and Torricelli (Brewer and Torricelli, 2007). None of these approaches improved the cell isolation protocol substantially (Fig. 4B). Since it seemed that the problem was at the tissue

dissociation step, and accutase enzyme was unable to digest the tissue appropriately, a comparative experiment was included by incubating the tissue with accutase or papain (Sigma-Aldrich Chemie GmbH, Taufkirchen, Germany) enzymes at 4°C and 37°C. Nuclear staining with DAPI revealed that digestion with accutase resulted in higher nuclear yield, but at expense of nuclear integrity that appeared fragmented in many cases. In contrast, papain enzyme digestion led to the isolation of fewer, but morphologically intact nuclei.

3.3.2 Isolation protocol according to Brewer and Torricelli (2007)

In order to further improve the neural cell isolation protocol, the procedure published by Brewer and Torricelli was applied, with some modifications (Brewer and Torricelli, 2007). In a first trial, the tissue was incubated with papain at a concentration of 2 mg/ml (Sigma Aldrich, Taufkirchen, Germany) at different temperatures and for different time periods under slight agitation. For further optimization, 0.1% ovomucoid (Sigma-Aldrich Chemie GmbH, Taufkirchen, Germany) was used as papain inhibitor to stop the digestion process. Moreover, DNAse (Sigma-Aldrich, Taufkirchen, Germany) was added to all the solutions in order to avoid the formation of DNA clumps. However, the papain enzyme used did not work very well as tissue digestion was still incomplete. Therefore, it was replaced by the same enzyme from a different provider as recommended by the authors in their original protocol (Brewer and Torricelli, 2007). Additionally, D-Trehalose was added to all the solutions applied during tissue digestion and disaggregation. According to the study by Saxena et al., the use of this sugar compound improves the yield of viable cells by 10-folds (Saxena et al., 2012). The Worthington alternative papain enzyme was tried at different concentrations ranging from 0.5 mg/ml to 2 mg/ml and at different incubation times. High enzyme concentrations led to increased cell damage and also to higher number of cellular clumps due to DNA released from broken cells.

Incubation with papain at 1 mg/ml and 37 °C for 30 min was finally selected as best working parameters for cortical neural cell isolation. The modified protocol yielded approximately 8 x 10^5 to 1.5 x 10^6 cells, starting from 30-40 mg of cortical murine tissue.

3.3.3 Development of an improved and reproducible cell isolation protocol

Based on the previous experiences, focus was next set on the tissue digestion step to further improve cellular integrity, purity and yield. Instead of incubating the cortical tissue with the papain solution at 37°C in a water bath, cortical tissue was now incubated with enzyme solution in a glass beaker on a hot plate. Prior to papain treatment, the tissue was first digested

with collagenase IA at 37°C to remove the collagen matrix. Then, the tissue was further dissociated by sequential treatment with different papain concentrations starting with 2 mg/ml, followed by 1 mg/ml, under very slight rotation. This gentle treatment ensured the loosening of the tissue layers and release of the cells with minimal harm to the cells. The tissue dissociation was further improved by triturating the tissue at intervals. DNAse and D-trehalose were used in all the solutions during the process. D-trehalose was added to improve the cell viability and membrane integrity by stabilizing the cells under stress (Saxena et al., 2012). The developed protocol worked equally well for young (3 months) and aged (24-30 months) mice from both C57BL/6 colonies.

3.4 Isolation of cortical neural cells with newly developed protocol

A calcium-free Hibernate A medium (BrainBits LLC, Springfield, IL, U.S.A) was made as shown in Tab. 2. Briefly, calcium-free Hibernate A medium was supplemented with 0.5 mM GlutaMax (Invitrogen, Darmstadt, Germany), 132 mM D-trehalose (Sigma-Aldrich, Taufkirchen, Germany) and 310 IU/ml of DNAse I (Sigma-Aldrich, Taufkirchen, Germany). Both enzymes, collagenase IA (Sigma-Aldrich, Taufkirchen, Germany) and papain (Cell Systems, Troisdorf, Germany,) as well as the papain inhibitor ovomucoid (Sigma-Aldrich, Taufkirchen, Germany) were diluted in the above mentioned Hibernate A working solution to the concentrations specified below. Hibernate A without calcium and magnesium (BrainBits, Springfield, LLC) was used for maximum enzyme activity and tissue digestion (Brewer and Torricelli, 2007).

The mouse head was placed in a 60 mm petri plate (VWR, Darmstadt, Germany) and arrested on an ice block. The skin around the skull was removed using sharp small scissors (FST GmbH, Essen, Germany). The skull bone was removed with the help of blunt forceps (FST GmbH, Essen, Germany) and the brain was exposed. The exposed tissue was slightly damped with 0.9% saline solution (Fresenius Kabi, Bad Homburg, Germany). The lepto-meninges were eliminated and bi-hemispherical cortices were exposed. Both cortices were made free of hippocampi and white matter regions and immediately processed for neural cell isolation.

To measure telomere length dynamics in murine brain cortex, cells were isolated according to the method delineated in the flow diagram given in Fig. 5. Briefly, freshly isolated bi-hemispherical cerebral cortices from young and aged murine brains were incubated with 3.0 ml of collagenase IA (1 mg/ml) for 30 min at 37°C under gentle agitation. In the meantime, papain was activated at 37°C for 30 min. Following incubation in collagenase IA for 30 min,

cortical tissue was transferred to a small glass tube containing 3 ml of papain solution (2 mg/ml). The solution was stirred with a magnetic stirrer and heated on a hot plate to attain a temperature of 37°C under slow agitation (~100 rpm) for 15 min to break cellular connections. To promote the release of the loosened cells from the softened tissue, cortices were treated sequentially with 3 ml of papain solution (1 mg/ml) under the same conditions (Fig. 4). Tissue was triturated 7-10 times with a smoothened fire-polished Pasteur pipette with 0.7-0.8 mm of tip diameter to enhance the mechanical dissociation. During the first round of trituration, the enzyme solution was gently streamed against the tissue using a Pasteur pipette in order to break it into smaller pieces, which were then further triturated. After trituration, the solution became turbid and thick. Remaining tissue pieces were allowed to settle down. The supernatant was removed and put on ice in a new 15 ml falcon tube.

Tab. 2: Solutions used for neural cell isolation.

Solutions	Ingredients
1 M trehalose stock solution	3.78 g D-trehalose, final volume up to 10 ml with distilled water
DNAse I stock solution	15.5 mg (~31,000 U) DNAse I,4 ml sterile Hibernate A minus calcium medium, aliquoted and stored at -20°C
1% ovomucoid stock solution	400 mg BSA, 400 mg ovomucoid in 25 ml sterile Hibernate A minus Ccalcium medium, adjust pH adjusted to 7.4, final volume up to 40 ml with Hibernate A minus calcium medium, aliquoted and stored at -20°C
Hibernate A-Ca working solution	25 µl Glutamax solution, 1.32 ml of 1 M trehalose stock solution, 400 µl of DNAse I stock solution, final volume up to 10 ml with Hibernate A minus calcium medium
0.1% ovomucoid working solution	1.32 ml of 1 M trehalose stock solution, 400 µl of DNAse I stock solution, 1 ml of ovomucoid stock solution, final volume up to 10 ml with Hibernate A minus calcium medium
PBS with trehalose	1.32 ml of 1 M trehalose stock solution, final volume up to 10 ml with PBS

Enzyme action was blocked afterwards with 0.1% ovomucoid. Leftovers of tissue pieces were again slightly agitated and mechanically dissociated in the pre-used papain solution (2 mg/ml) for 5-10 min until tissue dissociation was complete. Tissue lysis was blocked with equal volume of 0.1% ovomucoid. Following this step, tissue lysate was successively passed through 100 µm and 40 µm cell strainers and centrifuged at 500 x g for 5 min. The supernatant was removed and the pellet was re-suspended in 1 ml PBS containing 132 mM D-trehalose. The final neural cell suspension was incubated on ice for 15 min to stabilize the enzymatically and mechanically isolated cells. Cells were counted in a Neubauer counting chamber and immediately used for Flow-FISH, or immunohistochemistry for neural cell type identification.

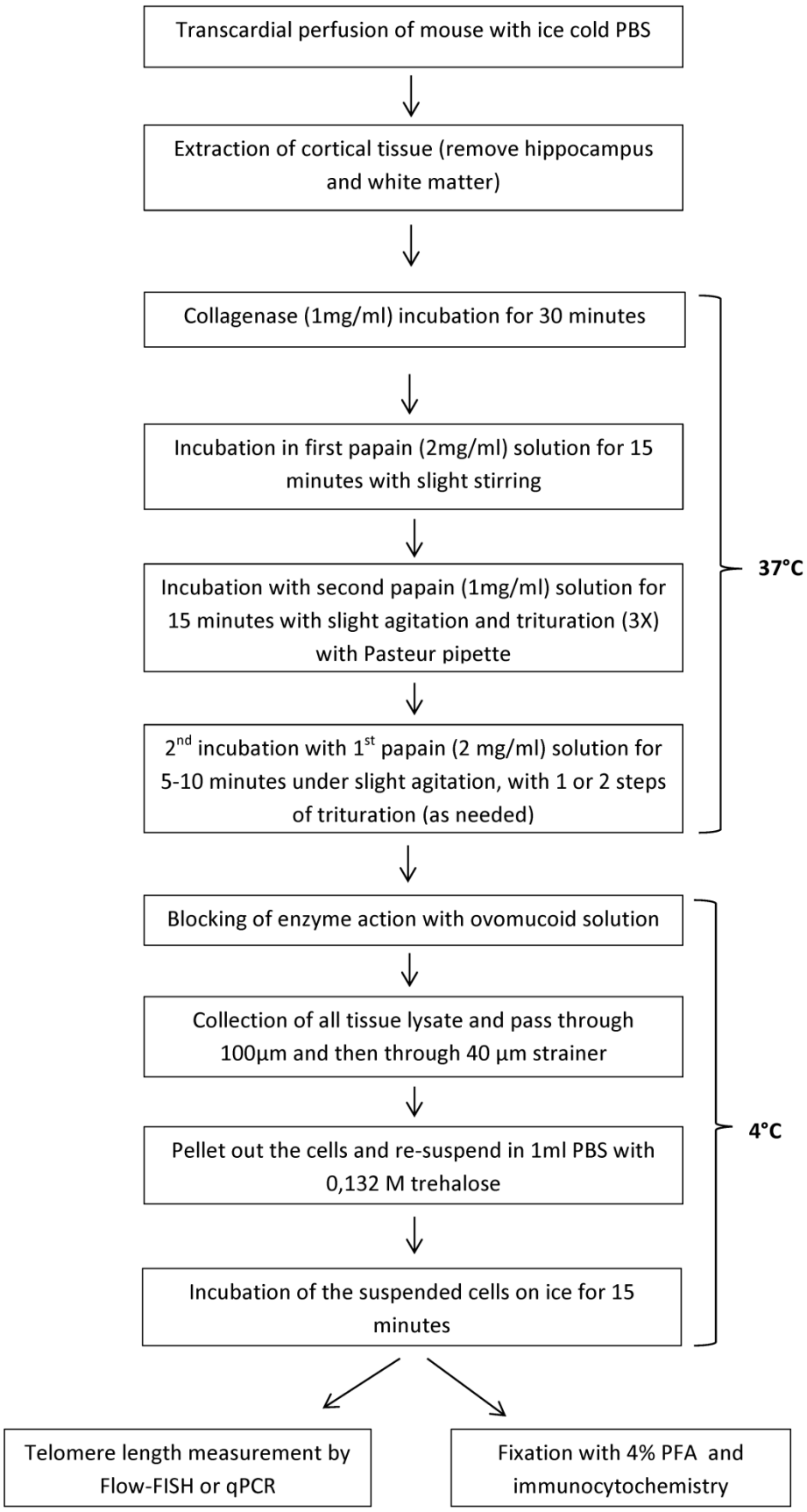

Fig. 5: Flow diagram of the cortical neural cell isolation protocol. A schematic presentation of the steps involved in neural cell isolation from murine brain cortex.

3.5 Immunocytochemistry and microscopy

To identify and characterize different cortical neural cell types isolated from young (3 months) and aged (27 months) mice, immunocytochemistry was performed for different cellular markers using primary and secondary antibodies listed in Tab. 3. The cells were fixed with 2% PFA for 20 min at room temperature (RT) and washed twice with 1x PBS. Fixation was followed by incubation with 10% normal donkey serum for 3 hours at RT to block the non-specific binding sites. Neural cells were then incubated with rabbit anti-ßIII-tubulin (1:250; Sigma, Taufkirchen, Germany) to mark neurons, with rabbit anti-CA-II (1:100; H-70, Santa Cruz, Heidelberg, Germany) to identify oligodendrocytes, with rabbit anti-Iba1 (1:250, Wako, Neuss, Germany) to discriminate microglia and with rabbit anti-S100ß to label astrocytes (1:1000; Synaptic Systems GmbH, Göttingen, Germany).

Tab. 3: Antibodies used for immunocytochemistry.

Antibody	Species	Dilution Factor	Catalogue No.	Company
anti-ßIII-tubulin	Rabbit	1:250	T2200	Sigma, Taufkirchen, Germany
anti-CA-II	Rabbit	1:100	SC-25596	Santa Cruz, Heidelberg, Germany
anti-Iba1	Rabbit	1:250	019-19741	Wako, Neuss, Germany
anti-S100ß	Rabbit	1:1000	287003	Synaptic Systems GmbH, Göttingen, Germany
anti NeuN	Mouse	1:250	MAB377	Millipore, Darmstadt, Germany
AF488 anti rabbit	Donkey	1:250	A21206	Invitrogen, Darmstadt, Germany

All the primary and secondary antisera were prepared in 10% normal donkey serum containing 0.3% permeabilizing Triton X-100. Incubation was continued overnight at 4°C under slow rotation. After incubation with primary antisera, cells were washed twice with 1x PBS and incubated with Alexa Fluor 488-conjugated donkey anti-rabbit IgG (H+L) secondary antibody diluted to 1:250 (Invitrogen, Darmstadt, Germany) for 30 min at RT under slow rotation. Cells were then washed twice with 1x PBS and treated with a DAPI solution for 5 min at RT to stain the nuclear DNA. Cells were again rinsed twice with 1x PBS and mounted on properly labelled clean glass slides. Photomicrographs were taken using a confocal laser

scanning microscopy (LSM 710 Zeiss, Jena, Germany) with a 63x oil immersion objective and appropriate lasers (488 nm laser for Alexa 488; 405 nm laser for DAPI).

Digital photomicrographs of freshly stained cell preparations were taken with the fluorescent microscope AxioPlan 2 equipped with AxioCam HRC camera and the AxioVision Rel. 4.8 software (Zeiss, Jena, Germany) to calculate the proportions of different neural cell types. Twenty images were taken from each of three preparations with a 40x objective, and assessed for each cellular marker by determining total DAPI-positive cell density and marker-specific cellular moieties from a display window of 360 x 275 µm, respectively. On average, a total of 500 cells were analyzed to determine the age-dependent neural proportions.

3.6 Extraction of microglia

To specifically determine changes in the telomere lengths of cortical microglia from hSOD1^{G93A} mutant mice with disease progression, microglia were extracted and purified by using a combined strategy, starting with the neural cell isolation protocol previously mentioned in section 3.3, with few modifications, and followed by a percoll gradient as described by Njie and colleagues (Njie et al., 2012). In order to be able to process brain cortices and isolate neural cells from a group of 5-6 mice in a single experimental session, the protocol was slightly modified. Briefly, animals were perfused with an ice cold PBS one after the other and both cortices were extracted and added to collagenase solution in individual tubes and kept on ice. Incubation on ice was continued until the last animal was perfused. Then all the cortices were processed simultaneously according to the protocol with the exception that all the incubations were carried out at 37°C in a water bath under slight agitation intervals. Moreover, the final cell suspension was not incubated on ice, but processed immediately to select microglia by centrifuging the final cell suspension at 1000 x g for 5 min. In the meanwhile, an isotonic percoll gradient (Sigma-Aldrich, Taufkirchen, Germany) was prepared as indicated in Tab. 4. The isotonic percoll gradient was diluted with 1x PBS to different percentages as mentioned in Tab. 5. The supernatant was discarded and the pellet was re-suspended in 6 ml of 75% percoll isotonic gradient. The cell suspension was equally distributed into 2 polystyrene tubes (3 ml of cell suspension in each tube). A total of 5 ml of 35% percoll gradient was layered slowly and gradually on top of a tube containing 3 ml of cell suspension. At the end, 2 ml of 1x PBS were layered on the top of this gradient. The gradient was centrifuged at 800 x g for 45 min in a hanging bucket centrifuge with brake and acceleration set at 0 and 3, respectively. Afterwards, the top layer containing debris was discarded. A very light band containing microglia was formed at the junction of 75% and 35%

gradient layer. This was carefully separated (5-6 ml volume together from both tubes), transferred into fresh 50 ml falcon tubes and washed with 50 ml of 1 x PBS at 1000 x g for 10 min using the same program settings. The supernatant was discarded and the pellet was re-suspended in 1 ml of 1x PBS. The microglial suspension was transferred to a sterile DNAse/RNAse free tube. The microglial cell number was determined for each individual sample. The purity of the isolated cells was 94-95%, as it was assessed by determining the number and percentage of Iba1 positive cells. The cell suspension was again centrifuged at 1000 x g for 5 min. The supernatant was carefully and completely aspirated and the microglia cell pellet was frozen in liquid nitrogen and stored at -80°C until the samples were further processed to extract the DNA.

Tab. 4: Recipe of isotonic percoll gradient

Volume of isotonic percoll gradient per brain (ml)	Volume of 10x PBS (ml)	Volume of percoll (ml)
4.5 + 3.5 = 8	0.8	7.2

Tab. 5: Preparation of isotonic percoll gradient with different percentages

Percentage (%) of isotonic percoll gradient	Volume required per brain (ml)	Volume of isotonic percoll (ml)	Volume of 1x PBS (ml)
75%	6	4.5	1.5
35%	10	3.5	6.5

3.7 DNA isolation from cells and tissues

DNA from the disseminated neural cells or homogenized CNS tissues was extracted using the NucleoSpin Tissue kit (Masherey Nagel, Düren, Germany) according to the kit's manual, with slight modifications. 200,000-300,000 cells were re-suspended in a final volume of 200 µl of buffer T1. Then, 25 µl of proteinase K solution and 200 µl of buffer 3 were added and samples were incubated at 70°C for 3 hrs. Alternatively, for tissues, 180 µl of buffer T1 were added to 25-30 mg of brain tissue. The tissue was homogenized with a motorized pestle and 25 µl of proteinase K were added. The tissue homogenate was vortexed and incubated overnight at 56°C in a pre-warmed heating block. On the next day, the tissue homogenate was

vortexed again and 200 µl of buffer B3 were added. The tissue homogenate was then vigorously vortexed and incubated at 70°C in a pre-tempered heating block for 10 min. After 10 min, the homogenate was vortexed again and if there were some pieces remaining, the homogenate was centrifuged at 11,000 x g for 5 min and the supernatant was transferred to the new tube.

All further steps of the protocol were identical for both, cells and tissue. 210 µl of ethanol were added to the samples and vortexed vigorously. Nucleospin columns were placed in the collection tubes and samples were applied on the columns. The samples were then centrifuged at 11,000 x g for 1 min. The flow-through was discarded and the columns were placed back in the collection tubes. Extracted DNA was washed by adding 500 µl of buffer BW and centrifuged for 1 min at 11,000 x g. The flow-through was again discarded. The DNA was washed by adding 600 µl of buffer B5 to the column and centrifuged for 1 min at 11,000 x g. Once again, the flow-through was discarded. Empty columns were centrifuged to dry the silica membrane. Columns were transferred to new sterile and labelled 1.5 ml tubes, and 50 µl of pre-warmed buffer BE (elution buffer) were added to the nucleospin column to elute the genomic DNA. Samples were incubated at RT for 2 min and centrifuged at 11,000 x g for 2 min. Quantification and purity determination of DNA was performed by spectrophotometry using a Nanodrop 2000/2000C device (ThermoFisher Scientific, Darmstadt, Germany). A ratio of absorbance of ~1.8 or higher at 260 nm/280 nm indicates the purity of the DNA and reflects that samples are free of proteins or other contaminants. For telomere length measurement by qPCR, samples were diluted to a concentration of 4 ng/µl. The stocks and dilutions were stored at 4°C.

3.7.1 Agarose gel electrophoresis

To further confirm the integrity of the extracted DNA, agarose gel electrophoresis was performed. To run genomic DNA, 0.8-1% (w/v) agarose gel (ThermoFisher Scientific, Darmstadt, Germany) was prepared in 1x TAE buffer (Tab. 6). The agarose gel was heated up in a microwave oven until it boiled and was completely dissolved into a clear transparent solution. The agarose gel was allowed to cool down to 60-70°C and ethidium bromide (Sigma-Aldrich, Taufkirchen, Germany) was added to a final concentration of 0.5 µg/ml from a stock of 10 mg/ml (5 µl stock/100ml gel) in order to stain the DNA. A comb was inserted carefully into the gel casting chamber. The agarose gel solution was poured into the gel casting tray and allowed to set and polymerize at least for 30 min. The polymerized gel was placed in the gel tank, which was filled with 1x TAE buffer. To track and visualize DNA

during the gel electrophoresis, 2 µl of 6 x DNA loading dye solution (ThermoFisher Scientific, Darmstadt, Germany) was mixed with 10 µl of DNA samples. Then, 10 µl of this mix were loaded into the sample wells. 100 bp or 1 Kb DNA ladders were also loaded as a reference size marker. The gel was monitored and run at 80-100 V until the loading dye reached 75% of the gel length. Afterwards, integrity of the DNA was visualized in SYNGENE G:BOX gel documentation system (VWR, Darmstadt, Germany) equipped with GeneSnap software version 7.09 (SYNGENE, Cambridge, UK).

Tab. 6: Recipe of buffers

Buffer	Ingredients
50x TAE	**Tris base = 242 g** **Glacial acetic acid = 57.1 ml** **EDTA = 18.6 gm** **Distilled water = up to 1 L**
1x TAE	**50X TAE = 20 ml** **Distilled water = 980 ml**

3.8 Gene expression analysis

3.8.1 RNA isolation from cortical tissue

In order to assess gene expressions, the RNA was isolated from the brain cortices of young (3 months) and aged (25-28 months) mice using QIAzol lysis reagent (QIAGEN, Hilden, Germany) according to the manufacturer's instructions. Briefly, the tissue was homogenized in 1200 µl of QIAzol lysis reagent for 30-45 sec using an Ultra-Turrax homogenizer (IKA Labortechnik, Staufen, Germany) and then incubated for 5 min at RT. Afterwards, 240 µl of chloroform (Sigma-Aldrich, Taufkirchen, Germany) were added and vortexed vigorously. The tissue homogenate was incubated for 3 min at RT and then centrifuged at 12000 x g for 20 min at 4°C. Centrifugation resulted into 3 phases. The upper transparent aqueous phase containing RNA was transferred to a sterile tube containing a 1.1-fold phase volume of ice cold isopropanol (Roth, Karlsruhe, Germany), and a 0.16-fold phase volume of 2M sodium acetate (pH = 4) (Sigma-Aldrich, Taufkirchen, Germany). The contents were mixed by shaking and incubated for 15 min at RT. Following incubation, the samples were again centrifuged at 12000 x g for 15 min at 4°C. The supernatant was carefully aspirated and discarded. The RNA pellet was washed twice with 75% ethanol and centrifuged at 7600 x g

for 5 min at 4°C. The RNA pellet was then air-dried and dissolved in 40 µl of nuclease-free water at 65°C for 5 min. Total RNA was quantified by spectrophotometry using a NanoDrop device (NanoDrop 2000c, Peqlab, Erlangen, Germany). The purity of the RNA samples was determined by the ratio of absorbance at 260 nm and 280 nm. The ratio of ~2.0 excludes the presence of relevant contaminants. For cDNA synthesis, RNA was diluted to 100 ng/µl and stored at -80°C.

3.8.2 cDNA synthesis

RNA was reversely transcribed to cDNA using the RevertAid First Strand cDNA Synthesis Kit (Life Technologies, Darmstadt, Germany) according to the manufacturer's instructions. Master Mix 1 and 2 were made as follows:

Mix 1	**Mix 2**
0.6 µl of oligo (dt) 18 primer	2.0 µl of 5x reaction buffer
0.5 µl of random hexamer primer	1.0 µl 0f 10 mM dNTPs
5.0 µl of RNA sample	0.5 µl RibolLock RNAse Inhibitor (20 U/µl)
	0.5 µl of RevertAid Reverse Transcriptase (200 U/µl)

Mix 1 containing the sample was incubated in a thermal cycler at 65°C for 5 min. Then, 4 µl of Mix 2 were added to Mix 1 to reversely transcribe the cDNA in a thermal cycler according to the following program:

Cycling Profile

Temperature	**Time**
25°C	5 min
42°C	60 min
70°C	5 min
4°C	∞

The cDNA was diluted with nuclease free water and adjusted to a final concentration of 5 ng/µl.

3.8.3 Real time PCR for analysis of RelA and c-Rel gene expression

In order to quantify the expression of *NF-kB RelA* and *c-Rel* in murine brain cortex, a one-step real-time qPCR was performed using Brillant II SYBR Green qPCR kit (Agilent Technologies, Frankfurt, Germany). To amplify only the genes of interest and to avoid genomic DNA amplification, primer pairs (Tab. 7) were designed to cover exon-exon boundaries. All the samples were run in technical duplicates from 5-6 biological replicates in each group.

The PCR reaction had the following composition:

10 µl of Brillant II SYBR Green qPCR Master Mix

2.5 µl of forward primer (2 µM)

2.5 µl of reverse primer (2 µM)

5.0 µl of cDNA sample (5 ng/µl)

The program used for the amplification of *RelA* and *c-Rel* cDNA is shown in Tab. 8. A melting curve was also generated to assess the specificity of the amplified PCR products by raising the temperature from 72°C to 95°C, with an increment of 0.5°C every 3 sec.

Tab. 7: Details of the primer pairs

Gene	Forward primer 5'→ 3'	Reverse primer 5'→ 3'	Product size (bp)
GAPDH	CAACAGCAACTCCCACTCTTC	GGTCCAGGGTTTCTTACTCCTT	164
RelA	GACCCTGACCATGGACGATC	CGGCTGTTCGATGATCTCCA	138
c-Rel	GGAAGTGTCAGGGGAGGAGA	GGCTACTTGGCGGTGTACAT	91

Changes in gene expression were analyzed according to Pfaffl (Pfaffl, 2001) using delta-delta threshold cycle ($\Delta\Delta C_t$) values. Data were normalized against expression of *GAPDH*, a housekeeping gene, which was co-amplified in the same run. Data were analyzed using the Rotor-Gene Q Series Software 2.3.1 (Qiagen, Hilden, Germany).

Tab. 8: Cycling profile for specific gene amplification

Step	Temperature	Time	Cycles
Initial denaturation	95°C	10 min	1 cycle
Denaturation	95°C	15 sec	40 cycles
Annealing	60°C	30 sec	
Elongation	72°C	30 sec	

3.9 RTL measurement

3.9.1 Flow-FISH

In order to evaluate age-associated changes in telomere length from the murine brain, cortical cells were freshly isolated from male C57BL/6 mice aged 3 months and 25-27 months as described, and telomere length was then determined by Flow-FISH. FISH (fluorescence *in situ* hybridization) represents a highly sensitive cytogenetic procedure to assess the copy number of repetitive genomic DNA elements by *in situ* hybridization. In Flow-FISH, this procedure is then coupled with flow cytometry to assess the relative telomere length.

Flow-FISH was performed on freshly isolated cortical cells by using a telomere PNA/FITC-based kit for flow cytometry (DAKO, Hamburg, Germany) according to the guidelines provided in the kit, with minor addition. Briefly, freshly isolated neural cells were processed with hybridization solution with or without telomere peptide nucleic acid (PNA) probe/FITC. In order to avoid DNA clumping during the denaturation step, 30 µl of DNAse I (310 IU/ml) were added to all the samples. DNA was denatured by heating to 82°C in a pre-warmed heating block for 10 min. Denatured DNA was allowed to hybridize with telomere PNA probe/FITC by incubating cells in the dark overnight at RT. Following overnight incubation, cells were washed twice in 1x washing solution (prepared from the 10x washing solution provided in the kit). To determine the sample-specific and background fluorescence intensities, cells were incubated with 1x propidium iodide (PI) solution or PBS for at least 3 hours at RT. The cell preparations were filtered through a 30 µm cell strainer into FACS tubes to get a single cell suspension and to avoid damage to the FACS device. Samples were run on a FACS Calibur flow cytometer (Becton Dickinson, Heidelberg, Germany). For detection of PNA-FITC and PI signal, FL1 and FL3 channels were selected, respectively.

As a first step, setup parameters were defined on the flow cytometer for the equipment settings and optimized for detector, amplifier and threshold. The setup defined was then kept constant for all other Flow-FISH runs. Calibration beads and blank beads (DAKO, Hamburg, Germany) were run prior to the sample runs and served as an internal reference to define the mean fluorescence intensity (MFI). Per group, 4-8 mice were analyzed and all the samples were run in technical duplicates. In order to ensure that the changes in MFI for PNA-FITC are valid and associated to the number of telomere repeats and not an artifact due to alterations in the total DNA content, the relationship between MFI and cell cycle phase-specific DNA content of each individual sample was analyzed. This was performed by normalizing the PNA-FITC-H-related MFI values against sample-specific DNA content (PI-A) in a cell cycle-dependent manner, according to the following formula:

$$(\text{MFI (PNA-FITC-H) } G_0/G_1)/ (\text{MFI (PI-A) } G_0/G_1)$$

and

$$(\text{MFI (PNA-FITC-H) } G_2)/ (\text{MFI (PI-A) } G_2)$$

Linearity between PNA-FITC-related MFI value and DNA content were represented as ratios of 1.0 ± 0.05 -fold s.d., whereas higher or lower ratios were likely to reflect MFI changes due to changes in sample-specific DNA amount.

3.9.2 Cell cycle-dependent gating strategies for neural cells

Analysis of cell cycle phase-specific RTL was performed in a stepwise manner as shown in Fig. 6. First, cells were sorted into different cell cycle phases and then analyzed for MFI using the FCS Express 5 Plus software equipped with Multi-cycle add-on plugin (De Novo Software, Glendale, CA, U.S.A).

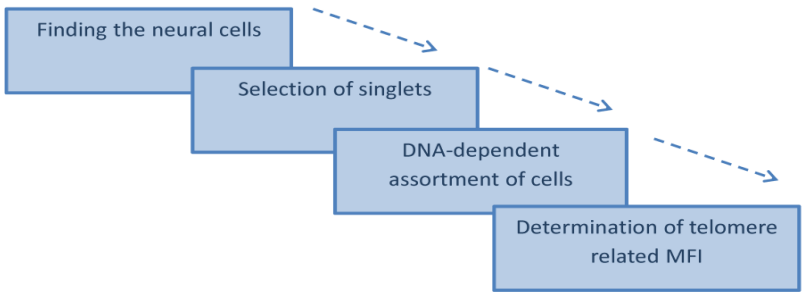

Fig. 6: Steps involved in analysis for relative telomere length measurement (RTL). Following neural cell selection, duplets were removed and the cells were identified in different cell cycle phases. RTL was then quantified in the selected cells according to their cell cycle status.

Recorded events were plotted as dot plots and overlaid with contour plots to separate and better discriminate the neural cells from the cellular debris and from dead cells. The neural cell population was characterized on the basis of the parameters ‘cell size’ and ‘granularity’ or ‘complexity’, determined by forward light scatter (FSC) and side light scatter (SSC), respectively, as shown in Fig. 7A and sorted as gate “Cells”. Singlets were selected, excluding the doublets out by applying an exclusion gate on selected cells via plotting dot plots of PI-A (FL3-Area) versus PI-H (FL3-Height) channels (Fig. 7B). To make a selection of cells according to the cell cycle phase, the inclusion gate for cells and exclusion gate for duplets was combined, and events were plotted as a function of PI-based DNA content, as depicted in Fig. 7C. The majority of the isolated cells were resident in the G_0/G_1 phase. The cells, which showed a doubled DNA content as compared with the cells in the G_0/G_1 phase, were gated as G_2 phase cells. MFI was realized for PNA probe/FITC stained and unstained samples for the gated cells both in the G_0/G_1 and G_2 phase (Fig. 7D). RTL was calculated by deducting the MFI of PNA probe/FITC-unstained sample from MFI of PNA probe/FITC-stained sample (ΔMFI).

Age-associated changes in the cell cycle proportions of isolated cortical cells were also determined by performing analyses on histograms showing DNA content of cortical cells isolated from 3 months and 25-27 months old mice. The cells were gated in different cell cycle phases on the basis of PI staining for DNA (Fig. 7C), and then their percentages were gathered for each cell cycle phase.

.

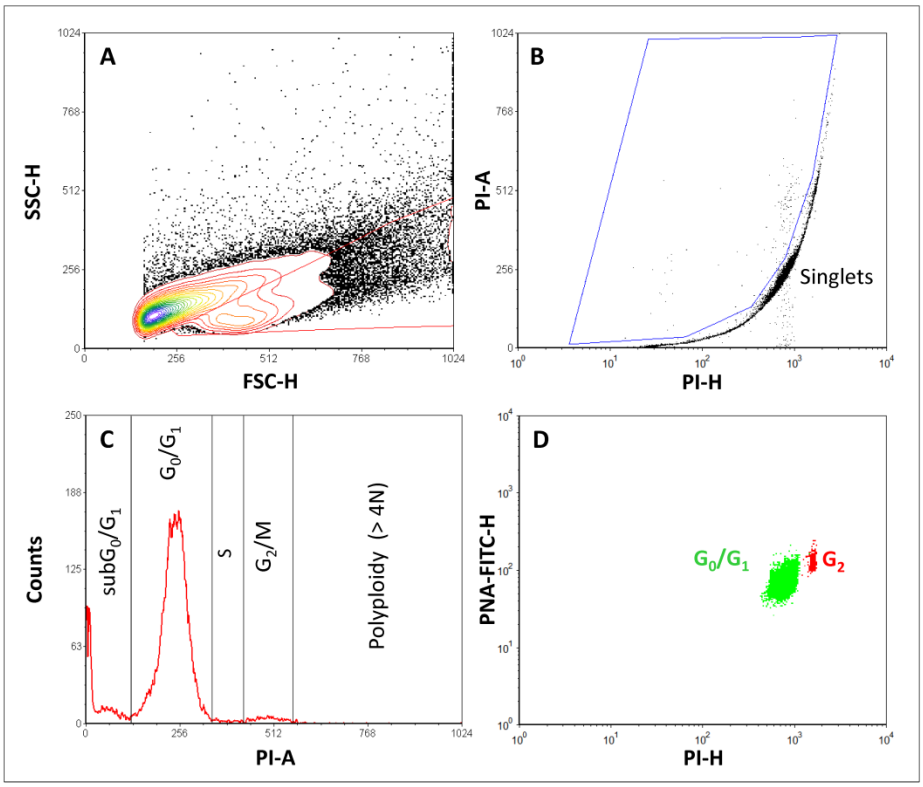

Fig. 7: Cell sorting strategies for relative telomere length (RTL) measurement. Representative images of isolated cortical cells from a 3 months old B6Je mouse. (A) Neural cell selection. The red gate "Cells" indicates vital neural cortical cells. (B) Omission of doublets. The blue gate "Singlets" specifies the exclusion of doublets. (C) Discrimination of cells in different cell cycle phases. The vast majority of neural cells reside in G_0/G_1, while only few cells are in G_2. Apoptotic cells are recognized as sub G_0/G_1 fraction. (D) Realization of cell cycle-dependent PNA-FITC MFI. Green color represents the MFI for G_0/G_1 cells and red for the cells in G_2 phase. PI-A, propidium iodide area; PI-H, propidium iodide height; PNA-FITC-H, peptide nucleic acid-fluorescein isothiocyanate height; SSC-H, side scatter height; FSC-H, forward scatter height.

3.9.3 qPCR

In order to assess RTL in complete cortical and cervical spinal cord tissue of hSOD1^{G93A} mutant mice, a q-PCR-based method developed by O'Callaghan and Fenech (2011) was used, with some modifications. This method was also applied to verify the Flow-FISH based results obtained for RTL in isolated cortical cells from young and aged C57BL/6 mice. Oligonucleotide primers against telomeric regions were utilized to amplify the telomere repeats in the genomic DNA in a specific sample. The 36B4 gene, which encodes an acidic ribosomal phosphoprotein, was used as a single copy gene to determine genome copies per sample. Genomic DNA samples from 5-6 biological replicates for each experimental group were run as technical duplicates for both, telomere repeats and the 36B4 gene in the same run. "No template control" was run for both the telomere and the single copy gene. Standards in the range of 1.56-25 ng/µl, made from serial dilutions of P1 C57BL/6 genomic DNA isolated

from the whole brain, were also run for both primer pairs to standardize the assay. Two master mixes were composed for each primer pair, each displaying the following composition:

12.5 µl of Light cycler 480 SybrGreen I Master (Roche, Mannheim, Germany)

0.5 µl of forward primer (5 µM)

0.5 µl of reverse primer (5 µM)

5.0 µl of DNA sample (4 ng/µl)

6.5 µl of nuclease free H_2O to make the volume up to 25 µl

The primer pairs used for both telomere repeats and the 36B4 gene (shown in Tab. 9) were identical to those used by O'Callaghan and Fenech (2011).

Tab. 9: Primer pairs used for RTL measurement.

Gene	Primer sequence 5'→ 3'	Product size (bp)
TeloF	CGGTTTGTTTGGGTTTGGGTTTGGGTTTGGG TTTGGGTT	>76
TeloR	GGCTTGCCTTACCCTTACCCTTACCC TTACCCTTACCCT	
36B4F	ACTGGTCTAGGACCCGAGAAG	78
36B4R	TCAATGGTGCCTCTGGAGATT	

The qPCR was run in a Rotor-Gene Q thermal cycler (QIAGEN, Hilden, Germany) applying the following cycling program:

10 min at 90°C…. 1 cycle

95°C for 15 sec
60°C for 1 min } 40 cycles

Melting curve

RTL was quantified in terms of the ratio of telomere repeat copy number "T" to single copy gene copy number "S" (T/S ratio), The relative T/S ratio was determined by the $2^{-\Delta\Delta Ct}$ method

as described by Richard M. Cawthon in 2002 (Cawthon, 2002),which determines how each DNA sample varies in its T/S ratio relative to the T/S ratio of a reference sample.

3.10 TRAP assay

3.10.1 Preparation of tissue lysate

To evaluate age- and disease-associated changes in telomerase (TERT) activity, TERT activity was measured using a telomeric repeat amplification protocol (TRAP)-based kit (Merck Millipore, Darmstadt, Germany), which was used according to the manufacturer's instructions. Briefly, animals were transcardially perfused with ice cold 1x TBS and different brain regions and cervical spinal cord tissue were extracted and transferred to pre-weighed RNAse/DNAse free tubes. The tissue was weighed and immediately froze in liquid nitrogen and then stored at -80°C.

The frozen tissue was thawed on ice, and 50 µl of CHAPS lysis buffer, supplemented with RNAse inhibitor (ThermoFisher Scientific, Darmstadt, Germany) at a final concentration of 100-200 IU/ml was added. Tissue was homogenized on ice using a motorized pestle. Volume of lysis buffer was adjusted to the wet weight of the tissue sample in order to achieve a final concentration of ~2 mg/µl. Tissue lysates were then incubated on ice for 30 min. Following incubation, samples were centrifuged at 12,000 x g for 20 min at 4°C and supernatants were collected. To avoid repetitive freeze-thaw cycles, all samples were aliquoted and then frozen at -80°C. According to the manual included in the kit, TERT activity in the tissue lysates is assumed to remain stable for at least one year if stored under proper conditions.

3.10.1 Protein estimation

In each of these final samples, total protein amount was measured with the Bradford assay. From each sample solution, 2 µl were pipetted to 250 µl of Bradford reagent (Bio-Rad, Munich, Germany) and incubated in the dark at RT for 15 min. Protein standards were prepared by diluting bovine serum albumin (BSA) (Sigma-Aldrich, Taufkirchen, Germany) in CHAPS lysis buffer within a range of 0.5-16 mg/ml. The standards were run in the same 96-well-plate together with the samples. Sample-specific protein content was estimated spectrophotometrically in a TECAN microplate reader (Tecan group Ltd., Männedorf, Switzerland) by measuring the absorbance of all the standards and the unknown samples at 590 nm. Protein amounts were then quantified based on the BSA standard curve. All the samples were then set to a final protein concentration of 500 ng/µl by dilution in CHAPS lysis buffer. For PCR-based TRAP assay, 1 µg of protein was used for each reaction.

3.10.2 TRAPeze RT telomerase activity assay

Real time quantification of TERT activity was performed by a qPCR-based assay to quantify the hexameric telomeric repeats added by the catalytic subunit TERT of the telomerase enzyme to the artificial oligonucleotide substrate (TS) provided in the reaction mix. The TERT product was then amplified by the Taq polymerase enzyme using the Amplifluor reverse primer (RP), which has a Fluorochrome and a quencher molecule like DABSYL. The quencher prevents the fluorochrome from emitting fluorescence as long as it is in close proximity to the fluorochrome as shown in Fig. 8. Once the hairpin containing both the quencher and the fluorochrome is incorporated in the amplified product, it is unfolded and the distance between both molecules increases, abolishing the quenching effect. Thus, these fluorescence energy transfer (ET) primers reduce amplification artifact because they emit fluorescence signals only when incorporated into amplified products. The emitted fluorescence then directly corresponds to the TERT product. Real time quantification of TERT activity was performed by qPCR. The master mix contained the following ingredients:

5.0 µl of 5x TRAPEZE RT reaction mix

0.4 µl of Titanium Taq Polymerase (2 U) (TaKara, Saint-Germain-en-Laye, France)

2.0 µl of sample *

(* All the controls, standards and samples with or without heat inactivation were added in the same volume)

The final volume of each reaction tube was adjusted to 25 µl and each sample was run in methodical duplicates with 5-6 animals in each group. The assay was standardized by adding internal positive and negative controls to each plate. TSR8 standard with a stock concentration of 20 amoles/µl and a sequence identical to the telomerase substrate was serially diluted within a range of 0.02-2.0 amoles/µl and run in each plate to assess the TERT activity.

The tissue lysate was incubated at 30°C for 30 min to allow the telomerase enzyme in the tissue lysate to add TTAGGG repeats to the artificial TS substrate provided in the reaction mix. Afterwards, the telomerase activity was inactivated by a hot start PCR and TERT product was amplified. The PCR was run according to the following cycling profile as shown in Tab. 10. TERT activity was quantified in terms of real time fluorescence emission (in arbitrary units – a.u.) corresponding to the average Ct value of each well and condition, and

compared to the emission signal derived from the TSR8 product. Data were normalized against the activity of a positive cell extract sample or positive control, run in each plate.

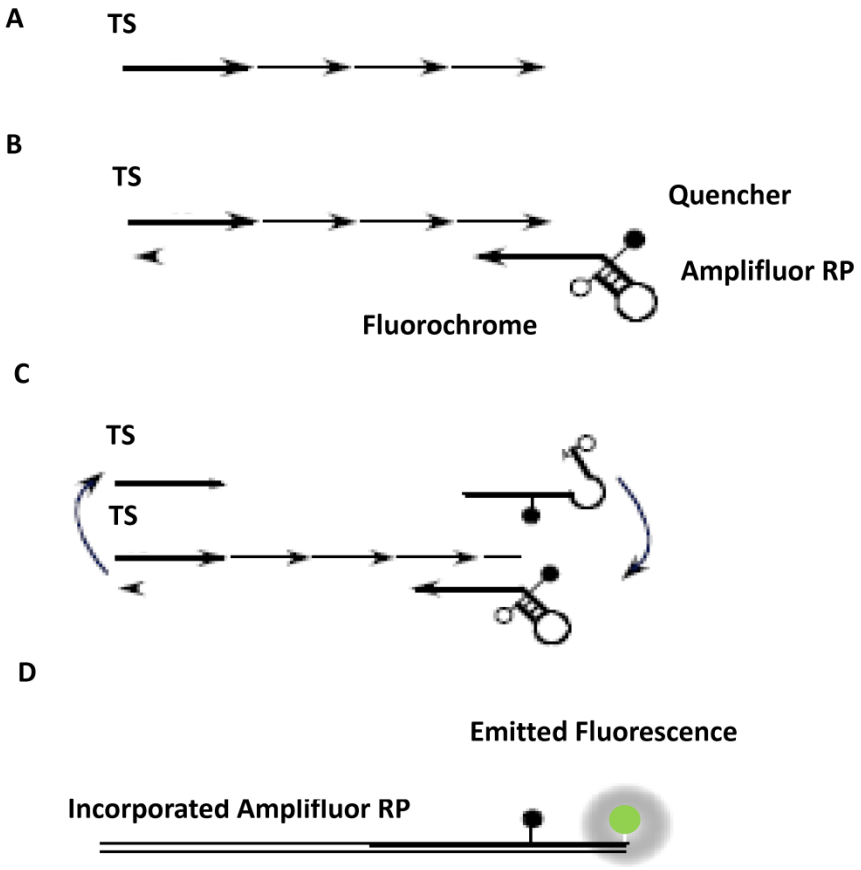

Fig. 8: Working principle of the TRAP assay. (A) Addition of TTAGGG repeats. Telomerase enzyme in the tissue lysate adds telomeric repeats to TS substrate. (B) Complementary strand synthesis. With the help of Amplifluor RP the lagging strand is generated. (C) Amplification of the generated product. Telomere repeats are amplified several folds by PCR. (D) Generation of fluorescence signal. Accumulated unquenched fluorescent signal is quantified and referred to as TERT activity (modified from TRAPeze RT telomerase detection kit manual).

Tab. 10: Cycling profile for TRAP assay.

Steps	Temperature	Time	Cycles
Addition of telomeric repeats to TS oligonucleotide	30°C	30 min	1
Inhibition of TERT activity	95°C	2.0 min	1
Amplification of telomerase product and data acquisition	94°C	15 sec	45
	59°C	60 sec	
	45°C	10 sec	

3.11 **Statistical Analysis**

Statistical analyses were performed using SigmaPlot (version 13.0) and IBM SPSS (version 22) software systems. Outliers were identified and excluded by the boxplot graphical tool. Two-tailed Student's t-test was applied for single pair comparison. Multiple groups were compared by One-way ANOVA, Two-way ANOVA or ANOVA on ranks. Holm-Šidák test was used as *post hoc* test. Significance levels are set as: n.s. $p > 0.05$, *$p < 0.05$, **$p < 0.01$ and ***$p < 0.001$.

4 RESULTS

4.1 Identification and quantification of neural cell types

With the newly established cell isolation protocol we obtained around 1.6-2.5 million cells per murine cortex from both the young and aged categories. To validate the efficiency of the isolation protocol, different neural cell types and their representative proportions in the isolates were characterized by immunocytochemistry. Apart from comparable cellular yields, the isolation protocol similarly preserved the cell vitality and viability in young and aged isolates from both murine cohorts. Neurons and oligodendrocytes were specified as ß-III-tubulin and CA-II positive entities, respectively (Fig. 9A and 9B). Microglial cells were identified by staining with Iba1, whereas astrocytes were distinguished by using S100-ß as marker (Fig. 9C and 9D). Different cell types were also identifiable by their morphological features like size, shape and cellular process-like extensions.

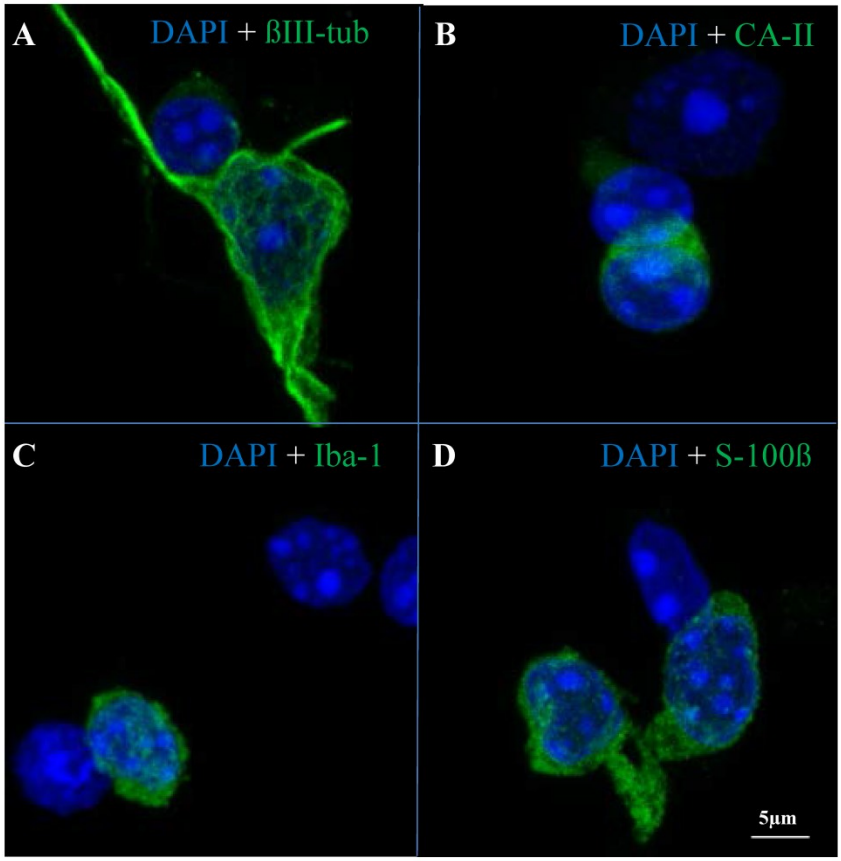

Fig. 9: Isolated cortical neural cells from 27 months old C57BL/6 Jena (B6Je) mice identified by labelling with different neural cell type markers. (A) Neurons: ß-III tubulin. (B) Oligodendrocytes: CA-II. (C) Microglia: Iba-1. (D) Astrocytes: S-100ß. Exemplified are the LSM micrographs taken at 63 x objective with oil immersion. Scale bar, 5µm.

The relative number of each neural cell type was determined from the total number of DAPI-positive cells within the isolate. The impact of ageing on the relative proportion of different cell types, isolated with our newly established protocol, was exemplified for the C57BL/6 Jena (B6Je) sub-strain. Likewise, effects of breeding strategies on the cellular proportions within the isolate were determined at 3 months of age for both strains. Quantifications showed that the cell isolation protocol yielded reproducible data, with individual cell proportions being preserved across ages and sub-strains. On average, 93.31±0.54% (3 months) and 94.19±0.46% (27 months) of the vital cells collected displayed neural identity (Fig. 10A), proving a similarly high efficiency rate of the protocol irrespective of the underlying tissue age. With respect to strain, no inter-strain differences were observed in the total content of individual neural cell types isolates at the age of 3 months. Altogether, a neural cellular identity was proven for 93.31±1.08% and 93.31±0.54% in the specimens derived from the B6J and B6Je colony, respectively (Fig. 10B).

Thus, the inter-age and inter-strain comparisons confirmed that the proportions of specific cell types remained constant with ageing in different strains and that the isolation protocol is not implementing any kind of selection bias for any of the age groups or strains. Moreover, neural cell proportions achieved for neurons, microglia and astrocytes were in close agreement with the reported distribution of these cells in the adult and mature murine brain (Lawson et al., 1990; Nedergaard et al., 2003; Herculano-Houzel et al., 2013).

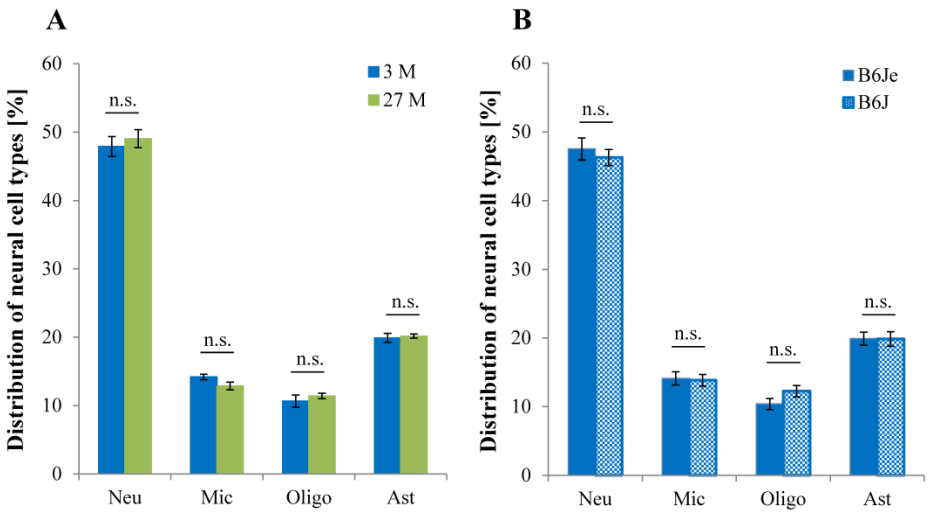

Fig. 10: Impact of ageing and inbreeding strategies on proportions of different cell types in neural cell isolates. (A) Age-dependent percentages of cells isolated from 3 versus 27 months old B6Je mice. (B) Strain-dependent distribution of different neural cell types obtained from 3 months old B6J and B6Je mice. Neu, neurons; Mic, microglia; Oligo, oligodendrocytes; Ast, astrocytes. N = 3 (~500 cell from each animal), Students's t-test; n.s. $p > 0.05$. Data are represented as means ± S.E.M.

4.2 Assessment of the telomere length in neural cells from murine brain

After neural cell isolation from murine brain, we were able to perform the primary aim of the study: to assess telomere length dynamics in the adult and aged murine brain. As a first approach, we focused on chromosome-specific telomere length determination by Q-FISH, a technique which enables to define absolute telomere length in a single cell and on each arm of the chromosome. In collaboration with the Laboratory of Molecular Cytogenetics at the Institute of Human Genetics in Jena, we started working on a Q-FISH protocol using our CNS cell isolates and, as a positive reference, on the ATCC-CRL 1722 murine lymphoma cell line (Fig. 11).

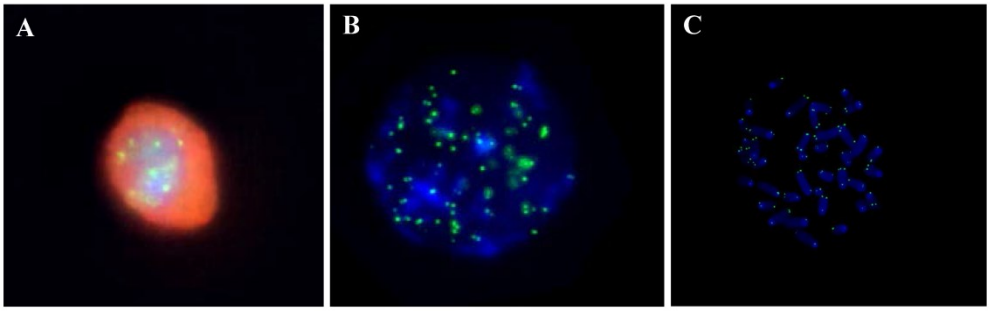

Fig. 11: Exemplified images of Q-FISH in interphase and metaphase cells. (A) A post-mitotic cortical neuron isolated from a 3 months old C57BL/6 (B6J) mouse following hybridization with a telomere specific peptide nucleic acid (PNA) probe and co-staining with the neuronal selection marker β-III tubulin. (B) An interphase cell and (C) a metaphase spread using the ATCC-CRL 1722 murine lymphoma cell line. Green, PNA probe specific for the telomeric TTAGGG sequence; red, β-III tubulin; blue, DAPI to stain nuclei. 100 x objective applying oil immersion (METASYSTEMS ISIS).

Molecular cytogenetic techniques including Q-FISH have been approved for diagnostics on interphase nuclei with the requirement of high throughput imaging and analytical tools (Canela et al., 2007; Iourov et al., 2007; Vorsanova et al., 2010). In the adult and aged brain, most inherent cell populations are post-mitotic or display only very low replicative activity and thus reside in the interphase of the cell cycle. In interphase cells, chromosomes are narrowly clustered and the FISH-signal for telomere probe, as it normally appears like two-paired dots for one chromosome in metaphase FISH, cannot be attributed to individual chromatids. Therefore, the Q-FISH protocol was not suited for telomere length analysis in murine brain tissue in our experimental paradigm (Fig. 11A). In contrast, in metaphase spreads as realized for a ATCC-CRL murine lymphoma cell line (Fig. 11C), the telomere ends belonging to the q- and p-arms of each of the chromosomes could easily be discriminated in each single cell, thus allowing quantification of the telomere length relative

to the internal reference probe-specific Q-FISH signal intensity. In contrast, strong cluster formation of chromosomes and the resulting superimposition of Q-FISH signals in the interphase clew impeded assessment of absolute telomere length in neurons (Fig. 11A and 11B). To overcome these obstacles, a Flow-FISH-based protocol was established for RTL measurement specifically in a mature neural environment.

4.2.1 Flow-FISH-based telomere length analysis

Fluorescent *in situ* hybridization was performed to label telomeres of the cortical neural cells and changes in RTL were then assessed by subsequent flow cytometry using a FACS-Calibur sorting device.

Analyses to determine RTL were performed with the FCS Express 5 Plus software plugged in with a Multi-cycle add-on (De Novo Software, Glendale, CA, U.S.A). The neural cell population was identified and separated from the smaller cluster of cellular debris, according to the analysis recently described by Guez-Barber and colleagues for adult rat neural cells, as shown in Fig. 12A (Guez-Barber et al., 2012).The light scatter obtained (Fig. 12B) was very similar to the one shown by Guez-Barber and colleagues (2012) (Fig. 12A).

Selection of the vital cell fraction was then followed by exclusion of cellular duplets to perform the analysis exclusively on single cells. Duplets were removed according to the selection parameters described by Wersto and colleagues (2001), either by plotting the gate parameters ‘height versus area’ or ‘width versus area’ in dot plots (Fig. 12C). Both parameters were tried, with better discrimination being achieved in dot plots of ‘height versus area’ in our set up (Fig. 12D). RTL was then indirectly determined in a cell cycle dependent manner and expressed as arbitrary units, with the values being referred to the mean fluorescence intensity (MFI) of PNA-FITC probes, which are specific for the telomere repeat sequence, and corrected against the background fluorescence intensity (ΔMFI) as shown in Fig. 13A and 13B.

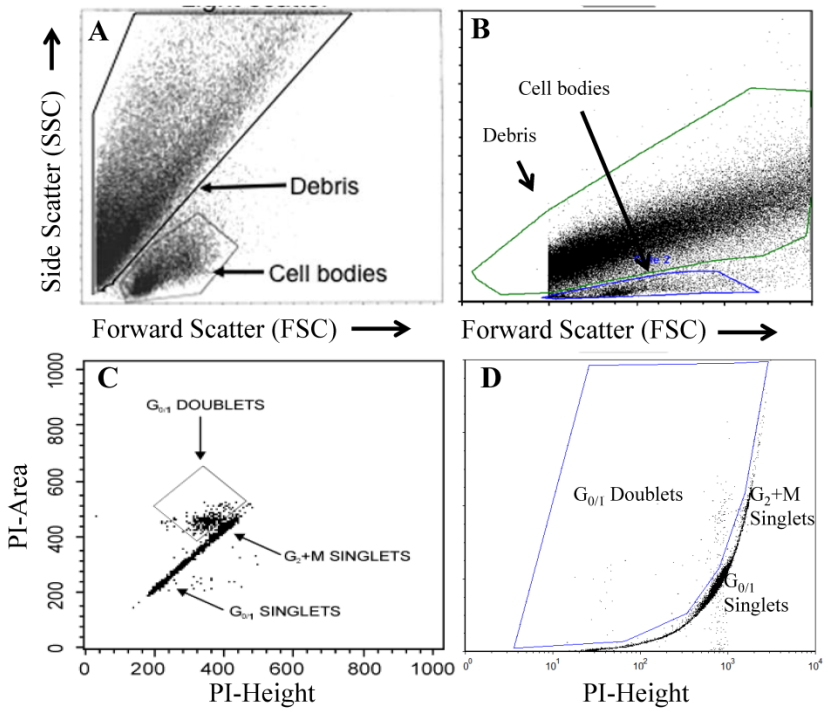

Fig. 12: Development of the cell gating strategy. (A,B) Identification of the neural cell population by the light scatter on the basis of size and granularity of the cells. (A) Modified image taken from Guez-Barber et al. (2012) representing the light scatter for rat neural cells. (B) Cortical neural cells isolated from a 3 months old B6J mouse. (C) Modified image from Wersto et al. (2001) to present the exclusion parameters for duplets. (D) Exclusion of duplets from the cortical neural cell selection taken from a 3 months old B6J mouse. PI-Height, propidium iodide height; PI-Area, propidium iodide area.

4.2.2 Age-dependent changes in telomere length dynamics and telomerase activity

4.2.2.1 Influence of ageing on the RTL of neural cortical cells residing in G_0/G_1

To quantify age-associated changes in RTL of brain telomeres isolated from C57BL/6 mice and their dependence on cell cycle activity, RTL of cortical neural cells were determined for G_0/G_1 and G_2 phases of the cell cycle, as selected on the basis of their DNA content. Ageing did not influence the telomere lengths of cortical neural cells arrested in G_0/G_1 phase in our conventionally inbred mouse strain (B6J). Accordingly, a non-significant decline in ΔMFI by only 1.55% was observed ($p = 0.857$; Fig. 13A). However, neural cells in the G_0/G_1 phase of the cell cycle, which were harvested from the hermetically inbred B6Je sister colony, exhibited a significant reduction in RTL by aging up to 25-27 months, thereby displaying a reduction in the corrected MFI of the telomere specific PNA-FITC probe values by 17.64% as compared with the young (3 months old) counterparts ($p = 0.007$; Fig. 13A). As delineated in Fig. 10A and exemplified for B6Je mice, neurons comprise 47.93 ± 1.59% and 48.78 ± 1.25% of the vital cell fraction in the cortical neural cell isolates from 3 months and 25-27 months old mice, respectively, indicating that approximately every second cell of the vital cell

fraction harbors a neuronal identity (p = 0.676; Fig. 10A). Moreover, the predominant fraction of these vital cells isolated either from the B6J (Fig. 13E) or B6Je (Fig. 13F) sister colony, resides in the G_0/G_1 phase of the cell cycle, which was proven for both young and aged conditions. From all these data, it is evident that the G_0/G_1 phase gated from neural cortical cell isolates comprises post-mitotic neurons up to 50% along with other neural cell types, inferring that these non-replicative neurons might also be susceptible to age-dependent telomere attrition.

4.2.2.2 Age-associated changes in RTL observed for replicative neural cells

In the CNS, neural cell entities that exit the G_0/G_1 phase and reach the G_2 phase of the cell cycle are mainly assumed to comprise microglia and astrocytes with moderate cell cycle activity, possibly complemented by neurons with an unscheduled and abortive cell cycle activity (Yang et al., 2001; Rehen et al., 2005). Cortical neural cells derived from the B6J colony, which adopted features of G_2 phase, as marked by a doubled DNA content in comparison to the G_0/G_1 cells, displayed no remarkable change in their RTL. This was reflected by a non-significant decrease of 19.85% in the ΔMFI values upon ageing up to 25 months (p = 0.052; Fig. 13B). In contrast, in the hermetically inbred B6Je colony, neural cells entities that reached the G_2 phase showed a drastic age-associated loss in the telomere lengths as depicted by a 44.72% decrease in the ΔMFI values in comparison to the young counterparts (p < 0.001; Fig. 13B).

4.2.2.3 High rate of telomere shortening in hermetically inbred mice

Generally, telomeres in inbred mice are longer than those in wild type mice (Hemann and Greider, 2000; Manning et al., 2002), and in this study appeared further elongated in our small, hermetically inbred B6Je sub-strain. In this genetically isolated colony, young mice showed a substantial increase in RTL compared with age-matched animals of the conventionally inbred B6J strain. This observation applied to cortical neural cells residing in G_0/G_1 and G_2 phase of the cell cycle. Thus, regardless of the specific cell cycle phase, B6Je mice on average displayed significantly longer telomeres than the conventionally inbred B6J strain at young state. Concretely, the G_0/G_1 and G_2 neural cell populations isolated from young B6Je mice exhibited a significant increment in their RTL by 23.83% and 23.16%, respectively, when compared with the young littermates from the B6J colony (for G_0/G_1: p < 0.001; for G_2: p = 0.003; Fig. 13A and 13B).

In spite of such longer RTL at young ages in B6Je colony, the age-associated decline in RTL assessed for both, replicative and non-replicative neural cell populations reached similar final

levels in the genetically isolated as well as the conventionally inbred strain (Fig. 13A and 13B). Henceforth, this indicates a faster rate of age-related telomere shortening in the B6Je sub-strain (Fig. 13A and 13B).

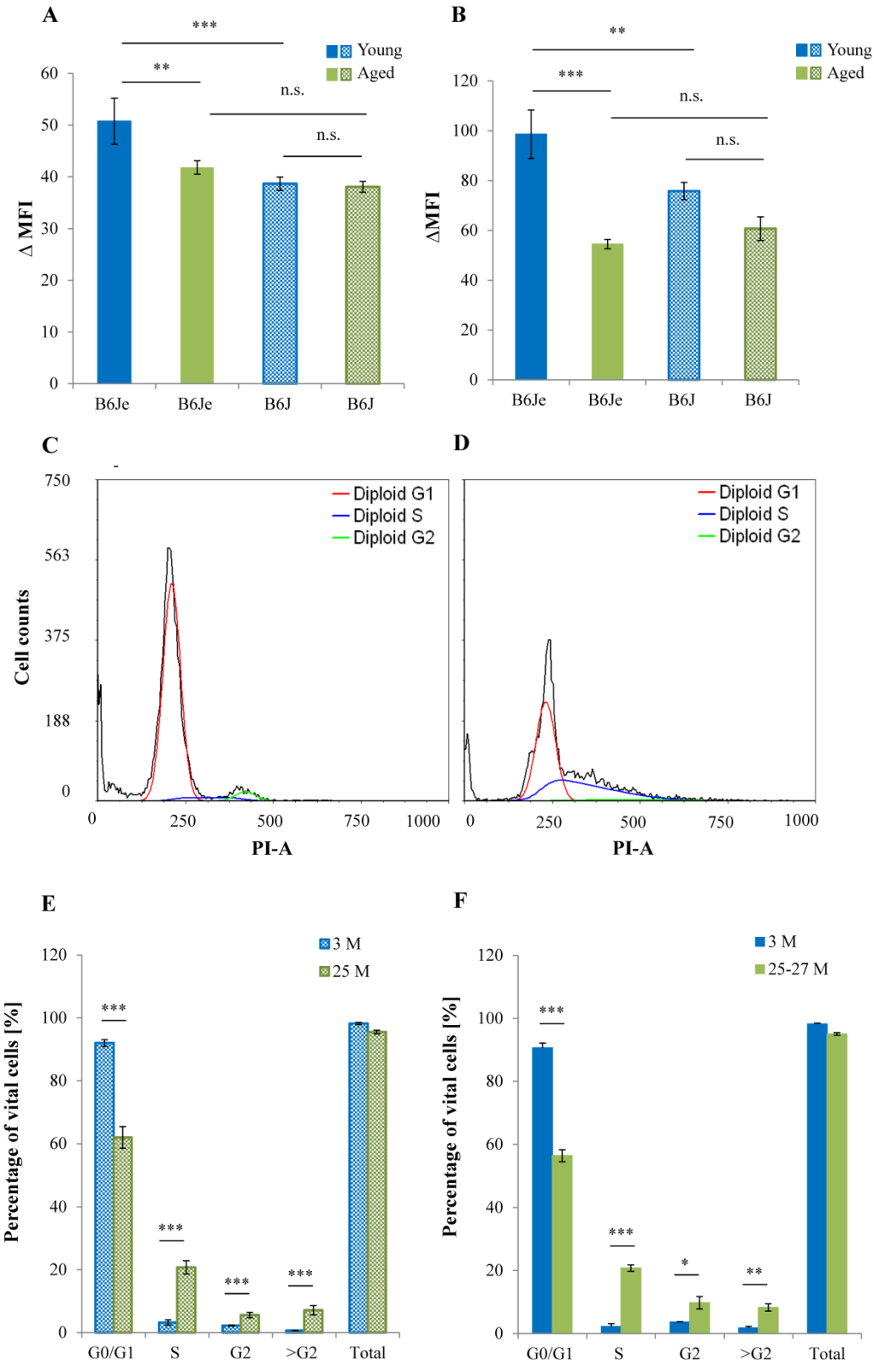

Fig. 13: Inter-strain comparison of the age-associated changes in RTL of cortical neural cells isolated from both B6 cohorts. For (A) cells residing in G_0/G_1 and (B) cell populations in G_2 phase. (C) Representative DNA histograms depicting an age-associated shift in cell cycle activity, as assessed by the PI staining of DNA. Data are exemplified for cortical cell isolates derived from B6Je mice at an age of 3 months and (D) 25-27 months. (E) Age-related distribution of the cortical neural cells in different cell cycle phases, given for the B6J and (F) B6Je colony. For (A) and (B) N = 3-8, Two-way ANOVA and Holm-Šidák post hoc test; n.s. $p > 0.05$, * $p < 0.05$, ** $p < 0.01$ and *** $p < 0.001$. Data are represented as means ± S.E.M. For (E) N = 6-10 and for (F) N = 4-8. For E and F, p values are calculated by Student's t-test; * $p < 0.05$, ** $p < 0.01$ and *** $p < 0.001$. Data are represented as means ± S.E.M.

Moreover, as delineated in Fig. 10B for the 3 months age group, proportions of the different neural cell populations in the cortical cell isolates were very similar for both C57BL/6 colonies, irrespective of the state of cell cycle activity, thus excluding the contribution of specific cell type preponderance to these remarkable inter-strain differences in RTL. Thus, the substantial inter-strain difference in RTL of young animals is putatively arising from strong inbreeding strategies. The inter-strain comparison of RTL between both replicative and non-replicative neural cell populations also implicates that, though hermetic inbreeding is negatively correlated with RTL in the aging murine brain, it is positively associated with RTL in the young and healthy state.

This conclusive finding about the faster rate of age-associated telomere shortening in the brain of the B6Je sub-strain particularly for the cells in G_2 phase is depicted in Fig. 14. Fig. 14 elucidates cell cycle-dependent telomere length dynamics for both sub-strains in terms of young:aged ratios. The decrement in RTL of the cells arrested in G_0/G_1 populations with ageing was moderate for B6Je mice and even absent in the B6J strain as reflected by young:aged RTL ratios of 1.15 ± 0.08 and 1.01 ± 0.07 ($p = 0.436$), respectively. In contrast, the rate of age-dependent decline in RTL for the neural cell populations with an active cell cycle was significantly faster for the B6Je cohort, displaying a ratio of 1.75 ± 0.11 in comparison to the B6J population (ratio: 1.38 ± 0.13) ($p = 0.037$; Fig. 14).

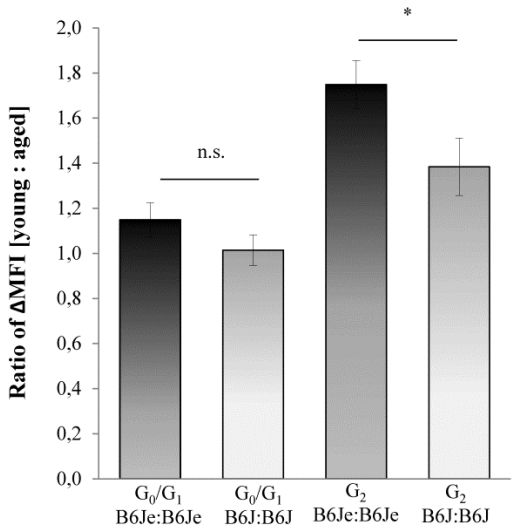

Fig. 14: Age-associated telomere length dynamics of cortical neural cells isolated from both C57BL/6 colonies. RTL dynamics were calculated in terms of young-to-aged ratios for RTL values and expressed as a function of cell cycle activity. N = 4-9, p values are calculated by Student's t-test; n.s. $p > 0.05$ and * $p < 0.05$. Data are represented as means ± S.E.M.

4.2.2.4 Higher ΔMFI values for the replicative cells in G_2 phase

Overall higher ΔMFI values were observed for the neural cell populations in G_2 phase from both young and aged cohorts of the two investigated C57BL/6 colonies, as compared with the cells residing in the G_0/G_1 phase, which is explained by the doubling of telomere repeat sequences following DNA content amplification in S phase (Fig. 15A). The increase in the telomere-specific ΔMFI signal for G_2 populations relative to the G_0/G_1 values was highest for the young mouse cohorts irrespective of the underlying breeding conditions, which displayed a 94.20% - 95.93% increment in ΔMFI signal for the B6Je and B6J strains, respectively (for B6Je: $p = 0.004$; for B6J: $p < 0.001$; Fig. 15A). The increment in ΔMFI values for the G_2 resident cells was reduced to 30.34% in the B6Je colony and 59.51% in the B6J cohort as compared with the G_0/G_1 signal at older ages (for B6Je: $p < 0.001$; for B6J: $p = 0.010$; Fig. 15A).

In order to confirm that the elevated ΔMFI values of G_2 cells over G_0/G_1 levels were due to an amplified DNA content, but not related to intrinsically longer telomeres, absolute telomere-related PNA-FITC-H values were normalized against sample-specific total DNA content in terms of PI-A for the G_0/G_1 and G_2 phase fractions from both underlying mouse colonies and from both age cohorts. The PNA-FITC-specific MFI values corrected against total DNA content in the young B6Je colony ranged between 0.306 ± 0.011 and 0.295 ± 0.009 for the cells residing in G_0/G_1 and G_2 phase, respectively, and between 0.270 ± 0.014 and 0.261 ± 0.009 in the aged B6Je group (Fig. 15B). In contrast, the ratios for G_0/G_1 and G_2 phase cell

moieties in the young and aged B6J mice span between 0.233 ± 0.011 - 0.223 ± 0.017 and 0.234 ± 0.025 - 0.237 ± 0.025, respectively (Fig. 15B). The stable ratios for G_0/G_1 and G_2 neural cell fractions at young and aged stages from both C57BL/6 cohorts support the conclusion that the higher ΔMFI values of G_2-phase cells originate from replicated telomere-specific DNA due to G_2-phase transition of the cells and not due to a genuine increase in telomere length. These calculations also validate the observation that the age-associated decline in ΔMFI values of both G_0/G_1 and G_2 phase fractions in the B6Je colony originate from a real loss of telomere sequence and are not arising from an artifact related to a decrease in total DNA content.

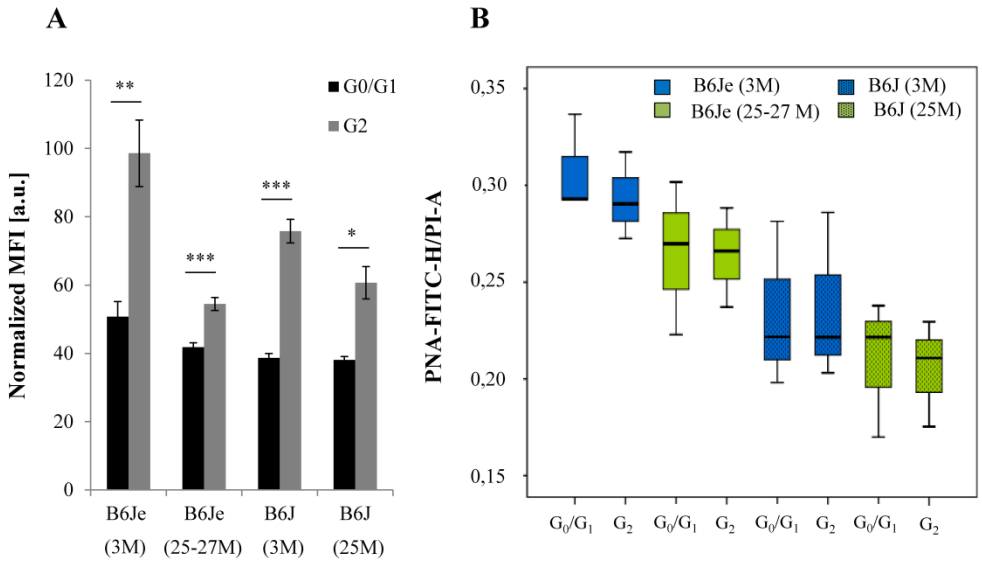

Fig. 15: Correlation between telomere-related DNA content and the total DNA content for different cell cycle phases in both young and aged cohorts of B6Je and B6J colonies. (A) ΔMFI values were higher in G_2 than in G_0/G_1 phase cells, both in the young and aged groups from the two colonies. N = 3-8, p values are calculated by Student's t-test; * $p < 0.05$, ** $p < 0.01$ and *** $p < 0.001$. Data are represented as means ± S.E.M. (B) Telomere-related DNA content normalized against total DNA content. Assessed are the ratios of absolute PNA-FITC-H signal and PI-A values for the G_0/G_1 and G_2 cell moieties, respectively, which were isolated from young and aged mice of both colonies. N = 3-8, Data are represented as means ± S.E.M. PI-A; propidium iodide area; PNA-FITC-H, peptide nucleic acid-fluorescein isothiocyanate height.

4.2.2.5 Age-associated shift in cell cycle activity

Moreover, the impact of ageing on cell cycle activity of neural cells was determined for both mouse colonies. Thereby, the distribution of neural cells in different cell cycle phases was analyzed according to their individual DNA content, as assessed on the basis of PI staining and executed for both C57BL/6 cohorts (Fig. 13E and 13F). As expected due to the post-mitotic nature of the brain, the majority of cortical cells were arrested in the G_0/G_1 phase in young mice from both, the B6J and B6Je colony (Fig. 13E and 13F). However, ageing resulted in a clear shift in cell cycle activity for both, the B6J and B6Je sister colonies, as demonstrated by an age-associated increase in the number of neural cells passing through the cell cycle as delineated in the DNA histograms given in Fig. 13C-D. As shown in Fig. 13E and 13F, the cell distribution analysis for different cell cycle phases exhibited a significant increase in the number of cells reaching criteria of S-, G_2- and $>G_2$- phases of the cell cycle, whereas the number of cells in G_0/G_1 phase declined significantly in aged animals from both strains.

4.2.2.6 Telomere length analysis based on qPCR techniques

Flow-FISH results were verified by measuring the RTL of cortical neural cells isolated from young and aged B6Je mice using the qPCR-based approach developed by Callaghan and Fenech (2011), with some modifications. Since RTL values cannot be assessed in a cell cycle phase-specific manner with the qPCR-based assay, values again reflect the average telomere length as determined by Flow-FISH, though without a selective gating strategy for underlying cell cycle phases. To allow for a comparison between both techniques, the parameters applied for Flow-FISH- related RTL analysis were now adjusted to qPCR criteria. Accordingly, RTL was measured in terms of PNA-FITC-related ΔMFI for the cells gated as “singlets”, which covered all the different cell cycle phases (Fig. 7B and 7C in section 3.9.2). As delineated in Fig. 16A, a significant reduction in RTL was observed for cortical neural cells isolated from aged B6Je animals as compared with their young counterparts, when assessed by Flow-FISH ($p < 0.001$). Likewise, a considerable age-associated decline in telomere length was detected in isolated cortical cells when the RTL was measured by qPCR in terms of the T/S ratio calculated, though the effect appeared less drastic relative to the Flow-FISH results ($p = 0.016$; Fig. 16B).

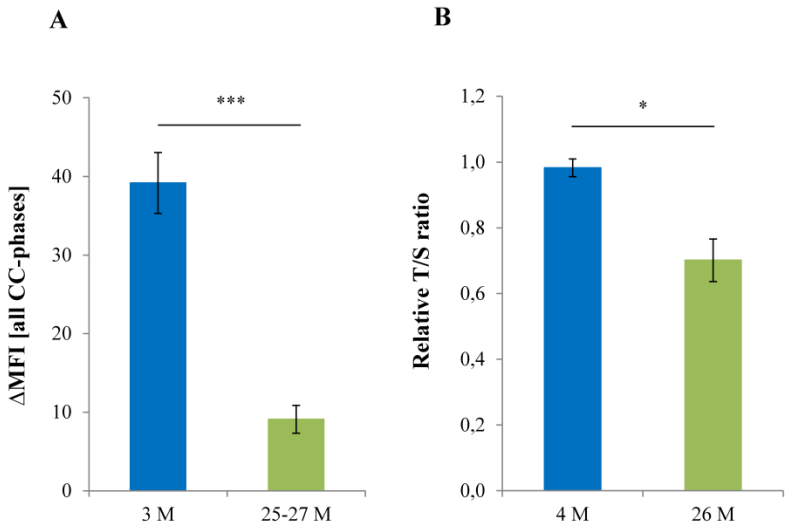

Fig. 16: Comparative analysis of telomere length alterations as assessed by Flow-FISH and by qPCR. (A) RTL measured as PNA-FITC-related ΔMFI for all cell cycle phases. (B) Relative T/S ratio measured by qPCR and corrected against a 4 months old control group. N = 3-4, Student's t-test; * $p < 0.05$, ** $p < 0.01$ and *** $p < 0.001$. Data are represented as means ± S.E.M.

4.2.3 Strain-specific changes in TERT activity with ageing

Telomere length is maintained by *de novo* addition of telomere repeats by the catalytically active reverse transcriptase (TERT) subunit of the enzyme telomerase, which uses an RNA component (TERC) as a template for the addition of tandem (TTAGGG)n repeats. Age-associated changes in TERT activity were determined in young and aged cortical tissues from both C57BL/6 colonies using a qPCR-based TRAP assay and normalized against a standardized positive control derived from a defined cell extract (Fig. 17A). In the B6Je strain, TERT activity levels remained unaltered as compared to the young control group ($p = 0.638$; Fig. 17A). However, TERT activity declined significantly with increasing age in the B6J colony ($p = 0.013$; Fig. 17A). Additionally, TERT activity displayed a similar level in the young control group from both, the B6Je and B6J colony ($p = 0.634$; Fig. 17A). At older ages, levels of TERT activity were not decreased in the B6Je colony relative to the B6J strain ($p = 0.095$), which might serve as a putative balancing mechanism to compensate for the shortened telomeres observed in the B6Je colony.

4.2.4 Age-dependent changes in NF-κB *RelA* and *c-Rel* gene expression

Ghosh and colleagues recently described the existence of a mechanistic feed-forward loop implicating reciprocal activating interaction between TERT and the RelA subunit of NF-κB in a malignant environment (Ghosh et al., 2012). In light of these findings, we analyzed relative mRNA expression of the NF-κB subunits *RelA* and *c-Rel* in cortical tissue from B6Je and B6J

cohorts in young and aged groups from both strains. Gene expression for each NF-κB subunit was corrected against the housekeeping gene *Gapdh* and represented as fold changes in transcript levels relative to young mice.

In line with the interaction between NF-κB RelA subunit and TERT established for a malignant environment, a significant up-regulation in the transcript levels of NF-κB *RelA* was found in aged B6Je mice relative to their young counterparts ($p < 0.001$). On the contrary, no age-associated changes in *NF-κB RelA* gene expression were observed in the B6J colony ($p = 0.403$; Fig. 17B). Moreover, *NF-κB RelA* gene expression levels in aged B6Je mice were also considerably higher than in aged B6J mice ($p < 0.001$; Fig. 17B). However, *c-Rel*, a heterodimer partner of RelA, for which a direct interaction with TERT is not yet described, showed no age-associated up-regulation in expression levels in the B6Je colony. In contrast, *c-Rel* gene expression displayed a substantial decrease with ageing in the B6J colony ($p = 0.001$; Fig. 17B). Moreover, expression levels of *c-Rel* appeared to be significantly lower in B6J mice as compared with B6Je mice ($p = 0.001$; Fig. 17B).

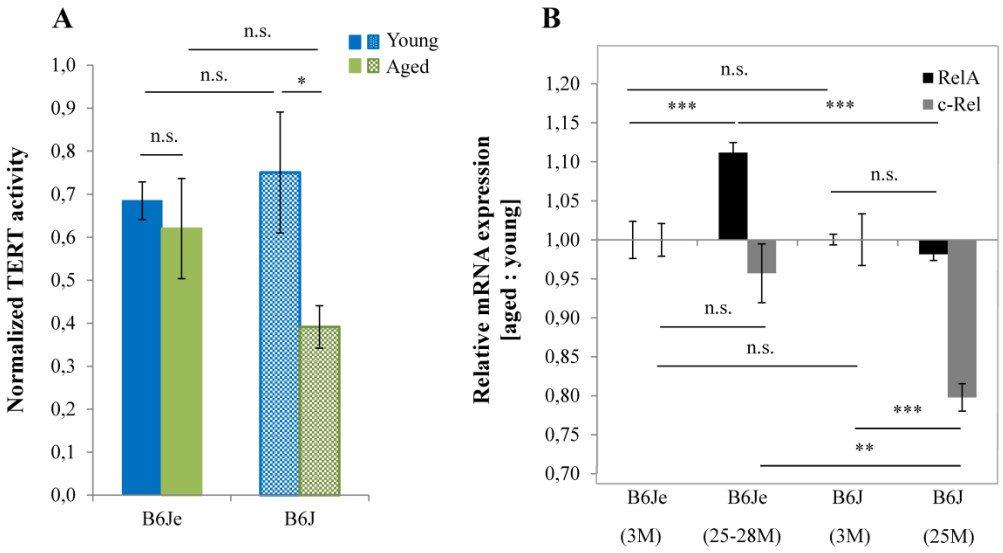

Fig. 17: Age-associated changes in the TERT activity and relative *RelA* and *c-Rel* mRNA expression levels in the murine cortex derived from B6Je and B6J mice. (A) Normalized TERT activity as a function of age. N = 5-6, Two-way ANOVA and Holm-Šidák *post hoc* test; n.s. $p > 0.05$ and * $p < 0.05$. Data are represented as means ± S.E.M. (B) Age-associated changes in the relative mRNA expression levels of canonical NF-κB *RelA* and *c-Rel* subunits, given in terms of aged:young ratios. N = 5-6, Two-way ANOVA and Tukey *post hoc* test; n.s. $p > 0.05$, * $p < 0.05$, ** $p < 0.01$ and *** $p < 0.001$. Data are represented as means ± S.E.M.

4.3 Changes in RTL with disease progression in the murine ALS-like model

4.3.1 RTL in disease susceptible cortex and spinal cord

In order to examine possible changes occurring in the telomere length of CNS tissue during the course of a neurodegenerative disease, hSOD1^{G93A} mutant mice, which serve as an established mouse model for ALS-like pathology, were used. The changes in RTL were investigated as a function of disease progression by means of the qPCR-based method already described and were specified for different disease-vulnerable CNS regions such as the cerebral cortex and, in particular, the spinal cord, which harbor primary and secondary motor neurons, respectively, and are strongly affected by the ALS pathology. For spinal cord analyses, the cervical segment was preferred since more distal regions are subjected to rapid motor neuron loss and apoptotic degeneration.

At the pre-symptomatic stage of the disease, no significant changes in the RTL were observed for the cortex and cervical spinal cord with respect to the control situation (for cortex: $p = 0.656$; for spinal cord: $p = 0.987$; Fig. 18). In contrast, a considerable increment in RTL was found for cortical tissue with disease progression, as compared with control animals ($p = 0.026$). Likewise, at the advanced stage of the disease, telomeres assessed in the cervical spinal cord tissue also showed a significant apparent elongation in comparison to the pre-symptomatic stage ($p = 0.014$), as well as relative to the healthy control situation ($p = 0.003$; Fig. 18).

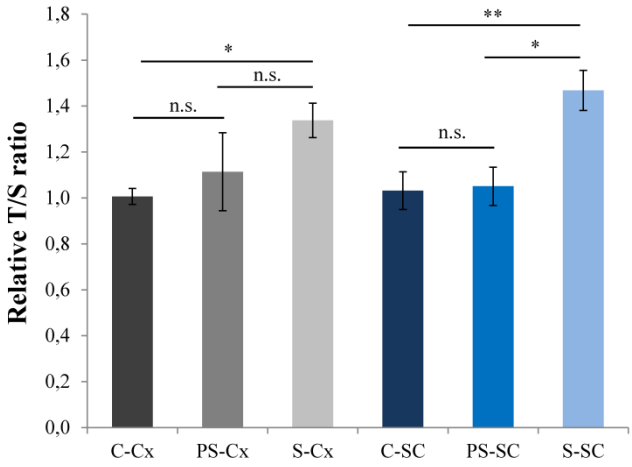

Fig. 18: Dynamics of RTL in hSOD1^{G93A} transgenic mice with disease progression. RTL assessed by a qPCR-based method for cortex (Cx) and cervical spinal cord (SC) derived from male hSOD1^{G93A} transgenic mice. RTL was analyzed at pre-symptomatic (PS) and symptomatic (S) disease stages and compared to RTL in respective healthy control tissues (C). N = 6, Two-way ANOVA; n.s. $p > 0.05$, * $p < 0.05$, ** $p < 0.01$ and *** $p < 0.001$. Data are represented as means ± S.E.M.

4.3.2 RTL in microglia

Since telomeres of both, cortex and cervical spinal cord tissue appeared to be longer at the advanced disease stage (Fig. 18), it raised the question about the cell type involved in the apparent change in RTL. A previous study by Linkus and colleagues found a tendency towards longer telomeres in microglia from the hippocampus of ALS patients relative to controls. However, they did not observe any alteration in the telomeres of neurons and astrocytes (Linkus et al., 2016). Though performed in human samples, their data provided a good reference point to set out and quantify RTL in purified microglia isolated from the cortex of the severely diseased hSOD1^{G93A} transgenic mice and in age-matched C57BL/6 control animals. Since RTL was found unchanged in the pre-symptomatic stage of the disease (Fig. 18), studies in microglia were restricted to the severe disease state. However, in our study, no elongation in RTL was observed in cortical microglia isolated at late disease stage (P = 0.406; Fig. 19). This ruled out microglia as the causal cell population responsible for the apparent increase in the RTL associated with severity of ALS disease.

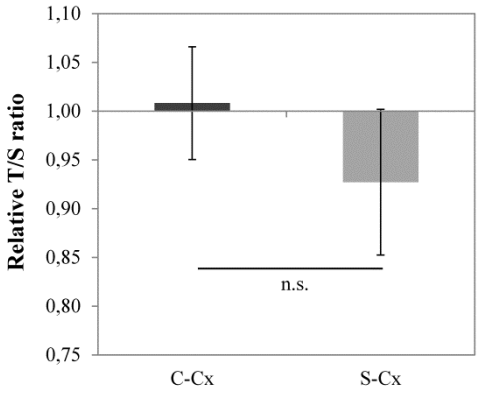

Fig. 19: Microglial telomere length. RTL was assessed in purified microglia isolated from the brain cortex (Cx) of male hSOD1^{G93A} mice at symptomatic (S) disease stage and compared to control values (C). N = 5-6, Student's t-test; n.s. $p > 0.05$. Data are represented as means ± S.E.M.

4.3.3 Region-specific changes in TERT activity with ALS disease progression

Using a qPCR-based TRAP assay, TERT activity was determined in different brain regions and in the cervical spinal cord of hSOD1^{G93A} transgenic mice at different stages of the disease. The region-specific TERT activity at pre-symptomatic (16-17 weeks) and symptomatic (19-21 weeks, clinical score 1 or 2) stages of the disease was normalized against values obtained at asymptomatic stage (6-7 weeks) for each corresponding region, and presented as arbitrary units (a.u.).

All brain regions examined displayed a similar trend towards an overall reduction in TERT activity at the symptomatic disease stage as compared with the asymptomatic control level

(Fig. 20A, B and C). The cortical region from hSOD1^{G93A} transgenic mice displayed a remarkable reduction in TERT activity with disease progression when compared with asymptomatic control levels (for presymptomatic stage: p = 0.014; for symptomatic stage: p = 0.022; Fig. 20A). In contrast, the cerebellum, which is less involved in the disease process, showed only a trend towards reduction at later disease stages (Fig. 20B). Hippocampus, a region which is involved in replicative cell renewal and cell cycle activity, presented a progressive decline in TERT activity at the presymptomatic stage (p = 0.008) and symptomatic stage (p = 0.796) relative to the control levels (Fig. 20C). In contrast, the cervical spinal cord tissue showed an up-regulation in the enzyme activity at the pre-symptomatic stage, relative to asymptomatic controls (p = 0.036), but exhibited a nonsignificant decline in enzyme activity along with further disease progression (p = 0.238; Fig. 20D).

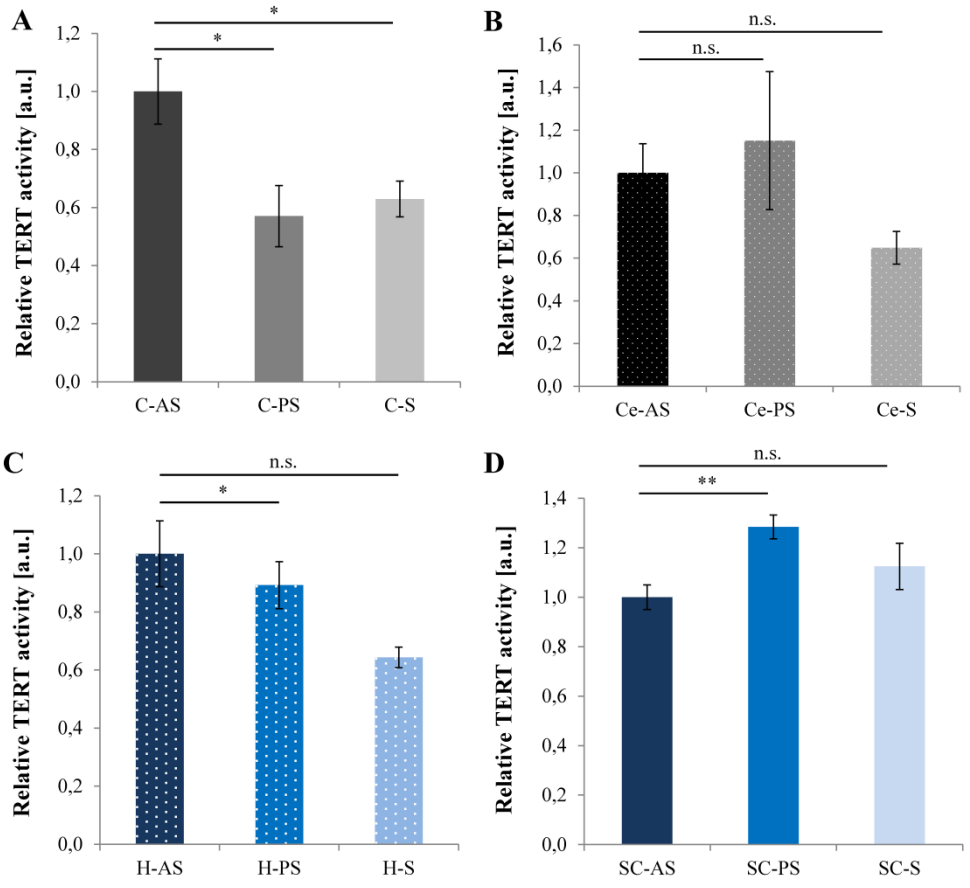

Fig. 20: TERT activity in different CNS regions as a function of disease progression. TERT activity in (A) cortex (C), (B) cerebellum (Ce), (C) hippocampus (H) and (D) cervical spinal cord (SC) tissue at asymptomatic (AS), pre-symptomatic (PS) and symptomatic (S) disease stages normalized against the asymptomatic group. N = 5-6; One way ANOVA applying Holm Šidák formula as p*ost hoc* test for A, B, D and ANOVA on rank for C; n.s. p > 0.05, * p < 0.05, ** p < 0.01 and *** p < 0.001. Data represented as means ± S.E.M.

5 DISCUSSION

Telomeres, the protective chromosomal caps, are shortened with each replicative cycle and are thus regarded as mitotic clocks, which limit replicative capacity of somatic cell. Hence, telomere ends are crucial for genome integrity and are assumed critical for lifespan of each individual organism. Though the knowledge regarding telomeres and their structural and functional regulation in dividing somatic tissues has grown enormously, corresponding issues in the post-mitotic brain are still not fully investigated. This is mainly due to the lack of adequate protocols for the isolation of neural cells and analysis of telomere length dynamics in interphase nuclei. In our study, we developed a protocol for the vital extraction of neural cells from the murine brain cortex, and combined this technique with a Flow-FISH-based approach in order to assess average telomere lengths in the healthy ageing murine brain (Ain et al., in preparation). As a further step, we assessed the effect of hermetic versus conventional inbreeding strategies on telomere length and integrity. Moreover, to determine the dependence of telomere length dynamics on the cell cycle activity in the post-mitotic interphase and moderately replicative neural cell populations in the CNS, we coupled Flow-FISH to PI-based DNA content analyses and specified RTL as a function of cell cycle activity. For some selected conditions, data obtained by Flow-FISH were verified by a PCR-based telomere length determination performed in isolated cells from corresponding tissue samples. Additionally, RTL dynamics were complemented by analyses on telomerase enzyme activity and NF-κB RelA expression. Furthermore, disease-associated changes in telomere length and telomerase activity were determined for different CNS regions in hSOD1^{G93A} transgenic mice, a well-established animal model for ALS.

5.1 Telomere length dynamics and telomerase activity in the ageing brain

In the first part of the study related to the healthy ageing model, we observed telomere shortening independently of any cell cycle activity in cortical neural cells isolated from a hermetically inbred mouse sub-strain, but not in the conventionally inbred sister colony. Comparing RTL of G_0/G_1 and G_2 phase cell populations from identical samples revealed that telomere attrition was more pronounced in the cells with active cell cycle. Telomere erosion in the neocortex of this hermetically inbred B6Je colony was accompanied by stabilized levels of TERT activity relative to the conventionally inbred B6J colony.

Since brain cortex is a region which shows a high vulnerability towards ageing-associated decay and thus is implicated in several neurodegenerative disorders (Ma et al., 2015; Raskin

et al., 2015), we specified the changes in RTL and telomerase activity primarily in the neocortex of the healthy young and senescent murine brain. Moreover, adult cortex is a non-neurogenic region, which is devoid of a self-replicative pool (Agasse et al., 2004). These features exclude a possible contribution of neural stem cells to the profound telomere shortening effect observed in the B6Je colony particularly for cell populations in the G_2 phase of the cell cycle. Furthermore, we regularly performed tissue perfusion prior to neural cell isolation to rule out any bias from the peripheral blood cell pool interfering with the telomere length measurements.

Isolation of neural cells from adult rodent brain tissue and downstream molecular analysis is technically challenging owing to the complex layered structure of several brain regions including the cortex (Lee et al., 2011), and is further complicated by the diverse cellular interactions between different neuronal and glial populations (Guez-Barber et al., 2012). Moreover, though there are many working protocols available for the isolation of neurons from different brain regions at embryonic and early postnatal ages (Pacifici and Peruzzi, 2012; Seibenhener and Wooten, 2012; Feldmann et al., 2014), only few working algorithms describe strategies for cell isolation from the mature CNS (Brewer, 1997; Brewer and Torricelli, 2007). Thus, the first step was to overcome these technical limitations and develop a protocol for the isolation of neural cells from the young as well as senescent murine CNS. The primary downstream application of such cell isolation was to measure RTL using an innovative Flow-FISH approach. Guez-Barber and his colleagues described means for neural cell isolation from the rat brain using accutase enzyme, followed by FACS purification of specific cell types (Guez-Barber et al., 2012). In analogy, we used this enzyme solution, composed of a mixture of collagenolytic and proteolytic enzymes, for neural cell isolation. However, the procedure failed technically in spite of a series of optimization steps, owing to the incomplete digestion of the tissue by this enzymatic compound, even when used at a working temperature optimal for such enzymes. Another potential problem could be the application to a brain region and species different from the experimental set up used in the work published by Guez-Barber and colleagues (Guez-Barber et al., 2012), both factors which implicate changes in tissue amount, composition and intercellular adhesion. Thereby, the authors (Guez-Barber et al., 2012) isolated cells from cerebral striatum or midbrain in the rat, whereas murine cortex was the region of interest in our study. Finally, by replacing accutase with papain enzyme and adding D-trehalose along with mechanical dissociation, we succeeded to develop a consistent working protocol for neural cell isolation from adult murine brain. Moreover, this newly established protocol proved to be a very valuable tool for cell

isolation from highly aged mice and for different CNS regions like cortex and spinal cord, thereby implicating that the isolated cells are suitable for many downstream applications including Flow-FISH, FACS, DNA extraction and qPCR (Ain et al., in preparation) and Comet assay (Penndorf et al., 2017).

To the best of our knowledge, this is the first study commencing telomere length determination under true neurosenescent conditions by using highly aged mice, beyond 24 months of age, and specified for replicative and non-replicative brain-derived neural cells. Though Flow-FISH, like TRF analysis and qPCR-based strategies, provides the average measurement of RTL, this approach was the only method currently available which enabled us to dissect between different cell cycle phases and thus bridged the knowledge between non-dividing interphase cells in G_0/G_1 phase and the cells with replicative potential, namely the G_2 phase moiety. One additional advantage of Flow-FISH over southern blotting and qPCR-based approaches is the putative cell type-specific analysis. However, coupling of Flow-FISH with classical immunocytochemistry under our conditions did not reach the required validity. We are currently optimizing Flow-FISH protocol coupled with a neuron-specific staining with Neu-O dye. Though yet not described as part of the thesis, this technique will now allow us to specify telomere length alterations directly in purified neurons (Ain et al., in preparation).

RTL determination in isolated cortical neural cells with Flow-FISH was later validated by qPCR-based telomere length measurement. Since qPCR-based strategies do not allow for cell cycle discrimination, Flow-FISH analysis and gating strategies required adjustment for comparison with qPCR-derived results. Thereby, RTL was evaluated selectively in the gate “singlets” without further discrimination of the cell cycle phases. Applying such comparison, age-associated reduction in RTL of cortical neural cells was confirmed with both methodological variants, though the effect was more pronounced when RTL was assayed by Flow-FISH as compared to the qPCR-based procedure. The difference observed in the severity of telomere length reduction might underlie several methodological and analytical reasons. In principal, the congruent pattern obtained by both methods substantiates the preciosity of our RTL determinations and might also support the establishment of a conclusive picture of telomere length dynamics in the ageing brain. Moreover, qPCR-based telomere length measurement in the murine CNS for different conditions like ageing and ALS provided an estimate of stable, reduced or even elongated telomeres which implicate the reliability and authenticity of the procedure. Further, currently ongoing analyses,

implementing Neu-O-based selection of neurons coupled with RTL measurement either by qPCR or Flow-FISH will further elucidate contribution of specific cell types to RTL changes in the CNS.

In this study, one of the novel and fundamental findings was that telomere shortening in the healthy ageing brain occurs not only in replication-active glial cells with a moderate but life-long cell cycle activity but also in non-replicative neural cells, seemingly including neurons. Though, telomere attrition in these non-dividing cells was less profound than in the cells with sustained cell cycle activity. However, this telomere shortening was only observed in the hermetically inbred B6Je colony. Moreover, though average telomere length in the replicative cortical cell population was not reduced by ageing in isolates derived from a conventionally inbred mouse strain, there was at least a strong tendency towards an age-associated shortening ($p = 0.052$). The telomere length in the G_0/G_1 arrested cell population remained unaffected by ageing in this mouse colony. Thus, the present data also substantiate that telomere integrity in the brain is affected by genomic factors, as demonstrated by the profound impact of breeding conditions on ageing-dependent and ageing-independent telomere length alterations. The presence of longer telomeres in the hermetically inbred young B6Je mice along with a higher rate of age-associated telomere attrition show that lack of genetic refreshment severely impacts on the length and integrity of the telomeres. Our data not only endorse previous findings about the lengthening of telomeres under consanguineous breeding conditions as described for blood cells (Manning et al., 2002) but also confirm it for brain cell populations. The data additionally provide evidence that hermetic inbreeding conditions reinforce telomere shortening with ageing in the murine brain, despite of its low replicative cell turnover. These observations are consistent with the notion that consanguinity exerts deleterious effects on the genome stability and integrity in general (Ruiz-Lopez et al., 2010). Moreover, exclusion of genetic refreshment as in the case of our B6Je colony can further lead to the occurrence of a genetic drift due to inheritance of deleterious genomic mutations (Casellas, 2011), a phenomenon which is associated with accelerated ageing and reduced lifespan in small inbred colonies (Lohr et al., 2014).

Owing to the basically post-mitotic nature of the CNS, there are only few studies addressing the subject of telomere length dynamics in the mammalian brain (Coviello-McLaughlin and Prowse, 1997; Takubo et al., 2002; Cherif et al., 2003; Flanary and Streit, 2003; Nakamura et al., 2007; Takubo et al., 2010; Dlouha et al., 2014). Flanary and Streit reported telomere shortening in the cortex and cerebellum of rat brains, with ages ranging between P21 and 5

months when analyzed by TRF (Flanary and Streit, 2003). However, brains at higher ages were not addressed in this study. In contrast, in a contemporary study, telomere lengths in the rat brain were described to remain stable at least up to the age of 15 months when compared to P21 and 3 months old controls, though region-specific telomere length dynamics were not concealed in this study (Cherif et al., 2003). In a previous study using southern blotting for the TRF-based telomere length assessment, no age-associated or region-dependent changes in the average telomere length were observed in the cerebellum, hippocampus and sub-ventricular zone of the murine brain, (Coviello-McLaughlin and Prowse, 1997). Likewise, in human postmortem cerebral cortex derived from individuals at ages between 0-104 years, no changes in the average length of those telomeres was detected (Takubo et al., 2002; Takubo et al., 2010). However, the rate of extremely short telomeres (<6kb) was found to be increased to an extent comparable with other replicative tissues (Takubo et al., 2010). In contrast, in the rat ageing brain no increase in the moiety of short telomeres was reported (Cherif et al., 2003).

The discrepancy in results obtained by different studies can be subjected to the variations arising from the different brain regions analyzed and heterogeneous age categories included in these studies. This also reflects the need for further approaches to clarify the nature of telomere length changes in the CNS. Subsequently, the strategy developed in our study represents a feasible approach to address this highly relevant issue.

The increase in the levels of reactive oxygen species (ROS) and subsequent DNA damage in the ageing brain (Ishii et al., 2017) serves as underlying mechanism in the pathology of various neurodegenerative diseases (Beal et al., 1997; Zhu et al., 2000). Additionally, guanine-rich telomeres are more prone to acquire permanent oxidation-mediated DNA damage and telomere erosion (Kawanishi and Oikawa, 2004; Coluzzi et al., 2014). Thus, beside the replication-associated telomere reduction, which is relevant in particular for our cells in G_2 phase, ROS-mediated telomere damage may contribute to the telomere attrition process and provide an explanation for the telomere shortening detected in the non-replicative neural cell pool. The coincidence of telomere erosion in both the replicative and non-replicative cell moieties of the B6Je strain with sustained levels of TERT activity may point to the induction of protective roles of the telomerase enzyme, which are known to counteract ROS-mediated cellular stress (Ahmed et al., 2008; Haendeler et al., 2009). However, the interplay between increased ROS-mediated DNA damage with ageing and TERT activity needs to be further elucidated.

Furthermore, our data show a shift in neural cell cycle activity with ageing, as marked by an increment in the DNA content of cortical neural cells isolated from both murine sister colonies. In general, the DNA histograms based on the PI staining established for the aged samples from both murine cohorts displayed a consistent pattern and exhibited a shift towards a higher frequency of cells with an increased DNA content as compared with the samples from young animals. Beside the observation that aged mice displayed an increment in the number of cells with higher DNA content, the proportion of the cells in G_0/G_1 phase decreased as compared to the young animals. Thus, our data provide evidence for the re-induction of the atypical cell cycle activity in the ageing brain as described previously (Zhang and Herrup, 2011). However, the identity of the cell types which displayed the DNA content variation due to regular or abortive cell cycle activity is yet not defined. Moreover, up to 50% of these neural cells in the cortical cell isolates appeared to have neuronal identity, reflecting that neurons are also subjected to DNA content variations along with glial cell populations, despite the existence of life-long intrinsic control processes to block replication (Herrup and Yang, 2007). This observation supports some previous evidences referring that up to 10-20% of the cortical neurons, both under healthy brain ageing and under AD pathology display a higher DNA content than expected for neurons in a stable, quiescent G_0 phase (Mosch et al., 2007; Fischer et al., 2012). The DNA content variations observed in these neurons might point to loss of control on cell cycle activity, which then can trigger aberrant and abortive cell cycle re-entry and ultimately leads to neuronal death (Arendt and Brückner, 2007; Zhang and Herrup, 2011).

The analysis of the activity of the TERT subunit of the telomerase enzyme, which is responsible for the *de novo* addition of the telomere repeats to the chromosomal ends, also showed strain-specific differences. The relatively maintained levels of TERT at higher age in the hermetically inbred sub-strain as compared to the conventionally inbred colony might reflect a sort of compensatory mechanism to overcome the faster rate of telomere erosion in the extremely inbred strain. Sustained levels of cortical TERT activity in the B6Je colony relative to the B6J mice might also be related to extra-telomeric functions of TERT. Likewise, TERT is thought to be involved in cell protective, anti-apoptotic, proliferative and survival functions. With regard to the canonical functions of the telomerase enzyme, TERT activity was long assumed to be restricted to highly proliferative organs such as the intestine, and to stem cell niches. However, different studies have pointed to the existence of substantial TERT expression and activity in the adult mammalian brain. Flanary and Streit showed a steady increment in the TERT activity levels in cortex and cerebellum of adult rats from day 21 up to

6 months of age. In their study, however, they did not explore the TERT activity in highly aged animals (Flanary and Streit, 2003). In the human brain, on the contrary, TERT activity was shown to already decline during fetal development and attain undetectable levels in adults. In contrast, TERT protein levels were discovered to increase steadily from development to adulthood in the human brain (Ishaq et al., 2016). Differential patterns of TERT protein expression and activity levels during development and adulthood suggest that these two elements do not correlate with each other. Eitan and colleagues (2016) further characterized the relationship between TERT protein and activity levels in different sub-cellular fractions of the murine cortex at ages ranging from prenatal day 14 to 20-22 months, and found a negative correlation between the TERT protein and enzyme activity level in the cytoplasmic and nuclear-bound fractions. In particular, the nuclear-bound fraction displayed low TERT activity levels at embryonic state but augmented activity levels with ageing, whereas the protein levels were decreased at adult stage (Eitan et al., 2016). In contrast, the cytoplasmic fraction presented very high TERT activity levels at the embryonic stage, which then decreased with ageing, while an opposite regulation was described for the TERT protein levels in the same fraction (Eitan et al., 2016). All these studies point to a differential regulation of TERT activity and protein and its involvement in non-canonical functions in the brain. Likewise, execution of conventional telomere elongation functions requires nuclear TERT protein expression and activity, whereas cytoplasmic location might implicate alternative TERT actions such as ROS-neutralization in mitochondria. Accordingly, constitutive TERT protein expression in different brain regions of rodents is assumed to be crucial for the regulation of normal organ function (Lee et al., 2010). Additionally, following oxidative stress exposure, 80-90% of TERT protein translocates from the nucleus to mitochondria and improves the mitochondrial function by causing an increase in mitochondrial membrane potential and by supporting the reduction of ROS production (Ahmed et al., 2008). Also, TERT has been shown to protect the mitochondrial DNA itself against UV-induced DNA damage (Haendeler et al., 2009). Spilsbury and colleagues showed similar nucleus-to-mitochondria translocation of TERT in the human hippocampus isolated from AD patients at advanced disease stages and pointed to a protective role against Tau-related pathology (Spilsbury et al., 2015). Furthermore, in somatic tissues including post-mitotic brain, TERT can improve tissue regeneration and rejuvenation and enhance cell survival, as TERT exerts anti-apoptotic functions in neurons after various kinds of ischemic and neurotoxic insults (Zhu et al., 2000; Fu et al., 2002; Kang et al., 2004; Jaskelioff et al., 2011). However, the requirement of a certain subcellular TERT location to perform such

rejuvenation and survival functions is still undefined. At least, these studies suggest the prevalence and functional relevance of enzymatically active and inactive TERT protein in the non-regenerative regions of the post-mitotic brain, not only at the developmental stages but also at higher chronological ages. In line with these findings, we observed substantial TERT activity in the non-neurogenic murine cortex isolated from young and aged mice of both B6 cohorts. Thus, detected shorter telomeres and sustained levels of TERT activity in the neocortex of aged B6Je mice as compared to their young counterparts might point to a counteracting response to reduce neurosenescence and maintain tissue homeostasis. However, a specific protective effect of TERT on the highly vulnerable telomeres in the ageing brain needs to be further elucidated.

TERT also interacts with different transcription factors and modulates several cell signaling pathways, for example the Wnt/β catenin pathway (Park et al., 2009; Zhang et al., 2012; Listerman et al., 2014) and NF-κB pathway (Yin et al., 2000; Ghosh et al., 2012). NF-κB is a cardinal regulator of ageing-associated genetic re-modelling in different tissues including the CNS. Constitutive activation of NF-κB and its downstream targets mediate chronic inflammation, also in the ageing brain via telomere dysfunction and accelerated senescence (Adler et al., 2007; Jurk et al., 2014). NF-κB interacts with TERT promoter regions and activates TERT expression (Yin et al., 2000) and, in turn, the NF-κB canonical pathway is regulated by a feed-forward interaction between TERT and the RelA subunit of NF-κB (Ghosh et al., 2012; Wu et al., 2016). In a malignant environment, NF-κB RelA and TERT expression levels are simultaneously augmented (Wang et al., 2004b; Ghosh et al., 2012). Moreover, in healthy to malignant cell transformation as assessed by *in vitro* systems, TERT directly stimulates the binding of RelA to the NF-κB downstream target gene promoters by inducing the RelA, but not c-Rel subunit of canonical NF-κB. Such interplay then leads to the up-regulation of the NF-κB inflammatory pathway. Subsequently, sustained and high levels of NF-κB target genes enhance the TERT expression via a feed-forward loop (Ghosh et al., 2012). A similar molecular interaction between TERT and NF-κB RelA subunit was recently proposed for the mouse model of alcoholic liver disease (ALD) (Wu et al., 2016).

In light of such evidences reported for malignant conditions, our findings regarding relatively sustained TERT activity levels in the neocortex of senescent B6Je mice prompted us to examine the expression levels of NF-κB RelA in the healthy ageing murine brain. Accordingly, RelA expression levels were found significantly higher in the neocortex of the aged B6Je colony as compared to their young littermates as well as relative to the aged B6J

mice, which showed significant age-associated reduction in the levels of the TERT activity. Thus, sustained TERT activity was accompanied by a corresponding up-regulation of RelA expression in the aged B6Je sub-strain, which displayed accelerated telomere erosion. These data also suggest that a similar feed-forward interaction between TERT and NF-κB RelA might exist in the CNS, as recently described in a malignant environment. In analogy, augmented RelA expression levels may partially contribute to the relatively unchanged TERT activity levels observed in the hermetically inbred aged B6Je colony. On the other hand, the observed increase in the RelA expression level in the ageing brain of the B6Je sub-strain also supports the prevailing notion of increased inflammation in the ageing brain (Gabuzda and Yankner, 2013). Such interplay may also accentuate the complex and indefinite role of NF-κB in healthy tissue aging in general, and underline its crucial role in mediating ageing-associated inflammation of the brain. We also observed a significant decrease in the expression levels of c-Rel in the aged B6J colony as compared to their young counterparts and also in comparison to the aged B6Je sub-strain, and this was accompanied by a significant reduction in TERT activity levels. Interestingly, knockout of c-Rel has been associated to an ageing phenotype in the mouse brain (Lanzillotta et al., 2015). Whether TERT is involved in direct or indirect regulation of c-Rel of canonical NF-κB is yet unclear and needs further examination. It will also be interesting to see whether TERT supports cell survival and homeostasis in the CNS, e.g., via interaction with canonical NF-κB subunits such as RelA and c-Rel. Furthermore, influence of breeding conditions and genetic refreshment on such molecular loops is not yet explored.

5.2 **Disease-associated changes in telomere length and telomerase activity**

Although the telomere length of the chromosomes in the healthy ageing human brain is currently thought to remain unaltered (Takubo et al., 2002; Takubo et al., 2010), loss of telomere integrity, either detected in blood or directly in CNS tissue, has indeed been associated with many neurodegenerative disorders (Panossian et al., 2003; Thomas et al., 2008; Kota et al., 2014). Nevertheless, such studies are still few, and only a rare number is addressing the role of telomere integrity and telomerase activity in the ALS disorder (Eitan et al., 2012; De Felice et al., 2014; Eitan et al., 2016; Linkus et al., 2016). ALS is an age-associated disease of the central and peripheral nervous system, which implicates progressive demise of motor neurons and associated neuro-muscular units. Its pathology is characterized by a rapidly progressing paralysis of bulbar, skeletal and respiratory muscles, which ultimately leads to the death of the individuals (reviewed by D'Amico et al., 2013; Paulukonis

et al., 2015).The underlying mechanisms involved in ALS-related pathological neurodegeneration are complex and not yet apprehended completely. A frequently used animal model resembling human ALS pathology is the hSOD1^{G93A} transgenic mouse model which expresses a high copy number of a mutated human super oxide dismutase 1 (*hSOD1*) gene.

In the second part of the study, we analyzed the disease-associated changes in telomere length dynamics in CNS regions principally affected by the disease course, including the neocortex and cervical spinal cord derived from hSOD1^{G93A} transgenic mice. Surprisingly, we observed a remarkable lengthening of telomeres at the advanced stage of the disease in both cortex and cervical spinal cord as compared with age-matched control and pre-symptomatic mice. These results are unexpected in light of the association of intact telomeres with genomic and functional cell preservation. Moreover, in a recent study Linkus and colleagues showed stable and unaltered telomere lengths in neurons and astrocytes from hippocampus of human ALS patients (Linkus et al., 2016). Interestingly, in the same study, Linkus and colleagues found a tendency towards longer telomeres in microglia as compared to the healthy controls (Linkus et al., 2016). Likewise, previous studies conducted with material derived from human patients suffering from neurodegenerative AD either showed unaltered telomere length (Lukens et al., 2009) or shortened telomeres as compared to healthy controls (Franco et al., 2006). However, in support of our findings, a recent study by Thomas and co-workers also discovered longer telomeres in hippocampi from AD patients as compared to the healthy controls, and this was seemingly observed without any gender effect (Thomas et al., 2008). Since hippocampus is known to possess regenerative capacity from its stem cell pool throughout the adult lifespan, which normally leads to telomere attrition in respective dividing populations, such findings of unaltered or elongated telomeres are similarly unexplained. They are also in opposition to a previous study showing telomere erosion in hippocampal neurons from AD patients (Franco et al., 2006). The possible mechanism responsible for the telomere lengthening observed in hippocampus is unknown, but it was proposed to result either from alternative lengthening of telomeres (ALT) or be due to a presumed lower frequency in regenerative cell cycle turnover in AD affected hippocampi (Thomas et al., 2008). Thus, discrepancies in telomere length assessments under neurodegenerative conditions are seemingly not restricted to ALS, but an issue unresolved also for AD and maybe other disease entities. Since in our study, both cortex and spinal cord tissue from the diseased hSOD1^{G93A} transgenic mice are devoid of proliferative activity, low regenerative capacity appears unlikely as a reason for the observed telomere lengthening. In contrast, the significant telomere lengthening, which occurred within

a short time of 4-5 weeks along with progression of the disease from the pre-symptomatic to the symptomatic stage, may be the result of ALT mechanisms. ALT, defined as molecular strategies to extend telomeres independently of telomerase activity, can arise from end-to-end fusion of very short telomeres, which may occur as a consequence, e.g., of the ALS disease process alongside with the loss of TERT activity. ALT is supposed to be active also in the absence of extremely short telomeres, can originate from extrachromosomal telomere circles or telomere copying events that form along with homologous recombination (HR) in a context of telomere instability and is most frequently found in immortalized or tumor cells (Cesare and Reddel, 2010, 2013; Samassekou et al., 2013). Moreover, irrespective of HR, extrachromosomal telomeric circles can be generated as a result of DNA damage or TERT overexpression (Wang et al., 2004a; Fasching et al., 2007; Pickett et al., 2009). The molecular bases for the possible role of ALT in the senescent and neurodegenerative CNS still has to be explored. Therefore, further analyses, e.g., based on 2D gel electrophoresis will reveal the presence of extrachromosomal telomeric circles and high telomere length heterogeneity, which serve as hallmarks of ALT (Nabetani and Ishikawa, 2011; Samassekou et al., 2013).

ALS is characterized by the severe loss of motor neurons especially in spinal cord tissue (Kiernan et al., 2011; Brettschneider et al., 2013). Hence, another possible explanation is that the increase in telomere length observed for cortex and spinal cord tissue at advanced disease stages results from the loss of neural cells with shorter telomeres, with preservation of cell populations with still intact telomere ends, thus leading to an apparent telomere elongation. Since many motor neurons are lost at advanced disease stage (Kiernan et al., 2011; Brettschneider et al., 2013) and microglia displayed a tendency towards longer telomeres in human ALS patients, we hypothesized that microglia could be the cell population responsible for the lengthening of telomeres detected at late disease stages in hSOD1^{G93A} mice. Moreover, microglia are assumed to play a dual role in ALS, with both neuroprotective and neurotoxic functions (Liao et al., 2012; Chiu et al., 2013). Therefore, we measured the telomere length in isolated cortical microglia from symptomatic and control mice. However, we did not observe any changes in microglial telomere length relative to the age-matched controls, which ruled out microglia as a potential contributing cell type to the observed lengthening of telomeres. Whether other neural cell types are likely to be involved in this increment in the average telomere length is still an open question and needs further investigation. Apart from average telomere length estimations, analyses on absolute telomere lengths are required to explore whether the recognition of longer telomeres under neurodegenerative conditions such as ALS

or AD have to be seen in the light of a relative pseudo-elongation, e.g. due to the loss of cells with short telomeres, or due to true TTAGGG sequence amplification.

In spite of the increasing knowledge on the role of TERT protein in the brain, a region-dependent profile of TERT activity in ALS-susceptible brain and spinal cord regions, and a corresponding mapping of enzyme activity versus protein expression levels, alongside with the disease process was not explored yet. Therefore in our study, we also assessed the changes in TERT activity as a function of the ALS disease progression in the hSOD1^{G93A} mutant strain, thereby addressing different CNS regions including the spinal cord. Using a qPCR-based TRAP assay, TERT activity was found reduced in all the brain regions investigated as compared to the asymptomatic mutant mice. In contrast, the cervical spinal cord tissue displayed a relative increment in the TERT activity along with disease progression. In a recent study, De Felice and colleagues described lower levels of TERT activity in terms of TERT protein expression in leucocytes and postmortem spinal cord tissue of ALS patients, relative to the controls. Moreover, lower TERT protein expression was also associated with shorter telomere lengths in blood leucocytes from these patients relative to the healthy controls (De Felice et al., 2014). It needs further determination whether a low TERT protein expression observed in ALS patients directly correlates with a low activity since a direct correlation between the TERT protein expression and TERT activity could not be established, at least for the murine organism (Eitan et al., 2016). Thus, our approach to define telomere length and TERT activity in a region-specific and disease state-dependent manner aimed to improve our current understanding of the telomere biology and specify it for the peculiar conditions of neurosenescence and neurodegeneration.

6 CONCLUSIONS AND OUTLOOK

In summary, this study addressed changes in the average telomere length occurring in the healthy ageing brain and under ALS-like neurodegenerative conditions. For the first time we analyzed telomere length dynamics selectively in replicative and non-replicative cell populations of the ageing murine brain and their dependency on genetic refreshment by using a Flow-FISH-based approach. Our data reveal that proliferation is not the only prerequisite for telomere shortening in the ageing brain. By applying hermetic inbreeding conditions we observed replication-independent telomere shortening in post-mitotic neural cells, a population which is assumed to contain up to 50% non-dividing neurons. Nonetheless, telomere shortening was found more pronounced in the dividing cell moiety. In addition to these observations, our data also showed an age-associated induction of cell cycle activity in the murine brain, a process recently found to contribute also to neuronal dysfunction and death. Further studies are now envisaged to identify the neural cell types responsible for the shift in the cell cycle activity and the observed telomere length shortening in the senescent brain. Our results also substantiate the influence of other factors like regular genetic refreshment on telomere length and rate of telomere erosion in the ageing brain. In this context, we show that neural telomere attrition is faster in animals which are devoid of genetic refreshment for longer periods. This observation suggests that the rate of telomere shortening and not the absolute telomere lengths might serve as a predictive factor for the ageing process of an organism. Moreover, under consanguineous breeding conditions, shorter telomere lengths both of the dividing and non-dividing neural cells were accompanied by stabilized activity levels of TERT subunit of the telomerase enzyme. The enzymatically active moiety of telomerase enzyme, which is responsible for preserving telomere length shares a mechanistic feed-forward loop with RelA subunit of canonical NF-κB, and this interaction might be involved in a putative TERT-RelA-mediated compensatory mechanism to compensate the faster rate of telomere shortening observed in the hermetic bred strain. Consistent with this hypothesis, unchanged TERT activity levels were accompanied by an increase in the expression levels of the NF-κB RelA subunit. Considering additional pleiotropic functions exerted by NF-κB in the CNS, molecular or pharmacological interference with TERT-RelA interplay may provide a possible target to prevent senescence and modulate degeneration in the CNS. However, the observed increase in RelA transcription levels may also due to the increased inflammation associated with ageing and thus it would underscore the ambivalent roles of NF-κB in the ageing brain. Therefore, one challenging aspect for future studies will be to investigate the intricate link between NF-κB pathway and chromosomal integrity and its

possible contribution to the underlying mechanism involved in neurosenescence and neurodegeneration.

As a second important aspect, this study provides a disease-associated profile of telomere length and telomerase activity in hSOD1^{G93A} mutant mice, an established model for ALS pathology. The molecular basis for the telomere lengthening observed in the cortex and spinal cord with severity of the disease is currently unknown. However, increased telomere lengths in CNS regions vulnerable to ALS-related pathobiology might also be indicative of an alternative telomere lengthening process. Such a process of conserved, but unconventional telomere elongation implicates an extensive erosion of telomeres as a first step, and a subsequent fusion of the arising critically short telomeres, which may be propagated with disease progression. It can also be a result of a TERT-independent telomere amplification from extrachromosomal telomere circles, though such a mechanism is not yet established independently of HR and thus requires consolidation for CNS circumstances. As an alternative explanation, the observed lengthening of telomeres might represent a pseudo-lengthening due to the loss of vulnerable cell populations with relatively short telomeres at advanced disease stages. Furthermore, our data also prove a region-specific regulation of TERT activity in the diseased CNS, which varies with disease progression. These observations provide a basis for future studies, aimed to elucidate the role of telomere biology in the pathophysiology of neurosenescence and neurodegeneration, like the ALS-related pathology.

7 LITERATURE

Adler AS, Sinha S, Kawahara TL, Zhang JY, Segal E, Chang HY (2007) Motif module map reveals enforcement of aging by continual NF-κB activity. Genes & development 21:3244-3257.

Agasse F, Roger M, Coronas V (2004) Neurogenic and intact or apoptotic non-neurogenic areas of adult brain release diffusible molecules that differentially modulate the development of subventricular zone cell cultures. European Journal of Neuroscience 19:1459-1468.

Ahmed S, Passos JF, Birket MJ, Beckmann T, Brings S, Peters H, Birch-Machin MA, von Zglinicki T, Saretzki G (2008) Telomerase does not counteract telomere shortening but protects mitochondrial function under oxidative stress. Journal of cell science 121:1046-1053.

Aida J, Izumiyama-Shimomura N, Nakamura K-i, Ishikawa N, Terai M, Matsuda Y, Aida S, Arai T, Takubo K (2014) Determination of telomere length by the quantitative fluorescence in situ hybridization (Q-FISH) method. American Journal of Analytical Chemistry 5:775.

Allshire RC, Dempster M, Hastie ND (1989) Human telomeres contain at least three types of G–rich repeat distributed non-randomly. Nucleic acids research 17:4611-4627.

Andrew T, Aviv A, Falchi M, Surdulescu GL, Gardner JP, Lu X, Kimura M, Kato BS, Valdes AM, Spector TD (2006) Mapping genetic loci that determine leukocyte telomere length in a large sample of unselected female sibling pairs. The American Journal of Human Genetics 78:480-486.

Arendt T (2012) Cell cycle activation and aneuploid neurons in Alzheimer's disease. Molecular neurobiology 46:125-135.

Arendt T, Brückner MK (2007) Linking cell-cycle dysfunction in Alzheimer's disease to a failure of synaptic plasticity. Biochimica et Biophysica Acta (BBA)-Molecular Basis of Disease 1772:413-421.

Aviv A (2002) Telomeres, sex, reactive oxygen species, and human cardiovascular aging. Journal of Molecular Medicine 80:689-695.

Baird DM (2005) New developments in telomere length analysis. Experimental gerontology 40:363-368.

Beal MF, Ferrante RJ, Browne SE, Matthews RT, Kowall NW, Brown RH (1997) Increased 3-nitrotyrosine in both sporadic and familial amyotrophic lateral sclerosis. Annals of neurology 42:644-654.

Brettschneider J, Del Tredici K, Toledo JB, Robinson JL, Irwin DJ, Grossman M, Suh E, Deerlin VM, Wood EM, Baek Y (2013) Stages of pTDP-43 pathology in amyotrophic lateral sclerosis. Annals of neurology 74:20-38.

Brewer GJ (1997) Isolation and culture of adult rat hippocampal neurons. Journal of neuroscience methods 71:143-155.

Brewer GJ, Torricelli JR (2007) Isolation and culture of adult neurons and neurospheres. Nature protocols 2:1490-1498.

Broer L, Codd V, Nyholt DR, Deelen J, Mangino M, Willemsen G, Albrecht E, Amin N, Beekman M, De Geus EJ (2013) Meta-analysis of telomere length in 19 713 subjects reveals high heritability, stronger maternal inheritance and a paternal age effect. European journal of human genetics 21:1163-1168.

Calado RT, Young NS (2008) Telomere maintenance and human bone marrow failure. Blood 111:4446-4455.

Calado RT, Dumitriu B (2013) Telomere dynamics in mice and humans. In: Seminars in hematology, pp 165-174: Elsevier.

Canela A, Vera E, Klatt P, Blasco MA (2007) High-throughput telomere length quantification by FISH and its application to human population studies. Proceedings of the National Academy of Sciences 104:5300-5305.

Casellas J (2011) Inbred mouse strains and genetic stability: a review. Animal 5:1-7.

Cawthon RM (2002) Telomere measurement by quantitative PCR. Nucleic acids research 30:e47-e47.
Cawthon RM (2009) Telomere length measurement by a novel monochrome multiplex quantitative PCR method. Nucleic acids research 37:e21-e21.
Cen J, Zhang H, Liu Y, Deng M, Tang S, Liu W, Zhang Z (2015) Anti-aging effect of estrogen on telomerase activity in ovariectomised rats–animal model for menopause. Gynecological Endocrinology 31:582-585.
Cesare AJ, Reddel RR (2010) Alternative lengthening of telomeres: models, mechanisms and implications. Nature reviews genetics 11:319-330.
Cesare AJ, Reddel RR (2013) Alternative lengthening of telomeres in mammalian cells.
Cherif H, Tarry J, Ozanne S, Hales C (2003) Ageing and telomeres: a study into organ-and gender-specific telomere shortening. Nucleic acids research 31:1576-1583.
Chiodi I, Mondello C (2012) Telomere-independent functions of telomerase in nuclei, cytoplasm, and mitochondria. Frontiers in oncology 2.
Chiu IM, Morimoto ET, Goodarzi H, Liao JT, O'Keeffe S, Phatnani HP, Muratet M, Carroll MC, Levy S, Tavazoie S (2013) A neurodegeneration-specific gene-expression signature of acutely isolated microglia from an amyotrophic lateral sclerosis mouse model. Cell reports 4:385-401.
Cohen SB, Graham ME, Lovrecz GO, Bache N, Robinson PJ, Reddel RR (2007) Protein composition of catalytically active human telomerase from immortal cells. Science 315:1850-1853.
Coluzzi E, Colamartino M, Cozzi R, Leone S, Meneghini C, O'Callaghan N, Sgura A (2014) Oxidative stress induces persistent telomeric DNA damage responsible for nuclear morphology change in mammalian cells. PLoS One 9:e110963.
Coviello-McLaughlin GM, Prowse KR (1997) Telomere length regulation during postnatal development and ageing in Mus spretus. Nucleic acids research 25:3051-3058.
D'Amico E, Factor-Litvak P, Santella RM, Mitsumoto H (2013) Clinical perspective on oxidative stress in sporadic amyotrophic lateral sclerosis. Free Radical Biology and Medicine 65:509-527.
Dalgård C, Benetos A, Verhulst S, Labat C, Kark JD, Christensen K, Kimura M, Kyvik KO, Aviv A (2015) Leukocyte telomere length dynamics in women and men: menopause vs age effects. International journal of epidemiology 44:1688-1695.
De Felice B, Annunziata A, Fiorentino G, Manfellotto F, D'Alessandro R, Marino R, Borra M, Biffali E (2014) Telomerase expression in amyotrophic lateral sclerosis (ALS) patients. Journal of human genetics 59:555-561.
De Lange T (2005) Shelterin: the protein complex that shapes and safeguards human telomeres. Genes & development 19:2100-2110.
De Meyer T, Rietzschel ER, De Buyzere ML, De Bacquer D, Van Criekinge W, De Backer GG, Gillebert TC, Van Oostveldt P, Bekaert S (2007) Paternal age at birth is an important determinant of offspring telomere length. Human molecular genetics 16:3097-3102.
Dlouha D, Maluskova J, Lesna IK, Lanska V, Hubacek J (2014) Comparison of the relative telomere length measured in leukocytes and eleven different human tissues. Physiological research 63:S343.
Eitan E, Hutchison ER, Mattson MP (2014) Telomere shortening in neurological disorders: an abundance of unanswered questions. Trends in neurosciences 37:256-263.
Eitan E, Tichon A, Priel E (2016) Dissociation between telomerase activity and expression during mice cortical development due to a DNA-bound telomerase inhibitor. Matters Select 2:e201604000008.
Eitan E, Tichon A, Gazit A, Gitler D, Slavin S, Priel E (2012) Novel telomerase-increasing compound in mouse brain delays the onset of amyotrophic lateral sclerosis. EMBO molecular medicine 4:313-329.
Epel ES, Blackburn EH, Lin J, Dhabhar FS, Adler NE, Morrow JD, Cawthon RM (2004) Accelerated telomere shortening in response to life stress. Proceedings of the National Academy of Sciences of the United States of America 101:17312-17315.

Erraji-Benchekroun L, Underwood MD, Arango V, Galfalvy H, Pavlidis P, Smyrniotopoulos P, Mann JJ, Sibille E (2005) Molecular aging in human prefrontal cortex is selective and continuous throughout adult life. Biological psychiatry 57:549-558.

Farzaneh-Far R, Lin J, Epel ES, Harris WS, Blackburn EH, Whooley MA (2010) Association of marine omega-3 fatty acid levels with telomeric aging in patients with coronary heart disease. Jama 303:250-257.

Fasching CL, Neumann AA, Muntoni A, Yeager TR, Reddel RR (2007) DNA Damage Induces Alternative Lengthening of Telomeres (ALT)–Associated Promyelocytic Leukemia Bodies that Preferentially Associate with Linear Telomeric DNA. Cancer research 67:7072-7077.

Feldmann M, Pathipati P, Sheldon RA, Jiang X, Ferriero DM (2014) Isolating astrocytes and neurons sequentially from postnatal murine brains with a magnetic cell separation technique. Journal of Biological Methods 1:e11.

Fischer HG, Morawski M, Brückner MK, Mittag A, Tarnok A, Arendt T (2012) Changes in neuronal DNA content variation in the human brain during aging. Aging Cell 11:628-633.

Flanary BE, Streit WJ (2003) Telomeres shorten with age in rat cerebellum and cortex in vivo. Journal of anti-aging medicine 6:299-308.

Floyd RA, Carney JM (1992) Free radical damage to protein and DNA: mechanisms involved and relevant observations on brain undergoing oxidative stress. Annals of Neurology 32.

Franco S, Blasco MA, Siedlak SL, Harris PL, Moreira PI, Perry G, Smith MA (2006) Telomeres and telomerase in Alzheimer's disease: Epiphenomena or a new focus for therapeutic strategy? Alzheimer's & Dementia 2:164-168.

Fu W, Lu C, Mattson MP (2002) Telomerase mediates the cell survival-promoting actions of brain-derived neurotrophic factor and secreted amyloid precursor protein in developing hippocampal neurons. Journal of Neuroscience 22:10710-10719.

Fumagalli M, Rossiello F, Clerici M, Barozzi S, Cittaro D, Kaplunov JM, Bucci G, Dobreva M, Matti V, Beausejour CM (2012) Telomeric DNA damage is irreparable and causes persistent DNA-damage-response activation. Nature cell biology 14:355-365.

Gabuzda D, Yankner BA (2013) Physiology: Inflammation links ageing to the brain. Nature 497:197-198.

Gardner M, Bann D, Wiley L, Cooper R, Hardy R, Nitsch D, Martin-Ruiz C, Shiels P, Sayer AA, Barbieri M (2014) Gender and telomere length: systematic review and meta-analysis. Experimental gerontology 51:15-27.

Garforth SJ, Wu YY, Prasad VR (2006) Structural features of mouse telomerase RNA are responsible for the lower activity of mouse telomerase versus human telomerase. Biochemical Journal 397:399-406.

Ghosh A, Saginc G, Leow SC, Khattar E, Shin EM, Yan TD, Wong M, Zhang Z, Li G, Sung W-K (2012) Telomerase directly regulates NF-κB-dependent transcription. Nature cell biology 14:1270-1281.

Greider CW, Blackburn EH (1987) The telomere terminal transferase of Tetrahymena is a ribonucleoprotein enzyme with two kinds of primer specificity. Cell 51:887-898.

Griffith JD, Comeau L, Rosenfield S, Stansel RM, Bianchi A, Moss H, De Lange T (1999) Mammalian telomeres end in a large duplex loop. Cell 97:503-514.

Guez-Barber D, Fanous S, Harvey BK, Zhang Y, Lehrmann E, Becker KG, Picciotto MR, Hope BT (2012) FACS purification of immunolabeled cell types from adult rat brain. Journal of neuroscience methods 203:10-18.

Haendeler J, Dröse S, Büchner N, Jakob S, Altschmied J, Goy C, Spyridopoulos I, Zeiher AM, Brandt U, Dimmeler S (2009) Mitochondrial telomerase reverse transcriptase binds to and protects mitochondrial DNA and function from damage. Arteriosclerosis, thrombosis, and vascular biology 29:929-935.

Harley CB, Vaziri H, Counter CM, Allsopp RC (1992) The telomere hypothesis of cellular aging. Experimental gerontology 27:375-382.

Hayflick L (1965) The limited in vitro lifetime of human diploid cell strains. Experimental cell research 37:614-636.
Hemann MT, Greider CW (2000) Wild-derived inbred mouse strains have short telomeres. Nucleic acids research 28:4474-4478.
Herculano-Houzel S, Watson C, Paxinos G (2013) Distribution of neurons in functional areas of the mouse cerebral cortex reveals quantitatively different cortical zones. Frontiers in neuroanatomy 7.
Herrup K, Yang Y (2007) Cell cycle regulation in the postmitotic neuron: oxymoron or new biology? Nature Reviews Neuroscience 8:368-378.
Höglinger GU, Breunig JJ, Depboylu C, Rouaux C, Michel PP, Alvarez-Fischer D, Boutillier A-L, DeGregori J, Oertel WH, Rakic P (2007) The pRb/E2F cell-cycle pathway mediates cell death in Parkinson's disease. Proceedings of the National Academy of Sciences 104:3585-3590.
Hollensworth SB, Shen C-C, Sim JE, Spitz DR, Wilson GL, LeDoux SP (2000) Glial cell type-specific responses to menadione-induced oxidative stress. Free Radical Biology and Medicine 28:1161-1174.
Iourov IY, Liehr T, Vorsanova SG, Yurov YB (2007) Interphase chromosome-specific multicolor banding (ICS-MCB): a new tool for analysis of interphase chromosomes in their integrity. Biomolecular engineering 24:415-417.
Ishaq A, Hanson PS, Morris CM, Saretzki G (2016) Telomerase activity is downregulated early during human brain development. Genes 7:27.
Ishii T, Takanashi Y, Sugita K, Miyazawa M, Yanagihara R, Yasuda K, Onouchi H, Kawabe N, Nakata M, Yamamoto Y (2017) Endogenous reactive oxygen species cause astrocyte defects and neuronal dysfunctions in the hippocampus: a new model for aging brain. Aging cell 16:39-51.
Jaskelioff M, Muller FL, Paik J-H, Thomas E, Jiang S, Adams AC, Sahin E, Kost-Alimova M, Protopopov A, Cadinanos J (2011) Telomerase reactivation reverses tissue degeneration in aged telomerase-deficient mice. Nature 469:102-106.
Jeng W, Loniewska MM, Wells PG (2013) Brain glucose-6-phosphate dehydrogenase protects against endogenous oxidative DNA damage and neurodegeneration in aged mice. ACS chemical neuroscience 4:1123-1132.
Jurk D, Wilson C, Passos JF, Oakley F, Correia-Melo C, Greaves L, Saretzki G, Fox C, Lawless C, Anderson R (2014) Chronic inflammation induces telomere dysfunction and accelerates ageing in mice. Nature communications 5.
Kang HJ, Choi YS, Hong S-B, Kim K-W, Woo R-S, Won SJ, Kim EJ, Jeon HK, Jo S-Y, Kim TK (2004) Ectopic expression of the catalytic subunit of telomerase protects against brain injury resulting from ischemia and NMDA-induced neurotoxicity. Journal of Neuroscience 24:1280-1287.
Kao H-T, Cawthon R, Delisi L, Bertisch H, Ji F, Gordon D, Li P, Benedict M, Greenberg W, Porton B (2008) Rapid telomere erosion in schizophrenia. Molecular psychiatry 13:118-120.
Kawanishi S, Oikawa S (2004) Mechanism of telomere shortening by oxidative stress. Annals of the New York Academy of Sciences 1019:278-284.
Kiernan MC, Vucic S, Cheah BC, Turner MR, Eisen A, Hardiman O, Burrell JR, Zoing MC (2011) Amyotrophic lateral sclerosis. The Lancet 377:942-955.
Kim NW, Piatyszek MA, Prowse KR, Harley CB, West MD, Ho PL, Coviello GM, Wright WE, Weinrich SL, Shay JW (1994) Specific association of human telomerase activity with immortal cells and cancer. Science:2011-2015.
Kipling D, Cooke HJ (1990) Hypervariable ultra-long telomeres in mice. Nature 347:400-402.
Kota LN, Bharath S, Purushottam M, Moily NS, Sivakumar PT, Varghese M, Pal PK, Jain S (2014) Reduced telomere length in neurodegenerative disorders may suggest shared biology. The Journal of neuropsychiatry and clinical neurosciences 27:e92-e96.
Lanzillotta A, Porrini V, Bellucci A, Benarese M, Branca C, Parrella E, Spano PF, Pizzi M (2015) NF-κB in innate neuroprotection and age-related neurodegenerative diseases. Frontiers in neurology 6.

Lawson L, Perry V, Dri P, Gordon S (1990) Heterogeneity in the distribution and morphology of microglia in the normal adult mouse brain. Neuroscience 39:151-170.

Lee J, Jo YS, Sung YH, Hwang IK, Kim H, Kim S-Y, Yi SS, Choi J-S, Sun W, Seong JK (2010) Telomerase deficiency affects normal brain functions in mice. Neurochemical research 35:211-218.

Lee J, Ehlers C, Crews F, Niethammer M, Budin F, Paniagua B, Sulik K, Johns J, Styner M, Oguz I (2011) Automatic cortical thickness analysis on rodent brain. In: Proceedings of SPIE--the International Society for Optical Engineering, p 7962481: NIH Public Access.

Levy MZ, Allsopp RC, Futcher AB, Greider CW, Harley CB (1992) Telomere end-replication problem and cell aging. Journal of molecular biology 225:951-960.

Liao B, Zhao W, Beers DR, Henkel JS, Appel SH (2012) Transformation from a neuroprotective to a neurotoxic microglial phenotype in a mouse model of ALS. Experimental neurology 237:147-152.

Linkus B, Wiesner D, MeΔner M, Karabatsiakis A, Scheffold A, Rudolph KL, Thal DR, Weishaupt JH, Ludolph AC, Danzer KM (2016) Telomere shortening leads to earlier age of onset in ALS mice. Aging (Albany NY) 8:382.

Listerman I, Gazzaniga FS, Blackburn EH (2014) An investigation of the effects of the core protein telomerase reverse transcriptase on Wnt signaling in breast cancer cells. Molecular and cellular biology 34:280-289.

Lohr JN, David P, Haag CR (2014) Reduced lifespan and increased ageing driven by genetic drift in small populations. Evolution 68:2494-2508.

Lu T, Pan Y, Kao S-Y, Li C, Kohane I, Chan J, Yankner BA (2004) Gene regulation and DNA damage in the ageing human brain. Nature 429:883-891.

Ludlow AT, Zimmerman JB, Witkowski S, Hearn JW, Hatfield BD, Roth SM (2008) Relationship between physical activity level, telomere length, and telomerase activity. Medicine and science in sports and exercise 40:1764.

Lukens JN, Van Deerlin V, Clark CM, Xie SX, Johnson FB (2009) Comparisons of telomere lengths in peripheral blood and cerebellum in Alzheimer's disease. Alzheimer's & Dementia 5:463-469.

Ma X, Zhang J, Zhang Y, Chen H, Li R, Wang J, Chen H (2015) Altered cortical hubs in functional brain networks in amyotrophic lateral sclerosis. Neurological Sciences 36:2097-2104.

Manning EL, Crossland J, Dewey MJ, Van Zant G (2002) Influences of inbreeding and genetics on telomere length in mice. Mammalian genome 13:234-238.

Marseglia L, Manti S, D'Angelo G, Nicotera A, Parisi E, Di Rosa G, Gitto E, Arrigo T (2014) Oxidative stress in obesity: a critical component in human diseases. International journal of molecular sciences 16:378-400.

Mayer S, Brüderlein S, Perner S, Waibel I, Holdenried A, Ciloglu N, Hasel C, Mattfeldt T, Nielsen K, Möller P (2006) Sex-specific telomere length profiles and age-dependent erosion dynamics of individual chromosome arms in humans. Cytogenetic and genome research 112:194-201.

McClintock B (1941) The stability of broken ends of chromosomes in Zea mays. Genetics 26:234.

McClintock B (1942) The fusion of broken ends of chromosomes following nuclear fusion. Proceedings of the National Academy of Sciences 28:458-463.

McShea A, Lee H-g, Petersen RB, Casadesus G, Vincent I, Linford NJ, Funk J-O, Shapiro RA, Smith MA (2007) Neuronal cell cycle re-entry mediates Alzheimer disease-type changes. Biochimica et Biophysica Acta (BBA)-Molecular Basis of Disease 1772:467-472.

Misiti S, Nanni S, Fontemaggi G, Cong Y-S, Wen J, Hirte HW, Piaggio G, Sacchi A, Pontecorvi A, Bacchetti S (2000) Induction of hTERT expression and telomerase activity by estrogens in human ovary epithelium cells. Molecular and cellular biology 20:3764-3771.

Möller P, Mayer S, Mattfeldt T, Müller K, Wiegand P, Brüderlein S (2009) Sex-related differences in length and erosion dynamics of human telomeres favor females. Aging (Albany NY) 1:733.

Montpetit AJ, Alhareeri AA, Montpetit M, Starkweather AR, Elmore LW, Filler K, Mohanraj L, Burton CW, Menzies VS, Lyon DE (2014) Telomere length: a review of methods for measurement. Nursing research 63:289.

Mosch B, Morawski M, Mittag A, Lenz D, Tarnok A, Arendt T (2007) Aneuploidy and DNA replication in the normal human brain and Alzheimer's disease. Journal of Neuroscience 27:6859-6867.

Moyzis RK, Buckingham JM, Cram LS, Dani M, Deaven LL, Jones MD, Meyne J, Ratliff RL, Wu J-R (1988) A highly conserved repetitive DNA sequence,(TTAGGG) n, present at the telomeres of human chromosomes. Proceedings of the National Academy of Sciences 85:6622-6626.

Muller HJ (1938) The remaking of chromosomes. Collecting net 13:181-198.

Nabetani A, Ishikawa F (2011) Alternative lengthening of telomeres pathway: recombination-mediated telomere maintenance mechanism in human cells. The Journal of Biochemistry 149:5-14.

Nakamura K-I, Takubo K, Izumiyama-Shimomura N, Sawabe M, Arai T, Kishimoto H, Fujiwara M, Kato M, Oshimura M, Ishii A (2007) Telomeric DNA length in cerebral gray and white matter is associated with longevity in individuals aged 70 years or older. Experimental gerontology 42:944-950.

Nawrot TS, Staessen JA, Gardner JP, Aviv A (2004) Telomere length and possible link to X chromosome. The Lancet 363:507-510.

Nedergaard M, Ransom B, Goldman SA (2003) New roles for astrocytes: redefining the functional architecture of the brain. Trends in neurosciences 26:523-530.

Njajou OT, Cawthon RM, Damcott CM, Wu S-H, Ott S, Garant MJ, Blackburn EH, Mitchell BD, Shuldiner AR, Hsueh W-C (2007) Telomere length is paternally inherited and is associated with parental lifespan. Proceedings of the National Academy of Sciences 104:12135-12139.

Njie EG, Boelen E, Stassen FR, Steinbusch H, Borchelt DR, Streit WJ (2012) Ex vivo cultures of microglia from young and aged rodent brain reveal age-related changes in microglial function. Neurobiology of aging 33:195. e191-112.

Nordfjäll K, Larefalk Å, Lindgren P, Holmberg D, Roos G (2005) Telomere length and heredity: Indications of paternal inheritance. Proceedings of the National Academy of Sciences of the United States of America 102:16374-16378.

Nordfjäll K, Svenson U, Norrback K-F, Adolfsson R, Roos G (2010) Large-scale parent–child comparison confirms a strong paternal influence on telomere length. European Journal of Human Genetics 18:385-389.

O'Callaghan NJ, Fenech M (2011) A quantitative PCR method for measuring absolute telomere length. Biological procedures online 13:3.

O'sullivan RJ, Karlseder J (2010) Telomeres: protecting chromosomes against genome instability. Nature reviews Molecular cell biology 11:171-181.

Pacifici M, Peruzzi F (2012) Isolation and culture of rat embryonic neural cells: a quick protocol. Journal of visualized experiments: JoVE.

Panossian L, Porter V, Valenzuela H, Zhu X, Reback E, Masterman D, Cummings J, Effros R (2003) Telomere shortening in T cells correlates with Alzheimer's disease status. Neurobiology of aging 24:77-84.

Park J-I, Venteicher AS, Hong JY, Choi J, Jun S, Shkreli M, Chang W, Meng Z, Cheung P, Ji H (2009) Telomerase modulates Wnt signalling by association with target gene chromatin. Nature 460:66-72.

Paulukonis ST, Roberts EM, Valle JP, Collins NN, English PB, Kaye WE (2015) Survival and cause of death among a cohort of confirmed Amyotrophic Lateral Sclerosis cases. PloS one 10:e0131965.

Penndorf D, Tadić V, Witte OW, Grosskreutz J, Kretz A (2017) DNA strand breaks and TDP-43 mislocation are absent in the murine hSOD1G93A model of amyotrophic lateral sclerosis in vivo and in vitro. PloS one 12:e0183684.

Pfaffl MW (2001) A new mathematical model for relative quantification in real-time RT–PCR. Nucleic acids research 29:e45-e45.

Pickett HA, Cesare AJ, Johnston RL, Neumann AA, Reddel RR (2009) Control of telomere length by a trimming mechanism that involves generation of t-circles. The EMBO Journal 28:799-809.

Poon HF, Hensley K, Thongboonkerd V, Merchant ML, Lynn BC, Pierce WM, Klein JB, Calabrese V, Butterfield DA (2005) Redox proteomics analysis of oxidatively modified proteins in G93A-SOD1 transgenic mice—a model of familial amyotrophic lateral sclerosis. Free Radical Biology and Medicine 39:453-462.

Prowse KR, Greider CW (1995) Developmental and tissue-specific regulation of mouse telomerase and telomere length. Proceedings of the National Academy of Sciences 92:4818-4822.

Ranganathan S, Bowser R (2003) Alterations in G 1 to S phase cell-cycle regulators during amyotrophic lateral sclerosis. The American journal of pathology 162:823-835.

Raskin J, Cummings J, Hardy J, Schuh K, A Dean R (2015) Neurobiology of Alzheimer's disease: integrated molecular, physiological, anatomical, biomarker, and cognitive dimensions. Current Alzheimer research 12:712-722.

Rehen SK, Yung YC, McCreight MP, Kaushal D, Yang AH, Almeida BS, Kingsbury MA, Cabral KM, McConnell MJ, Anliker B (2005) Constitutional aneuploidy in the normal human brain. Journal of Neuroscience 25:2176-2180.

Rolyan H, Scheffold A, Heinrich A, Begus-Nahrmann Y, Langkopf BH, Hölter SM, Vogt-Weisenhorn DM, Liss B, Wurst W, Lie DC (2011) Telomere shortening reduces Alzheimer's disease amyloid pathology in mice. Brain 134:2044-2056.

Ruiz-Lopez MJ, Evenson DP, Espeso G, Gomendio M, Roldan ER (2010) High levels of DNA fragmentation in spermatozoa are associated with inbreeding and poor sperm quality in endangered ungulates. Biology of reproduction 83:332-338.

Samassekou O, Malina A, Hébert J, Yan J (2013) Presence of alternative lengthening of telomeres associated circular extrachromosome telomere repeats in primary leukemia cells of chronic myeloid leukemia. Journal of hematology & oncology 6:26.

Saxena A, Wagatsuma A, Noro Y, Kuji T, Asaka-Oba A, Watahiki A, Gurnot C, Fagiolini M, Hensch TK, Carninci P (2012) Trehalose-enhanced isolation of neuronal sub-types from adult mouse brain. Biotechniques 52:381.

Seibenhener ML, Wooten MW (2012) Isolation and culture of hippocampal neurons from prenatal mice. Journal of visualized experiments: JoVE.

Shay JW, Wright WE (2000) Hayflick, his limit, and cellular ageing. Nature reviews Molecular cell biology 1:72-76.

Sibille E (2013) Molecular aging of the brain, neuroplasticity, and vulnerability to depression and other brain-related disorders. Dialogues in clinical neuroscience 15:53.

Smith C, Carney JM, Starke-Reed P, Oliver C, Stadtman E, Floyd R, Markesbery W (1991) Excess brain protein oxidation and enzyme dysfunction in normal aging and in Alzheimer disease. Proceedings of the National Academy of Sciences 88:10540-10543.

Song Z, Von Figura G, Liu Y, Kraus JM, Torrice C, Dillon P, Rudolph-Watabe M, Ju Z, Kestler HA, Sanoff H (2010) Lifestyle impacts on the aging-associated expression of biomarkers of DNA damage and telomere dysfunction in human blood. Aging cell 9:607-615.

Spilsbury A, Miwa S, Attems J, Saretzki G (2015) The role of telomerase protein TERT in Alzheimer's disease and in tau-related pathology in vitro. Journal of Neuroscience 35:1659-1674.

Takubo K, Izumiyama-Shimomura N, Honma N, Sawabe M, Arai T, Kato M, Oshimura M, Nakamura K-I (2002) Telomere lengths are characteristic in each human individual. Experimental gerontology 37:523-531.

Takubo K, Aida J, Izumiyama-Shimomura N, Ishikawa N, Sawabe M, Kurabayashi R, Shiraishi H, Arai T, Nakamura KI (2010) Changes of telomere length with aging. Geriatrics & gerontology international 10.

Thomas P, O'Callaghan NJ, Fenech M (2008) Telomere length in white blood cells, buccal cells and brain tissue and its variation with ageing and Alzheimer's disease. Mechanisms of ageing and development 129:183-190.

Tümpel S, Rudolph KL (2012) The role of telomere shortening in somatic stem cells and tissue aging: lessons from telomerase model systems. Annals of the New York Academy of Sciences 1266:28-39.

Turner MR, Barnwell J, Al-Chalabi A, Eisen A (2012) Young-onset amyotrophic lateral sclerosis: historical and other observations. Brain 135:2883-2891.

Unryn BM, Cook LS, Riabowol KT (2005) Paternal age is positively linked to telomere length of children. Aging cell 4:97-101.

Valdes AM, Andrew T, Gardner JP, Kimura M, Oelsner E, Cherkas LF, Aviv A, Spector TD (2005) Obesity, cigarette smoking, and telomere length in women. The lancet 366:662-664.

van Es MA, Hardiman O, Chio A, Al-Chalabi A, Pasterkamp RJ, Veldink JH, van den Berg LH (2017) Amyotrophic lateral sclerosis. The Lancet.

Vasa-Nicotera M, Brouilette S, Mangino M, Thompson JR, Braund P, Clemitson J-R, Mason A, Bodycote CL, Raleigh SM, Louis E (2005) Mapping of a major locus that determines telomere length in humans. The American Journal of Human Genetics 76:147-151.

Vera E, de Jesus BB, Foronda M, Flores JM, Blasco MA (2012) The rate of increase of short telomeres predicts longevity in mammals. Cell reports 2:732-737.

Verhoeven JE, Révész D, Epel ES, Lin J, Wolkowitz OM, Penninx BW (2014) Major depressive disorder and accelerated cellular aging: results from a large psychiatric cohort study. Molecular psychiatry 19:895-901.

Vorsanova SG, Yurov YB, Iourov IY (2010) Human interphase chromosomes: a review of available molecular cytogenetic technologies. Molecular cytogenetics 3:1.

Vulliamy TJ, Marrone A, Knight SW, Walne A, Mason PJ, Dokal I (2006) Mutations in dyskeratosis congenita: their impact on telomere length and the diversity of clinical presentation. Blood 107:2680-2685.

Wang RC, Smogorzewska A, De Lange T (2004a) Homologous recombination generates T-loop-sized deletions at human telomeres. Cell 119:355-368.

Wang W, Luo H-S, Yu B-P (2004b) Expression of NF-κB and human telomerase reverse transcriptase in gastric cancer and precancerous lesions. World journal of gastroenterology 10:177.

Wersto RP, Chrest FJ, Leary JF, Morris C, Stetler-Stevenson M, Gabrielson E (2001) Doublet discrimination in DNA cell-cycle analysis. Cytometry Part A 46:296-306.

Willeit P, Willeit J, Mayr A, Weger S, Oberhollenzer F, Brandstätter A, Kronenberg F, Kiechl S (2010) Telomere length and risk of incident cancer and cancer mortality. Jama 304:69-75.

Wright WE, Piatyszek MA, Rainey WE, Byrd W, Shay JW (1996) Telomerase activity in human germline and embryonic tissues and cells. Developmental genetics 18:173-179.

Wright WE, Tesmer VM, Huffman KE, Levene SD, Shay JW (1997) Normal human chromosomes have long G-rich telomeric overhangs at one end. Genes & development 11:2801-2809.

Wu X-q, Yang Y, Li W-x, Cheng Y-h, Li X-f, Huang C, Meng X-m, Wu B-m, Liu X-h, Zhang L (2016) Telomerase reverse transcriptase acts in a feedback loop with NF-κB pathway to regulate macrophage polarization in alcoholic liver disease. Scientific reports 6:18685.

Wu X, Amos CI, Zhu Y, Zhao H, Grossman BH, Shay JW, Luo S, Hong WK, Spitz MR (2003) Telomere dysfunction: a potential cancer predisposition factor. Journal of the national cancer institute 95:1211-1218.

Xu Q, Parks CG, DeRoo LA, Cawthon RM, Sandler DP, Chen H (2009) Multivitamin use and telomere length in women. The American journal of clinical nutrition:ajcn. 26986.

Yang Y, Geldmacher DS, Herrup K (2001) DNA replication precedes neuronal cell death in Alzheimer's disease. Journal of Neuroscience 21:2661-2668.

Yin L, Hubbard AK, Giardina C (2000) NF-κB regulates transcription of the mouse telomerase catalytic subunit. Journal of Biological Chemistry 275:36671-36675.

Zhang D, Cheng L, Craig DW, Redman M, Liu C (2010) Cerebellar telomere length and psychiatric disorders. Behavior genetics 40:250-254.

Zhang J, Herrup K (2011) Nucleocytoplasmic Cdk5 is involved in neuronal cell cycle and death in post-mitotic neurons. Cell cycle 10:1208-1214.

Zhang Y, Toh L, Lau P, Wang X (2012) Human telomerase reverse transcriptase (hTERT) is a novel target of the Wnt/β-catenin pathway in human cancer. Journal of Biological Chemistry 287:32494-32511.

Zhu H, Fu W, Mattson MP (2000) The Catalytic Subunit of Telomerase Protects Neurons Against Amyloid β-Peptide-Induced Apoptosis. Journal of neurochemistry 75:117-124.

8 APPENDIX

8.1 List of figures

8.2 List of tables

8.3 Acknowledgements

In the beginning I would like to pay my humble and immense gratitude to Almighty ALLAH for bestowing me this opportunity to carry out this work, and to give me enough courage and strength to withstand all the tough times and challenges during the course of my work.

Then I would like to thank Prof. O. W. Witte for trusting in me and appointing me to work on this project. His ingenious and knowledgeable suggestions and comments throughout the course of my studies always provided me with new insights to my work. I am thankful to him for his time and for always being there to listen to me and solve my problems either related to work or settling in Jena. I am also grateful to him for providing me excellent working conditions and continuous supply of material for the accomplishment of scientific experiments during the whole time. I am extremely grateful to Dr. Alexandra Kretz and Dr. Christian Schmeer for their continuous support, trust, motivation, encouragement, patience and excellent mentoring during the course of my whole studies. I am thankful to them for their precious time and countless efforts which they continuously dedicated for the establishment of experiments, discussing and analyzing their outcomes. I am also thankful to them for their valuable comments and guidance during the course of thesis writing.

I pay my sincere gratitude to Prof. Dr. Regine Heller whom if I call “Mother of Summer School students” will not be wrong. I am thankful to her for excellent summer school organization and for selecting me to be a part of Summer School Molecular Medicine in 2012. Since that first contact, she has proved to be always there to help me physically and morally. I am greatly thankful to our “ever growing international summer school community” for all the fun time and socializing events. I am also very lucky to have Dr. Tzvetanka Bondeva around me. I owe her big thanks for her unbounded love, excellent moral and physical support and for providing me kind, amazing and pleasurable company outside the lab. I am greatly thankful for her precious time, insightful and valuable suggestions for experimental design and data analysis. I am also sincerely obliged to Mrs. Nasim Kroegel for her immense help for dealing with all the administrative matters and for the preparation of all the documentations starting from my admission to the university until now. I am also greatly indebted to her for helping me in my settlement immediately after I arrived to Jena.

I am thankful to Graduate Academy, Friedrich Schiller University Jena for the provision of PhD stipend and for supporting me to attend the conferences which really gave me the chance to interact with the scientific community and helped me to groom my scientific knowledge. I

am also very thankful to the technical assistants especially Svetlana Tausch and Claudia Sommer for their excellent technical support during the performance of experiments.

I am deeply grateful to all the lab members and my office colleagues especially Dr. Benedict Grünewald and Dr. Mihai Ceanga for their valuable suggestions during the development of experiments. I thank Dr. Milan Stojiljkovic for great scientific discussions, comments and positive and intuitive criticism which led me for the critical analytical reasoning of the findings. I am also very thankful to my friends Vedrana Tadic and Diane Penndorf for their wonderful and enjoyable company and for helping me with language issues anytime I needed them. I also thank my "teacher" Dr. Sidra Gull for her selfless moral and physical support inside and outside the lab environment. I also thank my friends Hina, Anum, Seerat, Amama and Baila for their delightful company, fun, and humor which we shared together and which always helped me to release the stress.

I show my deepest gratitude to my prestigious homeland Pakistan, my all academic institutions, and all my teachers during the entire period of my studies for enabling me to reach to this point. Lastly, I cannot truly express my heart and gratitude to my family especially my loving parents and my sisters for their unconditional love, care, sacrifices, prayers and devotion. Thank you so much Mama, Papa and Naima for believing in me and allowing me to avail this opportunity and pursue my studies abroad.

8.4 Publications and conferences

8.4.1 Manuscripts in preparation

Ain Q*, Kretz A*, Bondeva T, Fischer M, Witte OW, Schmeer C. Telomere length dynamics and telomerase activity in the aging murine brain
Aging Cell (IF: 6.34) (under revision)

Ain Q, Schmeer C, Bondeva T, Großkreutz J, Witte OW, Kretz A. Telomere length dynamics and telomerase activity in the brain and spinal cord of the hSOD1^{G93A} mouse model of familial ALS
Journal envisaged: Molecular Neurodegeneration (IF: 6.78)

Ain Q, Kretz A, Witte OW, Schmeer C. Isolation and specification of CNS autochthonous cell populations for Flow-FISH analyses.
Journal envisaged: Nature Protocols (IF: 13.47)

** equal contribution*

8.4.2 Poster presentations

Ain Q, Schmeer C, Penndorf D, Fischer M, Bondeva T, Witte OW, Kretz A. Impact of hermetic inbreeding on telomere length dynamics and telomerase activity in the aging brain. 2nd Molecular Biology of Ageing Meeting, Groningen, Netherlands, 2017.

Ain Q, Kretz A, Penndorf D, Fischer M, Bondeva T, Witte OW, Schmeer C. Telomere length dynamics and telomerase activity in the aging murine brain. Annual Meeting of the Society for Neuroscience, San Diego, USA. Book of abstracts; Posters_4_Tue_AM, page 646, abstract no. 515, 2016.

Ain Q, Schmeer C, Bondeva T, Grosskreutz J, Witte OW, Kretz A. Telomere length dynamics and telomerase activity in the brain and spinal cord of diseased hSOD1^{G93A} mutant mice. 27th International Symposium on ALS/MND, Dublin, Ireland. Book of abstracts, page 150, abstract no. P109, 2016.

Ain Q, Kretz A, Penndorf D, Fischer M, Bondeva T, Witte OW, Schmeer C. Telomere length dynamics and telomerase activity in the aging murine brain. 13. Tag der Nachwuchswissenschaftler des Forschungszentrums (FZL), Jena University Hospital, Germany, 2016.

8.5 **Ehrenwörtliche Erklärung**

Hiermit erkläre ich, dass mir die Promotionsordnung der Medizinischen Fakultät der Friedrich-Schiller-Universität bekannt ist,

ich die Dissertation selbst angefertigt habe und alle von mir benutzten Hilfsmittel, persönlichen Mitteilungen und Quellen in meiner Arbeit angegeben sind,

mich folgende Personen bei der Auswahl und Auswertung des Materials sowie bei der Herstellung der Dissertation unterstützt haben:

Dr. Alexandra Kretz, Dr. Christian Schmeer, Prof. Dr. O. W. Witte, Diane Penndorf und Svetlana Würl

die Hilfe eines Promotionsberaters nicht in Anspruch genommen wurde und dass Dritte weder unmittelbar noch mittelbar geldwerte Leistungen von mir für Arbeiten erhalten haben, die im Zusammenhang mit dem Inhalt der vorgelegten Dissertation stehen,

dass ich die Dissertation noch nicht als Prüfungsarbeit für eine staatliche oder andere wissenschaftliche Prüfung eingereicht habe und dass ich die gleiche, eine in wesentlichen Teilen ähnliche oder eine andere Abhandlung nicht bei einer anderen Hochschule als Dissertation eingereicht habe.

Jena, Unterschrift des Verfassers